Institute of Thermoelectricity, Academy of Sciences and Ministry of Education and Science of Ukraine

# Journal of THERMOELECTRICITY

International Research

Founded in December, 1993

published 6 times a year

*No. 2* *2021*

## Editorial Board



## International Editorial Board

Founders – National Academy of Sciences, Ukraine
Institute of Thermoelectricity of National Academy of Sciences and Ministry of Education and Science of Ukraine

Certificate of state registration № КВ 15496-4068 ПР



Approved for printing by the Academic Council of Institute of Thermoelectricity of the National Academy of Sciences and Ministry of Education and Science, Ukraine

Address of editorial office:
Ukraine, 58002, Chernivtsi, General Post Office, P.O. Box 86.
Phone: +(380-372) 90 31 65.
Fax: +(380-3722) 4 19 17.
E-mail: jt@inst.cv.ua
http://www.jt.inst.cv.ua

Signed for publication 26.03.2021. Format 70×108/16. Offset paper №1. Offset printing.
Printer's sheet 11.5. Publisher's signature 9.2. Circulation 400 copies. Order 5.

Printed from the layout original made by "Journal of Thermoelectricity" editorial board
in the printing house of "Bukrek" publishers,
10, Radischev Str., Chernivtsi, 58000, Ukraine

**CONTENTS**

**V.G. Rifert,** *D.Sc. in Engineering*[1]
**L.I. Anatychuk,** *acad. of the NAS of Ukraine*[2,3]
**A.S. Solomakha,** *Ph.D. in Engineering*[1]
**P.O. Barabash,** *Ph.D. in Engineering*[1]
**V.G. Petrenko,** *Ph.D. in Engineering*[1]
**O.P. Snegovskoy**[1]

[1]NTUU "Ihor Sikorskyi KPI", 6, Politekhnicheskaya str,
Kyiv, 03056, Ukraine, *e–mail: vgrifert@ukr.net*;
[2]Institute of Thermoelectricity of the NAS and MES of Ukraine,
1, Nauky str., Chernivtsi, 58029, Ukraine, *e–mail: anatych@gmail.com*;
[3]Yuriy Fedkovych Chernivtsi National University,
2, Kotsiubynskyi str., Chernivtsi, 58012, Ukraine

# INFLUENCE OF THERMODYNAMIC CHARACTERISTICS OF A THERMOELECTRIC HEAT PUMP ON THE PERFORMANCE AND ENERGY CONSUMPTION OF A CENTRIFUGAL DISTILLER

*The paper analyzes the operation of a thermoelectric heat pump in combination with a centrifugal distiller for the regeneration of wastewater from a human life system in the conditions of future long-term space missions. The time dependence of the specific energy consumption of the system at different capacities of the heat pump is shown, the influence of the temperature difference of the heat carriers on the efficiency of the heat pump is analyzed. Bibl. 24, Fig. 5, Tabl. 2.*
**Key words**: thermoelectricity, heat pump, distiller.

**Nomenclature**

*CMED* – centrifugal distiller;
$c_p$ – heat capacity, J/(kg·K)
*G* – liquid flow rate, l/h;
*Q* – heat flow, W;
*G* – flow rate, kg/h;
*I* – current strength, A;
*N* – power delivered to THP, W;
*n* – revolutions, rpm;
*SPC* – specific power consumption, W·h/kg;
*THP* – thermoelectric heat pump;
*T, t* – temperature, °C;
*U* – voltage, V;
$\eta_{thp}$ – heat pump efficiency.

**Subscripts**

*h* – hot;
*c* – cold;
*d* – distiller;
*avg* – average;
*in* – inlet;
*out* – outlet;
*thp* – heat pump;
*cd* – motor

## Introduction

One of the important requirements for water recovery systems from liquid waste in the conditions of long-term space expeditions to the Moon, Mars and work on the International Space Station (ISS) is the minimum energy consumption.

A team of engineers and scientists from Igor Sikorsky Kyiv Polytechnic Institute, the Institute of Thermoelectricity of the National Academy of Sciences of Ukraine and the commercial company "Termodistillation RV" developed in the period 2000 - 2003 a wastewater treatment system for operation in microgravity conditions. In publications [1-5], this system is called the cascade distillation system (CDS). The more correct name used here is Centrifugal Multistage Distillation (CMED) system. The system contains two main components - the centrifugal multi-stage distiller itself and the thermoelectric heat pump. Two methods are used to reduce energy costs: 1) the principle of multi-stage evaporation and liquid concentration and 2) energy recovery through the use of a thermoelectric heat pump.

In [6 – 15], the integral characteristics of CMED of 3-stage and 5-stage distillation are given. Shown are the results of testing when concentrating urine, atmospheric moisture condensate, sanitary water and their mixtures at fixed operating parameters of the system, heat pump power (≈ 400 W), rotor motor speed, etc.

This paper shows the results of testing a centrifugal multi-stage distiller with a thermoelectric heat pump, which was developed at the Institute of Thermoelectricity of the National Academy of Sciences of Ukraine and manufactured by company ALTEC. The calculated characteristics of the parameters affecting the efficiency $\eta_{thp}$ are given.

## Methods for researching the characteristics of a centrifugal distiller with a thermoelectric heat pump

Three identical five-stage centrifugal distillers have been developed and manufactured by Termodistillation RV. Altec has manufactured two thermoelectric heat pumps designed and manufactured by the Institute of Thermoelectricity of the National Academy of Sciences and the Ministry of Education and Science of Ukraine (ITE). These distillers, together with thermoelectric heat pumps, were first tested at Termodistillation RV and later transferred to Honeywell International Inc. The devices were then tested at the Honeywell test benches and at the NASA test bench at the Marshall Space Flight Center.

The test results of distillers and THP presented here have not been previously published.

Fig. 1 shows a schematic diagram of a test bench for three distillers and two heat pumps.

The main and auxiliary equipment of the bench are connected by a system of pipelines that form two circulation circuits. In one of them ("hot") the evaporated solution circulates, and in the other ("cold") - distillate.

The test bench works as follows. The distiller's motor 1 is turned on, which provides the specified speed of the distiller's rotor, and the necessary pressure is set in the apparatus by the vacuum pump 7, which corresponds to the required boiling point of the solution. From the tank 13 the distillate fills the cold circuit, which ensures the circulation of the distillate through the condenser of the distiller 1, the salt meter 9, the rotameter 14, the cold side of THP 2, the heat exchanger-cooler 3 and again the condenser of the distiller. The "hot" circuit is filled from tank 4 to the level set by the regulator valve 6. In the "hot" circuit, the solution circulates from the distiller evaporator 1 through the rotameter 14, the hot side of the THP 2 and again into the distiller evaporator 1. When electricity is supplied to THP 2, the condensate is cooled in the "cold" circuit and the solution is heated in the "hot" circuit. The solution superheated in THP 2 relative to the saturation temperature in the CMED 1 evaporator is partially evaporated, and the resulting steam is used as a heating distiller in the subsequent evaporation stage; the steam obtained in the last stage of the distiller is condensed in a contact condenser CMED 1. During the evaporation process, the concentration of

dissolved substances in the hot circuit increases. Excess distillate from the "cold" circuit is automatically discharged into the distillate collector 5. The fresh solution is fed through valve 6. To ensure the stationary state of the distillation process, excess heat is removed by the heat exchanger-cooler 3 to the environment.

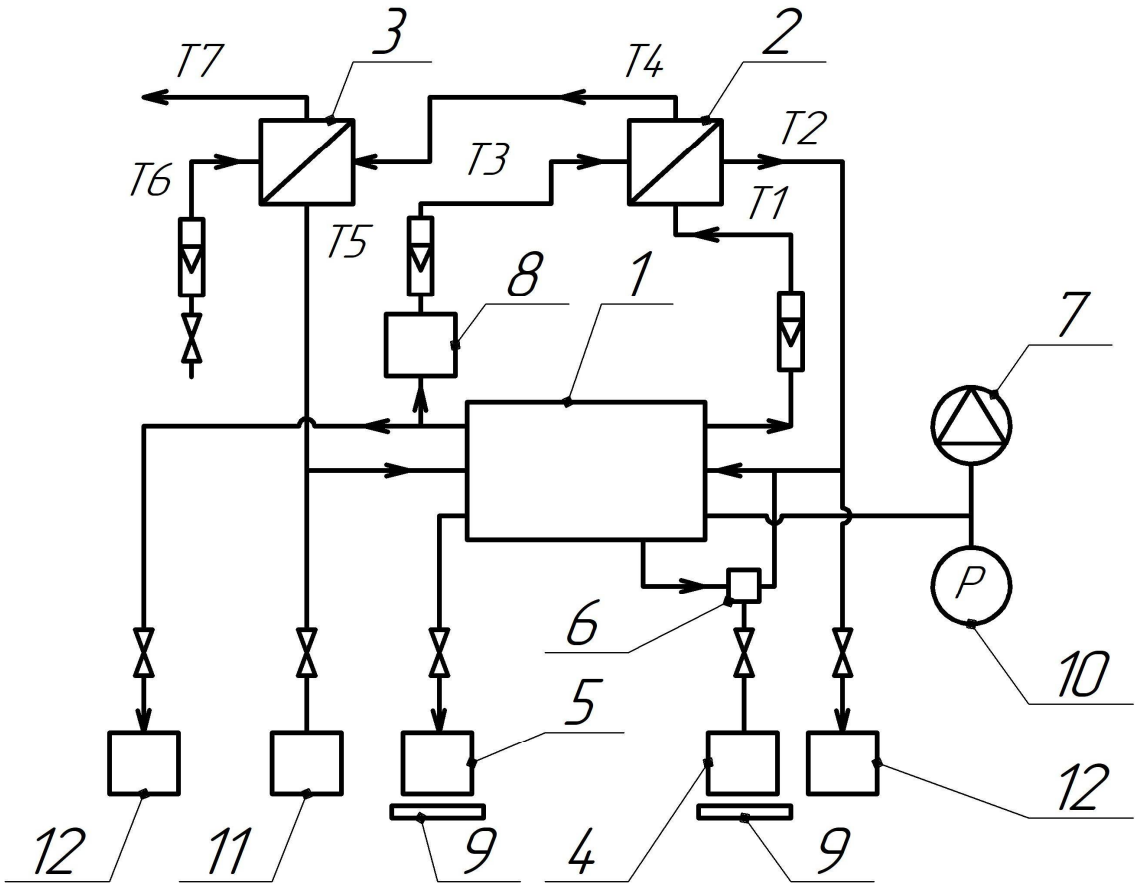


*Fig. 1. Schematic of the experimental test bench*
*1 – centrifugal vacuum distiller; 2 – thermoelectric heat pump;*
*3 – heat exchanger-cooler; 4 – initial solution; 5 – distillate collector; 6 – system power regulator valve; 7 – vacuum pump; 8 – salt meter; 9 – salt meter; 10 – electronic scales;*
*11 –vacuum gauge; 13 – container with distillate for refilling the cold circuit;*
*14 – rotameters; 15 – stop valve; 16 – containers for emptying circuits.*

After the end of the experiment, the power supply of THP 2 is turned off, and the "cold" and "hot" circuits are emptied into the corresponding containers 16.

The temperature was measured at the inlet and outlet of the thermopile on the hot ($t_1$, $t_2$) and cold sides ($t_3$, $t_4$), after the heat exchanger-cooler in the "cold" circuit ($t_5$) and at the inlet and outlet of the heat exchanger-cooler on the cooling side ($t_6$, $t_7$). The temperatures in the "hot" and "cold" circuits were measured by chromel-copel thermocouples, the measurement accuracy was ± 0.1 °C.

The pressure in the apparatus was measured with a vacuum gauge 11 with a measurement scale of

1 ... 0 bar (accuracy class 1.0) complete with a barometer.

The mass of the resulting distillate (product) and the initial solution was measured by electronic scales, measurement accuracy ± 2 g, measurement range ± 10 kg.

The salinity in the "cold" circuit was measured by the Hanna salt meter (0...999 ppm).

The motor and heat pump drive powers were measured with a voltmeter and an ammeter, accuracy class 0.5. The revolutions were measured with a tachometer with an accuracy of ±1 rpm.

The test time (one test) was 60...120 min.

## Results of the experimental study

At the Kiev Polytechnic Institute, studies (tests) of three CMEDs were carried out. Two heat pumps were used in the experiments. The rotation speed of the heat exchange surface varied from 900 to 1300 rpm, the power of the thermoelectric heat pump varied from 100 to 600 W. The working fluids were 1) distilled water; 2) NaCl solution with a concentration of 5 ... 30%; 3) urine with a concentration from 5 to 50%.

### Experimental determination of $\eta_{thp}$ depending on the input power and temperature difference

The heat flux generated at the outlet of the heat pump is defined as

$$Q_h = G_h c_p (t_2 - t_1), \tag{1}$$

where $t_2$ and $t_1$ are the outlet and inlet THP temperatures, respectively, °C.

$\eta_{thp}$ – the efficiency is determined as $\eta_{thp} = Q_h / N_{thp}$

SPC – specific power consumption is defined as the total cost of input energy (power supplied to the distiller's motor and power supplied to the thermopile) spent on the production of one kilogram of distillate

$$SPC = \frac{\left(N_{cd} + N_{thp}\right)}{G_d}, \tag{2}$$

The average temperature difference in a thermoelectric heat pump $\Delta T_{avg}$ is defined as:

$$\Delta T_{avg} = \frac{\left(t_1 + t_2\right)}{2} - \frac{\left(t_3 + t_4\right)}{2}, \tag{3}$$

where $t_1$ is temperature at the inlet to THP heating zone, °C; $t_2$ temperature at the outlet of THP heating zone, °C; $t_3$ is temperature at the inlet to THP cooling zone, °C; $t_4$ is temperature at the outlet of THP cooling zone, °C.

The temperature difference at the inlet to the thermoelectric heat pump $\Delta T_{in}$ is defined as:

$$\Delta T_{in} = t_1 - t_3, \tag{4}$$

Table 1 provides an example of one test performed on a CMED with 5 steps at $n$ = 1200 rpm on urine. All the initial values necessary to analyze the process are indicated: revolutions, power, time, temperature, costs, etc., and calculated values: supplied heat capacity, the degree of concentration of urine at the inlet and outlet of the device, the concentration in the residue, the efficiency of the heat pump.

Table 2 shows the main experimental parameters for each of the 32 tests performed in different periods of time on different devices. It should be noted that the main characteristics of the three manufactured centrifugal distillers, as well as two heat pumps, are identical (with the same parameters of the initial liquid, revolutions and power), as well as two heat pumps: performance, specific power consumption, distillate quality [16–19], which confirms the optimality of the developed CMED design in combination with THP.

*Table 1*

*Results of testing five-stage centrifugal distiller with thermoelectric heat pump (rotation speed 1100 rpm, working fluid – urine)*

| Time | Motor | | | THP | | | Weight | | | Flow rate | | | | Temperature | | | |
|---|---|---|---|---|---|---|---|---|---|---|---|---|---|---|---|---|---|
| | *U* | *I* | *N* | *U* | *I* | *N* | Initial liquid | Product (distillate) | Total dissolved solids | Hot, $G_h$ | Cold, $G_c$ | Performance | Specific power consumption SPC | Hot inlet to THP, $t_1$ | Hot outlet from THP, $t_2$ | Cold inlet to THP, $t_3$ | Cold outlet from THP, $t_4$ |
| min | V | A | W | V | A | W | gram | | mg/l | l/h | | kg/h | W·h/kg | °C | | | |
| 0 | 24.2 | 3.1 | 75 | 20.5 | 10.08 | 206.6 | 0 | 0 | 12 | 60 | 82 | 0 | 0 | 23.2 | 23.1 | 22.9 | 22.9 |
| 6 | 24.2 | 3.1 | 75 | 22.5 | 10.9 | 245.3 | 288 | 184 | 22 | 60 | 82 | 1.84 | 174.1 | 31.8 | 43.7 | 23.4 | 22.7 |
| 12 | 24.2 | 3.1 | 75 | 28.5 | 14.3 | 407.6 | 634 | 602 | 38 | 60 | 82 | 4.18 | 174.1 | 37.5 | 48.3 | 24.5 | 22.4 |
| **18** | **24.2** | **3.1** | **75** | **29.2** | **14** | **408.8** | **1122** | **1070** | **51** | **60** | **82** | **4.58** | **103.4** | **38.7** | **49.4** | **25.1** | **22.3** |
| 24 | 24.2 | 3.1 | 75 | 30 | 14.4 | 460.8 | 1584 | 1528 | 61 | 60 | 82 | 4.58 | 117.0 | 38.8 | 50.8 | 25.1 | 22.0 |
| 30 | 24.2 | 3.1 | 75 | 31.8 | 15.2 | 483.4 | 2078 | 2006 | 67 | 60 | 82 | 4.78 | 116.8 | 39.4 | 51.5 | 25.2 | 22.1 |
| 36 | 24.2 | 3.1 | 75 | 32.3 | 14.22 | 459.3 | 2592 | 2502 | 73 | 60 | 82 | 4.96 | 107.7 | 40.0 | 52.2 | 25.4 | 22.1 |
| 42 | 24.2 | 3.1 | 75 | 32.1 | 15.24 | 489.2 | 3110 | 3004 | 76 | 60 | 82 | 5.02 | 112.4 | 40.0 | 52.2 | 25.4 | 22.3 |
| 48 | 24.2 | 3.1 | 75 | 31.9 | 15.2 | 484.9 | 3628 | 3500 | 79 | 61 | 82 | 4.96 | 112.9 | 40.1 | 52.1 | 24.9 | 22.0 |
| 54 | 24.2 | 3.1 | 75 | 32.4 | 15.36 | 497.7 | 4136 | 3990 | 82 | 61 | 83 | 4.90 | 116.9 | 40.3 | 52.2 | 25.1 | 22.1 |
| 60 | 24.2 | 3.1 | 75 | 33 | 15.6 | 514.8 | 4656 | 4492 | 84 | 62 | 83 | 5.02 | 117.5 | 40.7 | 53.5 | 24.9 | 22.0 |
| 66 | 24.2 | 3.1 | 75 | 33.2 | 15.64 | 519.2 | 5182 | 5006 | 87 | 62 | 83 | 5.14 | 115.6 | 40.9 | 53.2 | 24.9 | 22.1 |
| 72 | 24.2 | 3.1 | 75 | 33.1 | 15.56 | 515 | 5702 | 5508 | 90 | 63 | 83 | 5.02 | 117.5 | 40.9 | 53.1 | 24.9 | 22.0 |
| 78 | 24.2 | 3.1 | 75 | 33 | 15.58 | 514.1 | 6220 | 6010 | 92 | 64 | 83 | 5.02 | 117.4 | 40.9 | 53.2 | 24.9 | 22.0 |
| 84 | 24.2 | 3.1 | 75 | 33.2 | 15.72 | 521.9 | 6740 | 6510 | 94 | 65 | 83 | 5.00 | 119.4 | 41.0 | 53.5 | 24.8 | 22.0 |
| 90 | 24.2 | 3.1 | 75 | 33.2 | 15.46 | 513.3 | 7250 | 7010 | 96 | 67 | 83 | 5.00 | 117.7 | 41.0 | 53.5 | 24.8 | 22.0 |
| 96 | 24.2 | 3.1 | 75 | 32.8 | 15.34 | 503.2 | 7755 | 7500 | 97 | 68 | 83 | 4.90 | 118.0 | 41.0 | 53.1 | 24.6 | 22.0 |
| 102 | 24.2 | 3.1 | 75 | 32.9 | 15.4 | 506.7 | 8175 | 8000 | 98 | 71 | 83 | 5.00 | 116.3 | 41.0 | 53.1 | 24.8 | 22.0 |
| 108 | 24.2 | 3.1 | 75 | 0 | 0 | 0 | 8280 | 8205 | 96 | 71 | 83 | | | | | | |

Fig.2 shows specific power consumption versus time for three five-stage distillers with a heat pump power of 400 W. In experiments on urine, the salt concentration increased over time up to 50%, and it should be noted that the efficiency of the system weakly depends on the concentration of the solution (see Fig. 2).

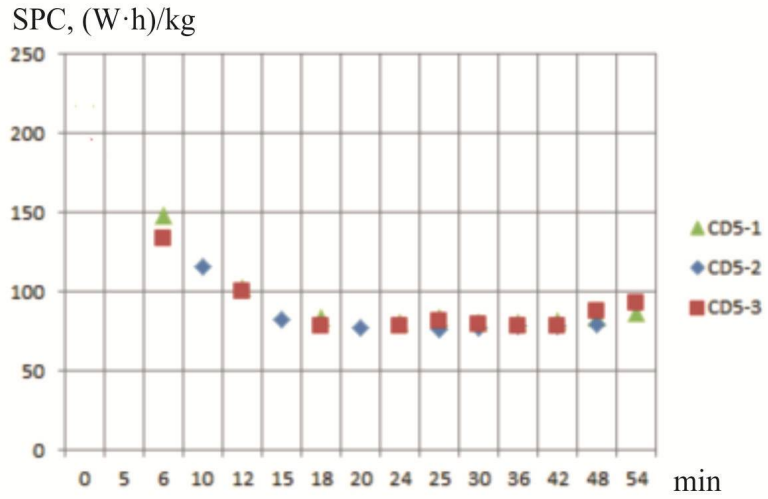


*Fig. 2. Specific power consumption versus time for urine, $N_{TTH}$ = 400 W, n = 1200 rpm.*

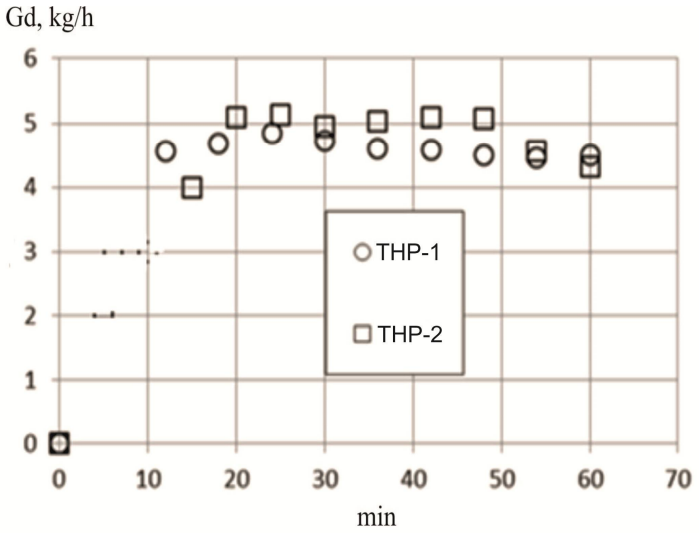


*Fig. 3. System performance versus time for two samples of thermoelectric heat pumps, $N_{thp}$ = 400 W, n = 1200 rpm.*

The most important indicator of heat pump efficiency, $\eta_{thp}$, has high values in the investigated range of current strength (see Table 2). In general, the efficiency of a thermoelectric heat pump depends on the average temperature difference and the temperature difference at the inlet to the heat pump. In our works [20-21], this is analyzed and it is shown that the implementation of the process in the field of action of centrifugal forces significantly intensifies heat transfer, which, in turn, favorably affects the efficiency of the thermoelectric heat pump. As a result, the $\eta_{thp}$ of the heat pump in our case varies from 2 to 5 depending on the current power.

NASA tested the TIMES distiller at the end of the 20th century. The system uses a polymer membrane that selectively allows water from the wastewater source to pass through. Power consumption is

minimized by using solid state heat pumps. As a result, in experimental tests with non-concentrated urine, the maximum efficiency of a thermoelectric heat pump was approximately equal to only two [22-24].

*Table 2*

*Main results of the experimental study for 32 selected tests*

| № | Liquid | Revolutions, $n$, rpm | Motor power, $N_p$, W | Heat pump power, $N_{thp}$, W | Current strength, $I$, A | Inlet temperature difference, $\Delta T_{in} = t_1 - t_3$ | Average temperature difference, $\Delta T_{avg} = (t_1 + t_2)/2 - (t_3 + t_4)/2$ | Delivered thermal power, $Q$, W | Heat pump efficiency, $\eta_{thp}$ |
|---|---|---|---|---|---|---|---|---|---|
| 1 | Urine | 1200 | 76 | 386 | 14.5 | 12.2 | 18.8 | 780 | 2.02 |
| 2 | Water | 1000 | 76 | 430 | 17.7 | 9 | 16.8 | 1000 | 2.33 |
| 3 | Urine | 1000 | 76 | 235 | 11 | 9 | 15.8 | 600 | 2.55 |
| 4 | Urine | 1000 | 77 | 240 | 11 | 9.7 | 15 | 614 | 2.56 |
| 5 | Urine | 1200 | 92 | 96.4 | 6.8 | 2.4 | 11.3 | 320 | 3.32 |
| 6 | Urine | 800 | 40 | 150 | 8.8 | 6.7 | 10 | 490 | 3.27 |
| 7 | Urine | 1000 | 71 | 150 | 8.8 | 8.8 | 12 | 459 | 3.06 |
| 8 | Urine | 1200 | 77 | 386 | 14 | 12 | 23.5 | 880 | 2.28 |
| 9 | Urine | 800 | 40 | 150 | 8.8 | 6.7 | 10 | 491 | 3.27 |
| 10 | Urine | 1000 | 70 | 150 | 8.8 | 8.8 | 12 | 459 | 3.06 |
| 11 | Urine | 1200 | 78 | 386 | 14 | 12 | 23.5 | 880 | 2.28 |
| 12 | Water | 1200 | 79 | 106 | 7.6 | 3.9 | 5.8 | 360 | 3.4 |
| 13 | Water | 1200 | 78 | 200 | 10.4 | 4.3 | 9.3 | 600 | 3.0 |
| 14 | Water | 1100 | 63 | 100 | 7.3 | 3.5 | 6.8 | 380 | 3.8 |
| 15 | Water | 1200 | 78 | 400 | 14.3 | 1.0 | 13.7 | 972 | 2.43 |
| 16 | Water | 1100 | 78 | 603 | 12.8 | 13.4 | 15.5 | 1110 | 1.84 |
| 17 | Urine | 900 | 59 | 150 | 8.7 | 5.3 | 10.5 | 495 | 3.3 |
| 18 | Urine | 1100 | 78 | 200 | 10.0 | 5.0 | 10.3 | 640 | 3.2 |
| 19 | Urine | 1300 | 100 | 63 | 2.0 | 1.5 | 3.8 | 351 | 5.4 |
| 20 | Urine | 1300 | 99 | 61 | 2.0 | 6.2 | 8.0 | 263 | 4.3 |
| 21 | Urine | 1300 | 98 | 100 | 7.0 | 3.2 | 7.3 | 330 | 3.3 |
| 22 | Urine | 1300 | 99 | 155 | 4.6 | 6.8 | 9.3 | 496 | 3.2 |
| 23 | Water | 1000 | 35.4 | 109 | 7.5 | 3.9 | 8.2 | 352 | 3.23 |
| 24 | Water | 1300 | 104 | 110 | 7.5 | 3.9 | 6.3 | 402 | 3.66 |
| 25 | Water | 900 | 35 | 200 | 10 | 5.1 | 10 | 492 | 2.46 |
| 26 | Water | 1300 | 98 | 200 | 10 | 4.5 | 10.2 | 528 | 2.64 |
| 27 | Water | 1100 | 78 | 606 | 17.6 | 10.5 | 16.5 | 196 | 1.94 |
| 28 | Water | 1000 | 51 | 101 | 7.3 | 3.5 | 6.8 | 379 | 3.75 |
| 29 | Urine | 1100 | 78 | 150 | 8.8 | 8.0 | 10.5 | 465 | 3.1 |
| 30 | Urine | 1100 | 77 | 150 | 8.8 | 5.7 | 9.2 | 540 | 3.6 |
| 31 | Urine | 1250 | 85 | 164 | 7.6 | 12 | - | 328 | 2.0 |
| 32 | Urine | 1100 | 79 | 165 | 13 | 13.5 | - | 396 | 2.4 |

The influence of the average temperature drop, the temperature difference at the THP inlet and the current strength on the efficiency of the ALTEC heat pump is shown in Fig. 4 and 5, respectively.

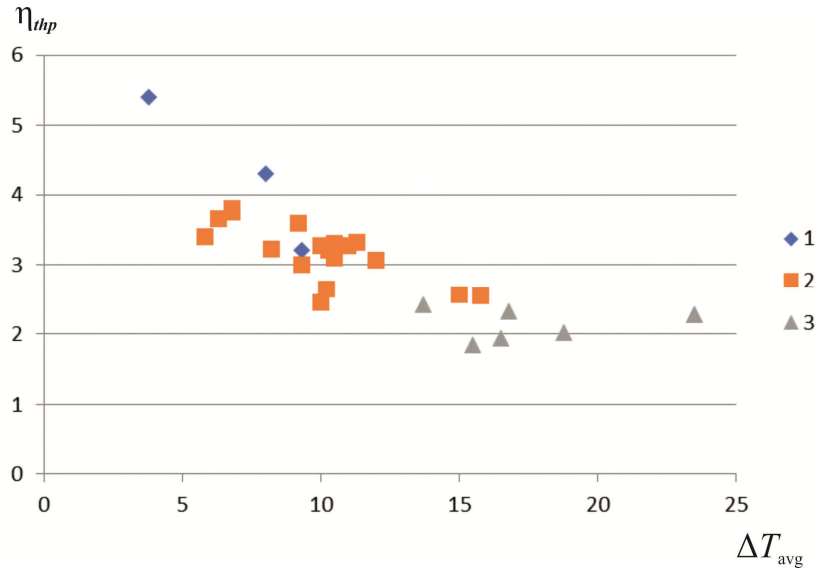


*Fig. 4 Dependence of heat pump efficiency on the average temperature difference; current strength: ◆ 1 – 2…4A; ■ 2– 7…10A; ▲ 3 13…17A;*

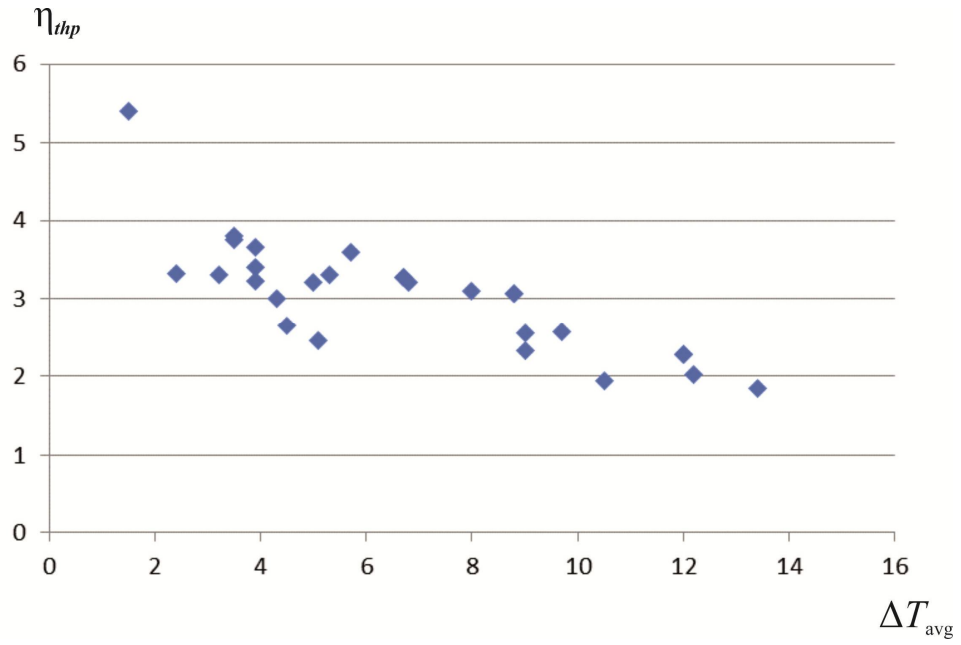


*Fig. 5 Dependence of heat pump efficiency on the temperature difference at the inlet to heat pump.*

## Conclusions

The conducted experimental studies have shown that in the developed system of a centrifugal distiller with a thermoelectric heat pump, it is possible to achieve high performance indicators of the thermopile, the heat pump efficiency $\eta_{thp}$ is in the range of 3…5. This can be achieved due to very intense heat transfer processes in the field of action of centrifugal forces, which makes it possible to maintain a minimum average temperature difference of the working fluids in a thermoelectric heat pump. The obtained data will be used to create a mathematical model of a water distillation system (centrifugal distiller + thermoelectric heat pump) and to design a water regeneration system for a given capacity with a predicted specific power consumption.

*The work was supported by the grant of the Ministry of Education and Science of Ukraine "Development and preparation of innovative distillers for the concentration of thermosensitive solutions", State registration number: 0121U110195.*

## References

1. Sargusingh M. J., Callahan M. R. (2015). Cascade distillation system design for safety and mission assurance. *45th International Conference on Environmental Systems ICES-2015-151* (12-16 July 2015, Bellevue, Washington).
2. Rifert V. G., Usenko V.I., Zolotukhin I.V., MacKnight A. and Lubman A. (2003). Cascaded distillation technology for water processing in space. SAE Paper 2003-01-2625. *34st International Conference on Environmental Systems* (Orlando, July 2003).
3. Lubman A., MacKnight A., Rifert V., Zolotukhin I. and Pickering K. (2006). Wastewater processing cascade distillation subsystem. Design and evaluation. *SAE International* (2006-01-2273, July 2006).
4. Lubman A., MacKnight A., Rifert V., and Barabash P. (2007). Cascade distillation subsystem hardware development for verification testing. *SAE International* (2007-01-3177, July 2007).

5. Callahan M., Patel V., Pickering K.D. (2010). Cascade distillation subsystem development: early results from the exploration life support distillation technology comparison test. *40th International Conference on Environmental Systems* (11 July 2010 - 15 July 2010, Barcelona, Spain).
6. Rifert V., Barabash P., Goliad N. (1990). Methods and processes of thermal distillation of water solutions for closed water supply systems, SAE Paper 901249. *20th Intersociety Conference on Environmental Systems* (Williamsburg, July 1990).
7. Samsonov N., Bobe L., Novikov V., Rifert V., et al. (1994). Systems for water reclamation from humidity condensate and urine for space station, SAE Paper 941536 *The 24th International Society Conference on Environmental Systems* (June, 1994).
8. Samsonov N.M., Bobe L.S, Novikov V., Rifert V.G., Barabash P.A., et al.(1995). Development of urine processor distillation hardware for space stations, SAE Paper 951605 *The 25th International Conference on Environmental Systems* (San Diego, July 1995).
9. Samsonov N.M., Bobe L.S, Novikov V., Rifert V.G., et al. (1997). Updated systems for water recovery from humidity condensate and urine for the International space station, SAE Paper 972559. *The 27th International Conference on Environmental Systems* (Nevada, July 1997).
10. Samsonov N.M., Bobe L.S, Novikov V., Rifert V.G., et al. (1999). Development and testing of a vacuum distillation subsystem for water reclamation from urine, SAE Paper 1999-01-1993. *The 29th International Conference on Environmental Systems* (Denver, July 1999).
11. Rifert V., Usenko V., Zolotukhin I., MacKnight A., Lubman A. (1999). Comparison of secondary water Processors using distillation for space applications, SAE Paper 99-70466. *The 29th International Conference on Environmental Systems* (Denver, July 1999).
12. Rifert V., Stricun A., Usenko V. (2000). Study of dynamic and extreme performances of multistage centrifugal distiller with the thermoelectric heat pump. SAE Technical Papers 2000. *The 30th International Conference on Environmental Systems* (Toulouse, France, 10-13 July 2000).
13. Rifert V., Usenko V., Zolotukhin I., MacKnight A. and Lubman A. (2001). Design optimisation of cascade rotary distiller with the heat pump for water reclamation from urine, SAE Paper 2001-01-2248. *The 31st International Conference on Environmental Systems* (Orlando, July 2001).
14. Rifert V.G., Anatychuk L.I., Barabash P.A., Usenko V.I., Strikun A.P., Prybyla A.V. (2017). Improvement of the distillation methods by using centrifugal forces for water recovery in space flight applications. *J.Thermoelectricity*, 1, 71-83.
15. Rifert V.G., Barabash P.A., Usenko V., Solomakha A.S., Anatychuk L.I., Prybyla A.V. (2017). Improvement the cascade distillation system for long-term space flights. *The 68th International Astronautical Congress (IAC)* (Adelaide, Australia, 25-29 September 2017). IAC-17-A1.IP.25.
16. Rifert Vladimir G., Anatychuk Lukyan I., Solomakha Andrii S., Barabash Petr A., Usenko Vladimir, Prybyla A.V., Naymark Milena, Petrenko Valerii (2019). Upgrade the centrifugal multiple-effect distiller for deep space missions. *The 70th International Astronautical Congress (IAC)* (Washington D.C., United States, 21-25 October 2019). IAC-19-A1, IP, 11x54316.
17. Rifert V.G., Anatychuk L.I., Barabash P.O., Usenko V.I., Strikun A.P., Solomakha A. S, Petrenko V.G., Prybyla A.V. (2019).Evolution of centrifugal distillation system with a thermoelectric heat pump for space missions. Part 3. Analysis of local and integral characteristics of centrifugal distillation system with thermoelectric heat pump. *J. Thermoelectricity*, 3, 5 – 19.
18. Rifert V.G., Anatychuk L.I., Barabash P.O., Usenko V.I., Strikun A.P., Solomakha A. S, Petrenko V.G., Prybyla A.V. (2019). Comparative analysis of thermal distillation methods with heat pumps for long space flights. *J.Thermoelectricity*, 4, 5 – 17.
19. Solomakha A.S., Anatychuk L.I., Rifert V.G., Barabash P.A., Usenko V., Petrenko V. (2020). Thermal distillation system for deep space missions: rationale for the choice. *The 71st International*

*Astronautical Congress (IAC)* (The CyberSpace Edition 12-14 October 2020). IAC-20-A1,VP,15,x61344. 7 pages.
20. Rifert V.G., Barabash P.A., Solomakha A.S., Usenko V., Sereda V.V., Petrenko V.G. (2018). Hydrodynamics and heat transfer in centrifugal film evaporator. *Bulgarian Chemical Communications*, Vol.50, Special Issue K., 49-57.
21. Rifert V.G., Solomakha A.S., Barabash P.A., Usenko V., Sereda V.V. (2020). Justification of the method for calculating heat transfer in film evaporators with a rotating surface. *Bulgarian Chemical Communications*, Vol.52, Special Issue F,95-102. DOI: 10.34049/bcc.52.F.0016
22. Thibaud-Erkey, C., Fort, J., and Edeen, M. (2000). A new membrane for the thermoelectric integrated membrane evaporative subsystem (TIMES). *SAE Technical Paper* 2000-01-2385 1999-01-1990
23. Dehner G.F. TIMES Regenerator Redesign Description Timothy D. Scull Hamilton Standard Space Systems International, Inc. Addendum development of a preprototype times wastewater recovery subsystem. Prepared under contract no. nas 9-15471, 1984.
24. A new membrane for the thermoelectric integrated membrane evaporative subsystem (TIMES) Catherine Thibaud-Erkey and James H. Fort Hamilton Sundstrand Space Systems International Marybeth A. Edeen NASA-Johnson Space Center Water Recovery Technology, *SAE Technical Paper* 820849, 1982. 2000-01-2385

Submitted 31.03.2021

**Ріферт В.Г.,** *док. техн. наук*
**Анатичук Л.І.,** *акад. НАН України*
**Соломаха О.С.,** *канд. техн. наук*
**Барабаш П.О.,** *канд. техн. наук*
**Петренко В.Г.,** *канд. техн. наук*
**Снеговской О.П.**

[1]НТУ «КПІ», вул. Політехнічна, 6, Київ, 03056, Україна; *e–mail: vgrifert@ukr.net*;
[2]Інститут термоелектрики НАН і МОН України, вул. Науки, 1,
Чернівці, 58029, Україна; *e–mail: anatych@gmail.com*
[3]Чернівецький національний університет ім. Юрія Федьковича,
вул. Коцюбинського 2, Чернівці, 58000, Україна

# ВПЛИВ ТЕРМОДИНАМІЧНИХ ХАРАКТЕРИСТИК ТЕРМОЕЛЕКТРИЧНОГО ТЕПЛОВОГО НАСОСА НА ПРОДУКТИВНІСТЬ ТА ВИТРАТИ ЕНЕРГІЇ ВІДЦЕНТРОВОГО ДИСТИЛЯТОРА

*У статті проведено аналіз роботи термоелектричного теплового насоса у комплексі з відцентровим дистилятором для регенерації стічних вод системи життєдіяльності людини в умовах майбутніх космічних місій. Показано залежність питомого споживання енергії системи від часу за різних потужностей теплового насоса, проаналізовано вплив різниці температур теплоносіїв на ефективність роботи теплового насоса. Бібл. 24, рис. 5, табл. 2.*
**Ключові слова:** кабіна: термоелектрика, тепловий насос, дистилятор.

**Риферт В.Г.,** *док. техн. наук* [1]
**Анатычук Л.И.,** *акад. НАН Украины*[2,3]
**Соломаха А. С.,** *канд. техн. наук*[1]
**Барабаш П.О.,** *канд. техн. наук*[1]
**Петренко В. Г.,** *канд. техн. наук*[1]
**Снеговской О. П.**

[1]НТУ «КПИ им. И. Сикорского», ул. Политехническая, 6,
Киев, 03056, Украина, *e–mail: vgrifert@ukr.net;*
[2]Институт термоэлектричества НАН и МОН Украины,
ул. Науки, 1, Черновцы, 58029, Украина,
*e–mail: anatych@gmail.com;*
[3]Черновицкий национальный университет
им. Юрия Федьковича, ул. Коцюбинского, 2,
Черновцы, 58012, Украина

# ВЛИЯНИЕ ТЕРМОДИНАМИЧЕСКИХ ХАРАКТЕРИСТИК ТЕРМОЭЛЕКТРИЧЕСКОГО НАСОСА НА ПРОИЗВОДИТЕЛЬНОСТЬ И РАСХОД ЭНЕРГИИ ЦЕНТРОБЕЖНОГО ДИСТИЛЛЯТОРА

*В статье проведен анализ работы термоэлектрического теплового насоса в комплексе с центробежным дистиллятором для регенерации сточных вод системы жизнедеятельности человека в условиях будущих длительных космических миссий. Показана зависимость удельного потребления энергии системы от времени при разных мощностях теплового насоса, проанализировано влияние разности температур теплоносителей на эффективность работы теплового насоса. Библ. 24, рис. 5, табл. 2.*

**Ключевые слова**: термоэлектрика, тепловой насос, дистиллятор.

## References

1. Sargusingh M. J., Callahan M. R. (2015). Cascade distillation system design for safety and mission assurance. *45th International Conference on Environmental Systems ICES-2015-151* (12-16 July 2015, Bellevue, Washington).
2. Rifert V. G., Usenko V.I., Zolotukhin I.V., MacKnight A. and Lubman A. (2003). Cascaded distillation technology for water processing in space. SAE Paper 2003-01-2625. *34st International Conference on Environmental Systems* (Orlando, July 2003).
3. Lubman A., MacKnight A., Rifert V., Zolotukhin I. and Pickering K. (2006). Wastewater processing cascade distillation subsystem. Design and evaluation. *SAE International* (2006-01-2273, July 2006).
4. Lubman A., MacKnight A., Rifert V., and Barabash P. (2007). Cascade distillation subsystem hardware development for verification testing. *SAE International* (2007-01-3177, July 2007).
5. Callahan M., Patel V., Pickering K.D. (2010). Cascade distillation subsystem development: early results from the exploration life support distillation technology comparison test. *40th International Conference on Environmental Systems* (11 July 2010 - 15 July 2010, Barcelona, Spain).
6. Rifert V., Barabash P., Goliad N. (1990). Methods and processes of thermal distillation of water solutions for closed water supply systems, SAE Paper 901249. *20th Intersociety Conference on*

*Environmental Systems* (Williamsburg, July 1990).

7. Samsonov N., Bobe L., Novikov V., Rifert V., et al. (1994). Systems for water reclamation from humidity condensate and urine for space station, SAE Paper 941536 *The 24th International Society Conference on Environmental Systems* (June, 1994).
8. Samsonov N.M., Bobe L.S, Novikov V., Rifert V.G., Barabash P.A., et al.(1995). Development of urine processor distillation hardware for space stations, SAE Paper 951605 *The 25th International Conference on Environmental Systems* (San Diego, July 1995).
9. Samsonov N.M., Bobe L.S, Novikov V., Rifert V.G., et al. (1997). Updated systems for water recovery from humidity condensate and urine for the International space station, SAE Paper 972559. *The 27th International Conference on Environmental Systems* (Nevada, July 1997).
10. Samsonov N.M., Bobe L.S, Novikov V., Rifert V.G., et al. (1999). Development and testing of a vacuum distillation subsystem for water reclamation from urine, SAE Paper 1999-01-1993. *The 29th International Conference on Environmental Systems* (Denver, July 1999).
11. Rifert V., Usenko V., Zolotukhin I., MacKnight A., Lubman A. (1999). Comparison of secondary water Processors using distillation for space applications, SAE Paper 99-70466. *The 29th International Conference on Environmental Systems* (Denver, July 1999).
12. Rifert V., Stricun A., Usenko V. (2000). Study of dynamic and extreme performances of multistage centrifugal distiller with the thermoelectric heat pump. SAE Technical Papers 2000. *The 30th International Conference on Environmental Systems* (Toulouse, France, 10-13 July 2000).
13. Rifert V., Usenko V., Zolotukhin I., MacKnight A. and Lubman A. (2001). Design optimisation of cascade rotary distiller with the heat pump for water reclamation from urine, SAE Paper 2001-01-2248. *The 31st International Conference on Environmental Systems* (Orlando, July 2001).
14. Rifert V.G., Anatychuk L.I., Barabash P.A., Usenko V.I., Strikun A.P., Prybyla A.V. (2017). Improvement of the distillation methods by using centrifugal forces for water recovery in space flight applications. *J.Thermoelectricity*, 1, 71-83.
15. Rifert V.G., Barabash P.A., Usenko V., Solomakha A.S., Anatychuk L.I., Prybyla A.V. (2017). Improvement the cascade distillation system for long-term space flights. *The 68th International Astronautical Congress (IAC)* (Adelaide, Australia, 25-29 September 2017). IAC-17-A1.IP.25.
16. Rifert Vladimir G., Anatychuk Lukyan I., Solomakha Andrii S., Barabash Petr A., Usenko Vladimir, Prybyla A.V., Naymark Milena, Petrenko Valerii (2019). Upgrade the centrifugal multiple-effect distiller for deep space missions. *The 70th International Astronautical Congress (IAC)* (Washington D.C., United States, 21-25 October 2019). IAC-19-A1, IP, 11x54316.
17. Rifert V.G., Anatychuk L.I., Barabash P.O., Usenko V.I., Strikun A.P., Solomakha A. S, Petrenko V.G., Prybyla A.V. (2019).Evolution of centrifugal distillation system with a thermoelectric heat pump for space missions. Part 3. Analysis of local and integral characteristics of centrifugal distillation system with thermoelectric heat pump. *J. Thermoelectricity*, 3, 5 – 19.
18. Rifert V.G., Anatychuk L.I., Barabash P.O., Usenko V.I., Strikun A.P., Solomakha A. S, Petrenko V.G., Prybyla A.V. (2019). Comparative analysis of thermal distillation methods with heat pumps for long space flights. *J.Thermoelectricity*, 4, 5 – 17.
19. Solomakha A.S., Anatychuk L.I., Rifert V.G., Barabash P.A., Usenko V., Petrenko V. (2020). Thermal distillation system for deep space missions: rationale for the choice. *The 71st International Astronautical Congress (IAC)* (The CyberSpace Edition 12-14 October 2020). IAC-20-A1,VP,15,x61344. 7 pages.
20. Rifert V.G., Barabash P.A., Solomakha A.S., Usenko V., Sereda V.V., Petrenko V.G. (2018). Hydrodynamics and heat transfer in centrifugal film evaporator. *Bulgarian Chemical Communications*, Vol.50, Special Issue K., 49-57.

21. Rifert V.G., Solomakha A.S., Barabash P.A., Usenko V., Sereda V.V. (2020). Justification of the method for calculating heat transfer in film evaporators with a rotating surface. *Bulgarian Chemical Communications*, Vol.52, Special Issue F,95-102. DOI: 10.34049/bcc.52.F.0016
22. Thibaud-Erkey, C., Fort, J., and Edeen, M. (2000). A new membrane for the thermoelectric integrated membrane evaporative subsystem (TIMES). *SAE Technical Paper* 2000-01-2385 1999-01-1990
23. Dehner G.F. TIMES Regenerator Redesign Description Timothy D. Scull Hamilton Standard Space Systems International, Inc. Addendum development of a preprototype times wastewater recovery subsystem. Prepared under contract no. nas 9-15471, 1984.
24. A new membrane for the thermoelectric integrated membrane evaporative subsystem (TIMES) Catherine Thibaud-Erkey and James H. Fort Hamilton Sundstrand Space Systems International Marybeth A. Edeen NASA-Johnson Space Center Water Recovery Technology, *SAE Technical Paper* 820849, 1982. 2000-01-2385

Submitted 31.03.2021

**V.A.Romaka,** *doc. techn sciences, professor*[1],
**Yu.V. Stadnyk,** *cand. chem. of science*[2],
**V. V. Romaka,** *doc. techn sciences,*
*cand. chem. of science, professor*[3]
**Demchenko P.Yu.,** *cand. chem. of science*[2]
**L.P. Romaka,** *cand. chem. of science*[2],
**V.Z. Pashkevych ,** *cand. tehn. of science*[1]
**A.M. Horyn,** *cand. chem. of science*[2],
**A.Ya. Horpeniuk,** *cand. tehn. of science*[1]

[1]National University "Lvivska Politechnika", 12, S. Bandera Str., Lviv, 79013, Ukraine,
*e-mail: vromaka@polynet.lviv.ua;*
[2]Ivan Franko National University of Lviv, 6, Kyryla and Mefodiya Str., Lviv, 79005, Ukraine,
*e-mail: lyubov.romaka@lnu.edu.ua*
[3]Technische Universität Dresden, Bergstrasse 66, 01069 Dresden, Germany

# INVESTIGATION OF PROPERTIES OF NEW THERMOELECTRIC MATERIAL $Lu_{1-x}Sc_xNiSb$

*The crystalline and electronic structures, thermodynamic, kinetic, energy and magnetic properties of the thermoelectric material $Lu_{1-x}Sc_xNiSb$ at temperatures T = 80 – 400 K have been studied. Depending on the concentration of the alloying component in the solid solution $Lu_{1-x}Sc_xNiSb$, different mechanisms of Sc atoms entering the semiconductor matrix have been established, which leads to different rates of generation of structural defects of acceptor and donor nature. The ratio of the concentrations of existing defects of donor and acceptor nature determines the position of the Fermi level $\varepsilon_F$ and the conduction mechanisms in $Lu_{1-x}Sc_xNiSb$. The investigated solid solution $Lu_{1-x}Sc_xNiSb$ is a promising thermoelectric material. Bibl. 18, Fig. 8.*
**Key words**: electronic structure, electric resistivity, Seebeck coefficient.

## Introduction

In [1 – 7], a study of a new class of semiconductor thermoelectric materials based on *RNiSb* compounds (*R – Y, Gd – Lu*), which have a high efficiency of converting thermal energy into electricity [8], was initiated. The study of *RNiSb* compounds showed that they crystallize in the structural type of *MgAgAs* ($F\bar{4}3m$) [9], and their crystal structure is defective: in the crystallographic positions of 4*a* *R* atoms and 4*c* *Ni* atoms there are vacancies. In turn, these vacancies form in the band gap $\varepsilon_g$ of *p-RNiSb* semiconductors structural defects of acceptor nature and the corresponding acceptor levels (zones), which confirm the results of kinetic studies [10].

Thermoelectric materials based on *p-RNiSb* (*R – Er, Lu*) [4 – 6] were obtained by doping semiconductors with *Zr* or *Sc* atoms by substituting rare earth metal atoms in the crystallographic position

4a. This was accompanied by the generation of structural defects of donor or neutral nature, which allowed to optimize the values of the of Seebeck coefficient $\alpha(T,x)$, thermal conductivity $\kappa(T,x)$ and electric conductivity $\sigma(T,x)$ [8]. Thus, doping *p*-(*Er*,*Lu*)*NiSb* with *Zr* atoms ($4d^25s^2$) [4, 5] led to the following changes in crystal and electronic structures:

– substitution at position 4*a* of *Er* or *Lu* atoms for *Zr* atoms generates structural defects of donor nature, because *Zr* has a larger number of *d*-electrons than, for example, the *Lu* atom ($5d^16s^2$). In this case, an impurity donor zone $\varepsilon_D^1$ appears in the band gap $\varepsilon_g$;

– occupation of vacancies in position 4*a* by *Zr* atoms simultaneously eliminates structural defects of acceptor nature and generates defects of donor nature and donor zone $\varepsilon_D^2$.

In the case of doping of *p-ErNiSb* with *Sc* atoms ($3d^14s^2$) in the $Er_{1-x}Sc_xNiSb$ semiconductor, no donor level was formed, because *Er* and *Sc* atoms are located in the same group of the Periodic Table of the Elements [6]. On the other hand, the occupation of vacancies in position 4*a* by *Sc* atoms creates defects of donor nature with the appearance of the donor zone $\varepsilon_D^2$ in the band gap $\varepsilon_g$.

The following results of the study of structural, thermodynamic, kinetic, energy and magnetic properties of semiconductor solid solution $Lu_{1-x}Sc_xNiSb$ will establish the nature of structural and energy defects, which will make the process of optimizing the characteristics of thermoelectric material predictable to maximize thermal energy conversion efficiency.

## Research methods

The crystal structure, the distribution of the density of electronic states (DOS), and the magnetic, thermodynamic, kinetic, and energy properties of $Lu_{1-x}Sc_xNiSb$ have been studied. The samples were synthesized by fusing the charge of the initial components in an electric arc furnace in an inert argon atmosphere, followed by homogenizing annealing for 720 h at a temperature of 1073 K. Diffraction data arrays were obtained using a powder diffractometer STOE STADI P ($Cu\text{K}\alpha_1$-radiation). Crystallographic parameters were calculated using the program Fullprof [11]. The chemical and phase compositions of the samples were monitored by an energy-dispersive *X*-ray analyzer (EPMA) [12]. Calculations of DOS, electron localization function (ELF), enthalpy of mixing ($\Delta H_{\text{mix}}$), and optimization of $Lu_{1-x}Sc_xNiSb$ crystal structure parameters were performed using the Korringa-Kohn-Rostocker (KKR) method in the coherent potential (CPA) and local density approximation (LDA) and the full-potential method of linearized plane waves (FLAPW). KKR simulations were performed using the AkaiKKR software package [13] in the local density approximation for the exchange-correlation potential with parameterization by Moruzzi, Janak, Williams [14] in the semi-relativistic consideration of the core level and spin-orbit interaction. Elk software package was used in FLAPW calculations [15]. Calculations were performed for a 10×10×10 *k*-grid in both the LDA and generalized gradient approximations (GGA). The Brillouin zone was divided into 1000 *k*-points, which were used to calculate the Bloch spectral function (band spectrum) and the density of electronic states. The width of the energy window was chosen so as to capture the semi-core states of the *p*-elements. Visualization of volumetric data was performed using the program VESTA [16]. Topological analysis and interpretation of DOS and ELF was performed within the framework of Bader's theory [10]. The accuracy of calculating the position of the Fermi level was $\varepsilon_F \pm 6$ meV. Temperature and concentration dependences of resistivity ($\rho$) and the Seebeck coefficient ($\alpha$) were measured with respect to copper and magnetic susceptibility ($\chi$) (Faraday's method) of $Lu_{1-x}Sc_xNiSb$ samples, $x = 0 – 1.0$, in the temperature range $T = 80 – 400$ K.

## Investigation of structural characteristics of $Lu_{1-x}Sc_xNiSb$

Microprobe analysis of the concentration of atoms on the surface of the samples established their correspondence to the initial composition of the charge (Fig. 1), and *X*-ray phase and structural analyzes showed that the diffraction patterns of samples $Lu_{1-x}Sc_xNiSb$, $x = 0 - 0.1$, and *ScNiSb* are indexed in the *MgAgAs* [9] structural type and contain no traces of other phases (Fig. 2*a*).

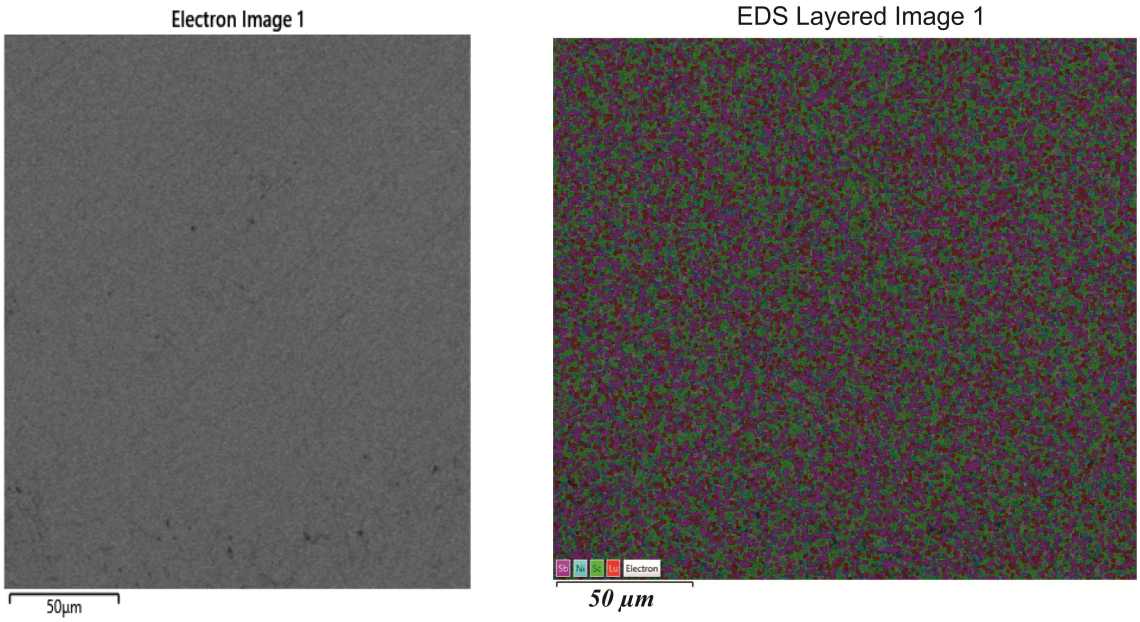


*a)* *b)*

*Fig. 1. Photograph of the surface (a) and distribution of components (b) of the sample $Lu_{0.98}Sc_{0.02}NiSb$*

Given that the atomic radius of *Lu* ($r_{Lu} = 0.173$ nm) is larger than *Sc* ($r_{Sc} = 0.164$ nm), it is assumed that the values of the unit cell period a(*x*) $Lu_{1-x}Sc_xNiSb$ decrease when the *Lu* atoms are replaced by *Sc* atoms (Fig. 4*a*. 2*b*). In this case, structural defects of neutral nature are generated in the $Lu_{1-x}Sc_xNiSb$ semiconductor (*Lu* and *Sc* atoms contain the same number of external *d*-electrons). However, as can be seen from the insert of Fig. 2*b*, the decrease in the values of the period a(*x*) $Lu_{1-x}Sc_xNiSb$ at concentrations *x*=0–0.1 is nonlinear, which may indicate more complex structural changes than the replacement of *Lu* atoms by *Sc*. Such changes can be caused by partial occupation of *Sc* vacancies at positions 4*a* of *Lu* atoms and/or 4*c Ni* atoms. This will lead to the deformation of the unit cell and change its period a(*x*). However, the accuracy of *X*-ray diffraction studies does not directly identify these changes.

Therefore, from the results of *X*-ray structural studies we can assume that the structure of the semiconductor $Lu_{1-x}Sc_xNiSb$ may simultaneously undergo the following changes:

– substitution at position 4*a* of *Lu* atoms by *Sc* atoms generates defects of neutral nature;

– occupation of vacancies in position 4*a* by *Sc* atoms simultaneously eliminates the structural defect of acceptor nature and the corresponding acceptor zone $\varepsilon_A^1$ in the band gap $\varepsilon_g$. At the same time, structural defects of donor nature and the corresponding donor zone $\varepsilon_D^1$ are formed;

– occupation of vacancies by *Sc* atoms in position 4*c* of *Ni* atoms simultaneously eliminates structural defects of acceptor nature and the corresponding acceptor zone $\varepsilon_A^2$, and in the band gap $\varepsilon_g$ a structural defect of donor nature is formed with the appearance of donor zone $\varepsilon_D^2$.

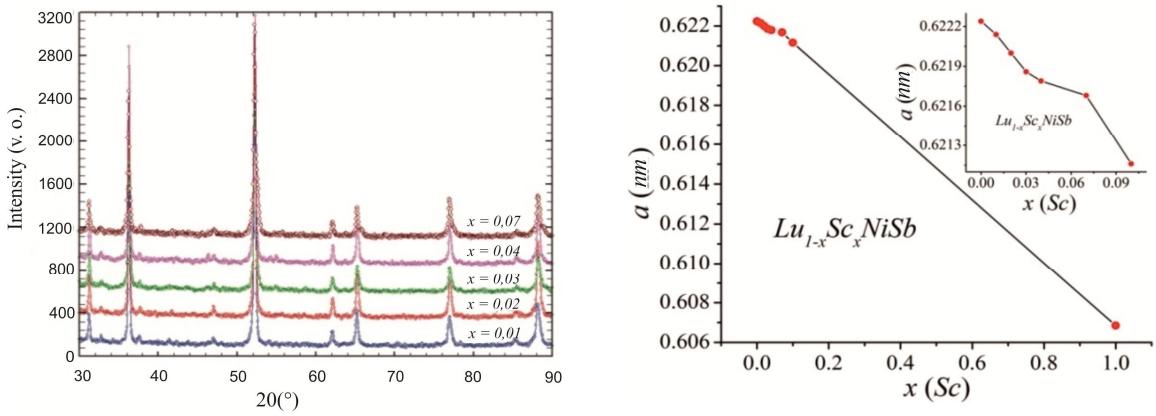


*a)* *b)*

*Fig. 2. Diffractograms of samples (a) and change of the period of the unit cell a (x) (b) $Lu_{1-x}Sc_xNiSb$*

We simulated the change in the values of the period of the unit cell a($x$) $Lu_{1-x}Sc_xNiSb$ for the ordered variant of its crystal structure (all atoms occupy their own crystallographic positions) using software packages AkaiKKR [13] and Elk [15] (Fig. 3*a*).

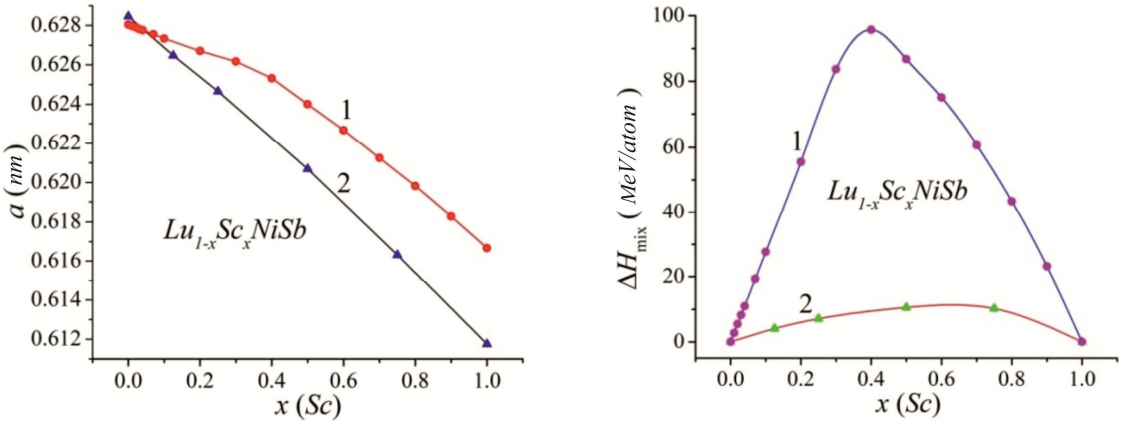


*a)* *b)*

*Fig. 3. Calculation of the change in the period of the unit cell a(x) (a) and the enthalpy of mixing ΔH(x) (b) solid solution $Lu_{1-x}Sc_xNiSb$: 1 – software package AkaiKKR, 2 – software package Elk*

The results of modeling a($x$) $Lu_{1-x}Sc_xNiSb$ are close to the results of *X*-ray diffraction studies (Fig. 2*b*). Using the Elk software package we get a linear decrease of a($x$) $Lu_{1-x}Sc_xNiSb$, whereas modeling with the AkaiKKR software package yields an inflection of $x \approx 0.4$ on the dependence of a($x$).

Modeling of the electronic structure and experimental studies of the properties of $Lu_{1-x}Sc_xNiSb$ will show the degree of adequacy of the assumptions made and will allow us to understand the mechanism of entry of *Sc* atoms into the *p-LuNiSb* matrix.

## Modeling of thermodynamic characteristics and electronic structure of $Lu_{1-x}Sc_xNiSb$

Modeling of thermodynamic characteristics for a hypothetical solid solution $Lu_{1-x}Zr_xNiSb$, $x = 0 – 1.0$, in the approximation of harmonic oscillations of atoms in the framework of density functional theory (DFT) allows us to establish the energy feasibility of the existence of a substitutional solid solution. Fig.3*b* shows the results of modeling by the KKR [13] and FLAPW [15] methods of changing the enthalpy of mixing $\Delta H_{mix}(x)$ $Lu_{1-x}Zr_xNiSb$. The nature of the behavior of the $\Delta H_{mix}(x)$ dependences obtained by both modeling methods shows the energy feasibility of the existence of a substitutional solid solution for the studied $Lu_{1-x}Zr_xNiSb$, $x = 0 – 0.10$. In turn, the dependences $\Delta H_{mix}(x)$ $Lu_{1-x}Zr_xNiSb$ differ slightly. Thus, the dependence $\Delta H_{mix}(x)$, obtained using the Elk software package [15], shows that its growth in the concentration range $x = 0 – 0.4$ is associated with the energy feasibility of forming a substitutional solid solution when *Lu* atoms in crystallographic position 4*a* are replaced of atoms *Sc*. In addition, from Fig. 3*b*, curve 1, it is also seen that the enthalpy dependence of the mixing $\Delta H_{mix}(x)$ $Lu_{1-x}Sc_xNiSb$ passes through the maximum at $x \approx 0.4$, and then decreases monotonically. In turn, the dependence $\Delta H_{mix}(x)$ $Lu_{1-x}Sc_xNiSb$, obtained using the software package AkaiKKR [13], contains a maximum of $x \approx 0.7$.

Important parameters that characterize the results of doping the *LuNiSb* semiconductor with *Sc* atoms to obtain the thermoelectric material $Lu_{1-x}Sc_xNiSb$ are the behavior of the Fermi level $\varepsilon_F$, the band gap $\varepsilon_g$ and the zones of continuous energies. Based on the assumption that the crystal structure of $Lu_{1-x}Sc_xNiSb$ is ordered, using the Elk software package [15], the distribution of the density of electronic states (DOS) was modeled (Fig. 4*a*). It is seen that in *LuNiSb* the Fermi level $\varepsilon_F$ lies in the middle of the band gap $\varepsilon_g$, which is characteristic of intrinsic semiconductors [17], and the band gap $\varepsilon_g = 190.5$ meV.

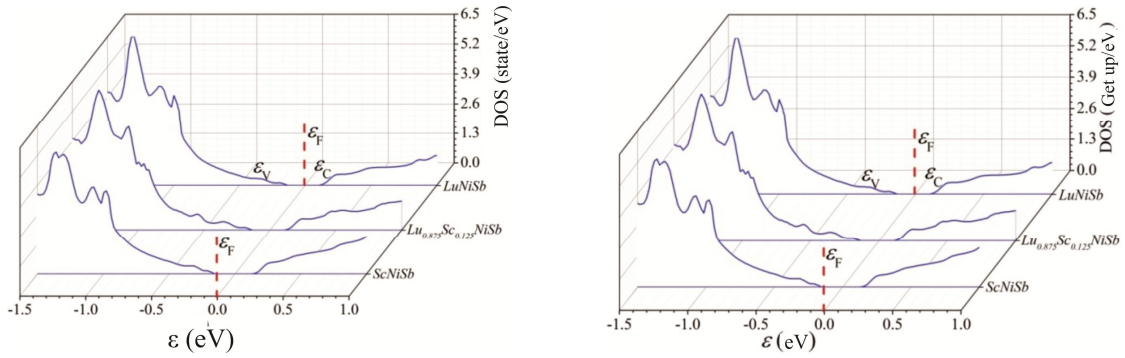


*a)* *b)*

*Fig. 4. Calculation of DOS (Elk software package) for ordered (a) and unordered (AkaiKKR software package) (b) variants in the crystal structure $Lu_{1-x}Sc_xNiSb$*

The results of DOS modeling for the ordered variant of the crystal structure $Lu_{1-x}Sc_xNiSb$, $x = 0.125$, (Elk software package [15]) show the redistribution of DOS (Fig. 4*a*) and the increase in the band gap $\varepsilon_g$. The Fermi level $\varepsilon_F$ lies in the middle of the band gap $\varepsilon_g$, because the atoms *Lu* and *Sc* are located in the same group of the Periodic Table of the Elements, and the generated structural defects are neutral.

DOS simulation for the ordered variant of the *ScNiSb* crystal structure ($Lu_{1-x}Sc_xNiSb$ for $x = 1.0$) gives a band gap $\varepsilon_g = 247.6$ meV, which is greater than that of *LuNiSb*. In this case, the Fermi level $\varepsilon_F$ also lies in the middle of the band gap $\varepsilon_g$. We can predict that *p-ScNiSb* will become the basic semiconductor for thermoelectric materials.

Therefore, DOS simulations for the ordered variant of the *LuNiSb* and *ScNiSb* structure do not correspond to the results of experiment [2, 3, 5, 6], which show that the main carriers are holes (*p*-type

conductivity) and the Fermi level $\varepsilon_F$ lies near the valence band $\varepsilon_V$. Based on these results, a model of the crystal structure of *p-LuNiSb* and *p-ScNiSb* was proposed, the essence of which is the presence of vacancies in positions 4*a* and 4*c* of *Lu* (*Sc*) and *Ni* atoms, respectively.

The DOS calculation for the disordered variant of the $Lu_{1-x}Sc_xNiSb$ crystal structure (Fig. 4*b*) was performed using the model we proposed in the DOS calculations for the *YNiSb* compound [7]. The model of the structure of the semiconductor $Lu_{1-x+y}Sc_xNi_{1-2y}Sb$ is considered, in which at position 4*a* the *Lu* atoms are replaced by *Sc* atoms. In addition, the *Lu* atoms partially move to the 4*c* position of the *Ni* atoms, and a vacancy (Vac) occurs simultaneously in this position. Moreover, how many *Lu* atoms additionally move to the 4*c* position of *Ni* atoms, so many vacancies appear in this position. That is, if the atoms of *Lu* at the number $x$=0.01 move to the position 4*c* of the atoms of *Ni*, then there are additional vacancies with a concentration of $x$=0.01 Therefore, at position 4*c* of *Ni* atoms we have: Ni – $x = 0.98$, Lu – $x = 0.01$, Vac – $x = 0.01$. In this model of the $Lu_{1-x}Sc_xNiSb$ crystal structure, the calculation of the distribution of DOS shows the presence of the band gap $\varepsilon_g$, and the Fermi level $\varepsilon_F$ lies near the valence band $\varepsilon_V$ (Fig. 4*b*). This means that the values of the Seebeck coefficient $\alpha(T,x)$ at all investigated concentrations and temperatures will be positive in the experiment.

It is clear that this model is correct only for a small number of *Sc* impurity atoms, because even partial occupation of the position 4*c* of *Ni* atoms by *Lu* atoms significantly deforms the structure with its subsequent decay. The disadvantage of this model is also the generation of a significant number of energy levels in the band gap $\varepsilon_g$, which intersect with the zones of continuous energies and fix the Fermi level εF. This makes it difficult to determine the real band gap $\varepsilon_g$ and the value of the activation energy $\varepsilon_1^{\rho}(x)$ from the Fermi level $\varepsilon_F$ to the valence band $\varepsilon_V$.

Modeling the electron density distribution and the Elk electron localization function by introducing *Sc* atoms into the *LuNiSb* compound structure by substituting *Lu* atoms in the 4*a* crystallographic position (Fig. 5) gives a clear idea of changes in the crystal and electronic structures of $Lu_{1-x}Sc_xNiSb$ thermoelectric material.

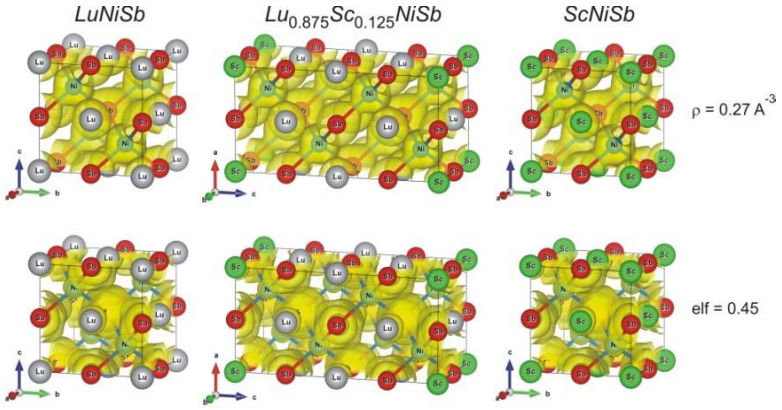


*Fig. 5. Simulation of electronic density of $Lu_{1-x}Sc_xNiSb$, x=0–1.0, (Elk software package)*

The following results of experimental studies of kinetic, energy and magnetic properties will show the degree of adequacy of the proposed disordered model of the crystal structure of $Lu_{1-x}Sc_xNiSb$ to the real structure of the semiconductor.

## Investigation of kinetic, energy and magnetic properties of $Lu_{1-x}Sc_xNiSb$

Temperature and concentration dependences of resistivity ρ and the Seebeck coefficient α of $Lu_{1-}$

$_xSc_xNiSb$ samples are shown in Fig. 6, 7. The dependences ln(ρ(1/*T*)) and α(1/*T*) are typical for doped and compensated semiconductors with high- and low-temperature activation sites, which indicates the presence of several activation mechanisms of conductivity [17]. In addition, high-temperature activation regions on the ln(ρ(1/*T*)) dependences for all studied samples $Lu_{1-x}Sc_xNiSb$ (Fig. 6*a*) show that the Fermi level $\varepsilon_F$ is located in the forbidden band $\varepsilon_g$, and positive values of the Seebeck coefficient α(*T*) (Fig. 6*b*) that specify its position – near the valence band $\varepsilon_V$. Thus, holes are the main carriers of $Lu_{1-x}Sc_xNiSb$ electricity at almost all temperatures studied.

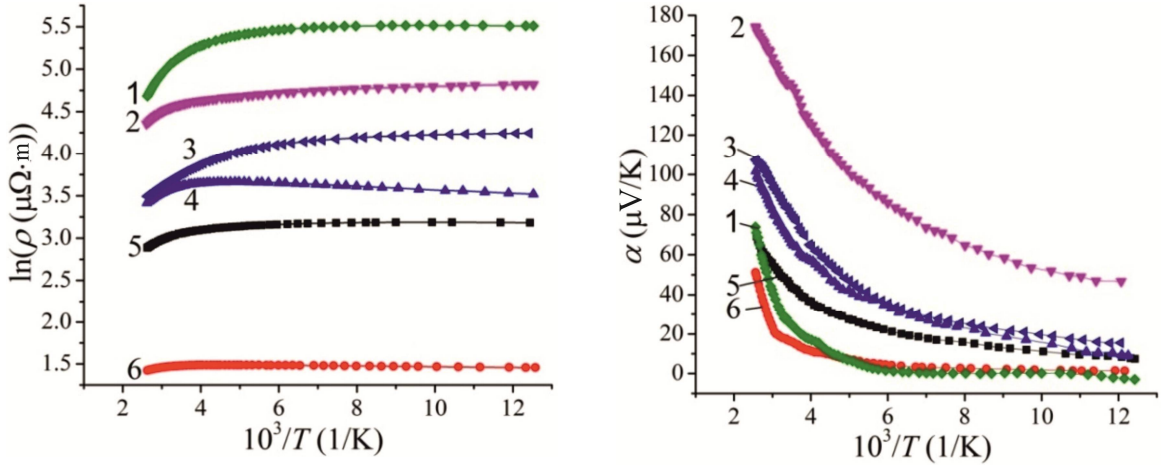


*a)* *b)*

*Fig. 6. Temperature dependences of resistivity ln(ρ(1/T)) (a) and the Seebeck coefficient α(1/T) (b) $Lu_{1-x}Sc_xNiSb$; 1 – x=0.1; 2 – x=0.07; 3 – x=1; 4 – x=0.04; 5 – x=0; 6 – x=0.01*

The change in the values of the resistivity ln(ρ(1/*T*)) $Lu_{1-x}Sc_xNiSb$ is described by the known expression (1):

$$\rho^{-1}(T) = \rho_1^{-1} \exp\left(-\frac{\varepsilon_1^{\rho}}{k_B T}\right) + \rho_3^{-1} \exp\left(-\frac{\varepsilon_3^{\rho}}{k_B T}\right), \quad (1)$$

where the first high-temperature term describes the activation of current carriers $\varepsilon_1^{\rho}(x)$ from the Fermi level $\varepsilon_F$ to the level of continuous energy zones, and the second, low-temperature term, is the jumping conductivity at impurity states $\varepsilon_3^{\rho}(x)$ with energies close to the Fermi level $\varepsilon_F$.

Temperature dependences of the Seebeck coefficient α(1/*T*) $Lu_{1-x}Sc_xNiSb$ (Fig. 6*b*) are described using expression (2) [18]:

$$\alpha = \frac{k_B}{e}\left(\frac{\varepsilon_i^{\alpha}}{k_B T} - \gamma + 1\right), \quad (2)$$

where γ is a parameter that depends on the nature of the scattering mechanism. From high- and low-temperature activation regions of the α(1/*T*) dependence, the values of activation energies $\varepsilon_1^{\alpha}(x)$ and $\varepsilon_3^{\alpha}(x)$, respectively, were calculated, which, as shown in [10], are proportional to the amplitude of large-scale fluctuation of continuous energy zones and small-scale fluctuation of heavily doped and compensated semiconductors [17].

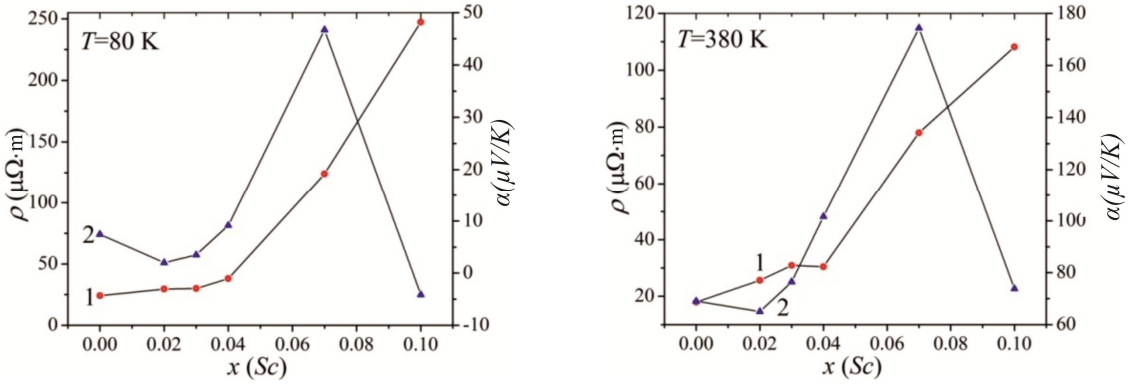


*Fig. 7. Change in the values of resistivity ρ(x,T) (1) and the Seebeck coefficient α(x,T) (2) $Lu_{1-x}Sc_xNiSb$ at different temperatures*

Thus, in the case of *p-LuNiSb*, the Fermi level $\varepsilon_F$ is located at a distance $\varepsilon_1^{\rho} = 10.2$ meV from the valence band $\varepsilon_V$, and the amplitude of modulation of continuous energy bands is $\varepsilon_1^{\alpha} = 35.7$ meV. For the *p-ScNiSb* semiconductor, the Fermi level $\varepsilon_F$ lies at a distance $\varepsilon_1^{\rho} = 30.1$ meV from the valence band $\varepsilon_V$, and the amplitude of modulation of the continuous energy bands is $\varepsilon_1^{\alpha} = 23.1$ meV. High values of activation energy $\varepsilon_1^{\alpha}$ in both *p-LuNiSb* and *p-ScNiSb* semiconductors indicate the presence of a significant number of uncontrolled donors, and the position of the Fermi level $\varepsilon_F$ is determined by the ratio of concentrations of ionized acceptors and donors. And if the nature of the acceptors in *p-LuNiSb* and *p-ScNiSb* is due to the presence of structural defects in the form of vacancies, the origin of the donors lies in the plane of purity of the original components and sampling technology.

Note that only in the semiconductors *p-LuNiSb*, $Lu_{0.93}Sc_{0.07}NiSb$, $Lu_{0.90}Sc_{0.10}NiSb$ and *p-ScNiSb* in the low-temperature regions of the dependences $\ln(\rho(1/T))$ there are activation regions, indicating the mechanism of hopping $\varepsilon_3^{\rho}$ localized states. On the other hand, the presence of $\varepsilon_3^{\rho}$-conductivity in a *p*-type semiconductor with a significant concentration of acceptors (vacant nature of defects in the structure of *p-LuNiSb* and *p-ScNiSb*) indicates the presence of a compensating donor impurity. And if in the form of *p-LuNiSb* and *p-ScNiSb* the presence of donors can be explained by the degree of purity of the components and the peculiarities of its synthesis and homogenizing annealing, then what generates jump $\varepsilon_3^{\rho}$-conductivity at concentrations *Sc*, $x = 0.07$ та $x = 0.10$?

And why for other samples of $Lu_{1-x}Sc_xNiSb$ at low temperatures the values of resistivity increase with increasing temperature (metallic conductivity)?

The answers to these questions lie in the plane of changes in the structure of $Lu_{1-x}Sc_xNiSb$, which will be shown below. Metallization of low-temperature conductivity for individual $Lu_{1-x}Sc_xNiSb$ samples indicates the close location of the Fermi level $\varepsilon_F$ to the valence band flow level, which significantly facilitates the ionization of acceptors and the appearance of a significant number of free holes of the valence band $\varepsilon_V$. It is known that the activation energy of the jumping conductivity $\varepsilon_3^{\rho}$ shows the degree of filling of holes in the *p*-type semiconductor of the conductivity of small-scale fluctuations. As soon as the holes are filled with small-scale fluctuations, the activation of the holes between the potential wells will not be carried out, and there will be no low-temperature activation sites on the resistivity dependences $\ln(\rho(1/T))$. It is obvious that in samples $Lu_{1-x}Sc_xNiSb$, $x = 0.01 – 0.04$, there is a significant number of ionized acceptors at low temperatures, which leads to overlapping of wave functions of impurity states near the Fermi level $\varepsilon_F$ and, as a consequence, to the absence of jumping mechanism $\varepsilon_3^{\rho}$-conductivity. In this case, the impurity acceptor zone intersects with the valence band $\varepsilon_V$, forming a "tail", which is manifested by metallic conductivity at low temperatures. These experimental results are close to those calculated when modeling the distribution of DOS for the disordered variant of the $Lu_{1-x}Sc_xNiSb$ structure (Fig. 4*b*).

Fig. 8*a* shows the change in the values of the activation energy of current carriers $\varepsilon_1^{\rho}$ from the Fermi level $\varepsilon_F$ to the valence band flow level (positive values of the Seebeck coefficient $\alpha(x,T)$ (Figs. 6*b*, 7)). We can see that doping the base semiconductor *p-LuNiSb* with a neutral impurity *Sc* leads to a drift of the Fermi level $\varepsilon_F$ from the flow rate of the valence band towards the middle of the band gap $\varepsilon_g$. Recall that in *p-LuNiSb* the Fermi level was at a distance $\varepsilon_1^{\rho} = 10.2$ meV from the valence band $\varepsilon_V$, and in the case of $Lu_{1-x}Sc_xNiSb$, $x = 0.10$, at a distance $\varepsilon_1^{\rho} = 67.9$ meV. This is possible either in the case of the emergence and increase in the number of donors, or a decrease in the number of acceptors with a constant number of donors.

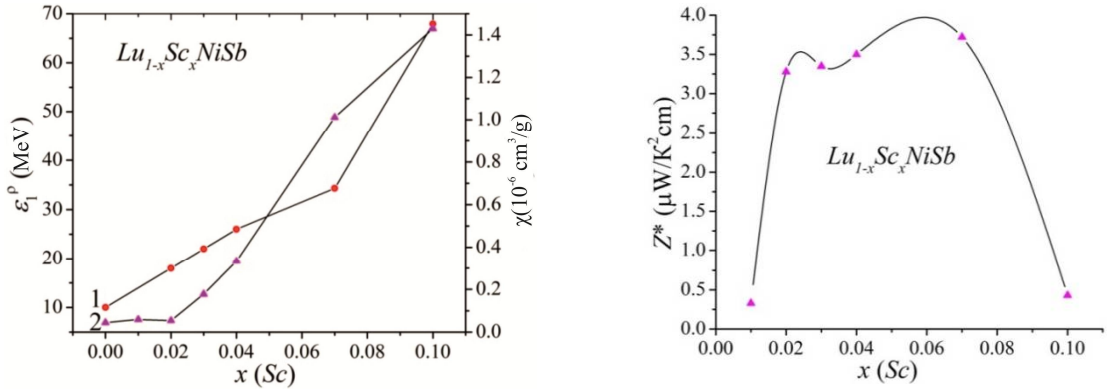


*a* *b*

*Fig. 8. Change in the values of activation energy $\varepsilon_1^{\alpha}(x)$ (1) and specific magnetic susceptibility $\chi(x)$ (2) (a) and thermoelectric power Z* (b) $Lu_{1-x}Sc_xNiSb$*

In the analysis of structural changes, we noted that as a result of the introduction of *Sc* atoms into the structure of the *LuNiSb* compound, it is possible for *Sc* atoms to occupy vacancies in position 4*a*, which simultaneously eliminates the structural defect of acceptor nature and the corresponding acceptor level. This creates a structural defect of donor nature with the appearance in the band gap $\varepsilon_g$ of the corresponding donor band $\varepsilon_D^1$, which supplies free electrons, making the semiconductor $Lu_{1-x}Sc_xNiSb$ strongly doped and compensated. This mechanism of structural changes of $Lu_{1-x}Sc_xNiSb$, which generate the appearance of the donor zone $\varepsilon_D^1$, is the most real in the semiconductor and is consistent with the results of kinetic and energy studies.

The following interesting feature follows from the nature of the behavior of $\varepsilon_1^{\rho}(x)$ $Lu_{1-x}Sc_xNiSb$ (Fig. 8*a*). We can see that at the concentration range $x = 0 - 0.07$ the change of activation energy values $\varepsilon_1^{\rho}(x)$ is almost linear, and the velocity of the Fermi level $\varepsilon_F$ from the valence band $\varepsilon_V$ is constant and is $\Delta\varepsilon_F/\Delta x = 4.9$ meV/%*Sc*. At a concentration of $x \geq 0.07$, the angle of inclination of the dependence $\varepsilon_1^{\rho}(x)$ becomes steeper, which indicates an increase in the velocity of the Fermi level $\varepsilon_F$ from the valence band $\varepsilon_V$ to $\Delta\varepsilon_F/\Delta x = 11.2$ meV/%*Sc*. Different velocities of the Fermi level $\varepsilon_F$ from the valence band $\varepsilon_V$ to the middle of the band gap $\varepsilon_g$ $Lu_{1-x}Sc_xNiSb$ show different velocities of generation of structural defects of acceptor and donor nature. It can be seen that at the concentration $x \geq 0.07$ the number of donors grows ~2 times faster than at the site $x = 0 - 0.07$. And the reason for this is different changes in the crystal structure of $Lu_{1-x}Sc_xNiSb$ depending on the concentration of *Sc* impurity atoms.

The results of changes in the values of resistivity $\rho(x,T)$, the Seebeck coefficient $\alpha(x,T)$ (Fig. 7) and Fermi level $\varepsilon_F$ (Fig. 8*a*, curve 1) are consistent with the results of experimental measurements of magnetic $\chi(x)$ $Lu_{1-x}Sc_xNiSb$, $x = 0 - 0.10$, at room temperature (Fig. 8*a*, curve 2). Studies have shown that the $Lu_{1-x}Sc_xNiSb$ semiconductor is a Pauli paramagnet in which the magnetic susceptibility is determined exclusively by the electron gas and is proportional to the density of states at the Fermi level $\varepsilon_F$. As can be

seen from Fig. 8*a*, curve 2, the dependence $\chi(x)$, as well as $\rho(x,T)$ and $\alpha(x,T)$ (Fig. 7), has a plateau in the area of concentrations $x = 0 – 0.02$, which we associate with insignificant concentration of free electrons generated by the formed donor band $\varepsilon_D$[1]. At higher concentrations *Sc*, the rate of change of the magnetic susceptibility $\chi(x)$ $Lu_{1-x}Sc_xNiSb$, as well as $\rho(x,T)$ and $\alpha(x,T)$, increases, showing an increase in the rate of free electron generation.

Thus, the study of electrokinetic, energy and magnetic properties of $Lu_{1-x}Sc_xNiSb$ showed at different concentrations different rates of generation of structural defects of acceptor and donor nature, which is due to different mechanisms of *Sc* atoms entering the semiconductor matrix. However, this issue requires additional research, including structural, and modeling of the electronic structure of the semiconductor solid solution $Lu_{1-x}Sc_xNiSb$ under different conditions of entry into the structure of *Sc* atoms, and the above results will serve as reference points in the calculations.

Studies of the solid solution $Lu_{1-x}Sc_xNiSb$ showed that it is a promising thermoelectric material at concentrations $x = 0.02 – 0.07$ with high values of the thermoelectric power factor (Fig. 8*b*).

## Conclusions

The complex nature of structural changes has been established as a result of a comprehensive study of crystal and electronic structures, thermodynamic, kinetic, energy and magnetic properties of $Lu_{1-x}Sc_xNiSb$ thermoelectric material obtained by doping *p-LuNiSb* with *Sc* atoms by substituting atoms in 4*a* crystallographic position. It is shown that, depending on the concentration of *Sc* atoms, they can occupy different crystallographic positions in the $Lu_{1-x}Sc_xNiSb$ semiconductor matrix, which leads to different rates of generation of structural defects of acceptor and donor nature. The ratio of the concentrations of existing defects of donor and acceptor nature determines the position of the Fermi level $\varepsilon_F$ and the conduction mechanisms in $Lu_{1-x}Sc_xNiSb$. The investigated solid solution $Lu_{1-x}Sc_xNiSb$ is a promising thermoelectric material.

## References

1. Karla I., Pierre J., Skolozdra R.V. (1998). Physical properties and giant magnetoresistance in *RNiSb* compounds. *J. Alloys Compd*., 265, 42–48.
2. Romaka V.V., Romaka L., Horyn A., Rogl P., Stadnyk Yu., Melnychenko N., Orlovskyy M., Krayovskyy V. (2016). Peculiarities of thermoelectric half-Heusler phase formation in *Gd-Ni-Sb* and *Lu-Ni-Sb* ternary systems. *J. Solid State Chem*., 239, 145–152.
3. Wolańska I., Synoradzki K., Ciesielski K., Załęski K., Skokowski P., Kaczorowski D. (2019). Enhanced thermoelectric power factor of half-Heusler solid solution $Sc_{1-x}Tm_xNiSb$ prepared by high-pressure high-temperature sintering method. *Materials Chemistry and Physics*, 227, 29–35.
4. Romaka V.A, Stadnyk Yu., Romaka L., Krayovskyy V., Horyn A., Klyzub P., Pashkevych V. (2020). Study of structural, electrokinetic and magnetic characteristics of the $Er_{1-x}Zr_xNiSb$ Semiconductor. *J. Phys. Chem. Sol. State*, 21(4), 689-694.
5. Romaka V.A., Stadnyk Yu.V., Romaka L.P., Pashkevych V.Z., Romaka V.V., Horyn A.M., Demchenko P.Yu. (2021). Study of structural, thermodynamic, energy, kinetic and magnetic properties of thermoelectric material $Lu_{1-x}Zr_xNiSb$. *J. Thermoelectricity*, 1, 32–50.
6. Romaka V.A, Stadnyk Yu., Romaka L., Krayovskyy V., Klyzub P., Pashkevych V., Horyn A., Garanyuk P. (2021). Synthesis and Electrical Transport Properties of $Er_{1-x}Sc_xNiSb$ Semiconducting Solid Solution. *J. Phys. Chem. Sol. State*, 22(1), 146-152.
7. Romaka V.V., Romaka L., Horyn A., Stadnyk Yu. (2021). Experimental and theoretical

investigation of the *Y–Ni–Sb* and *Tm–Ni–Sb* systems, *J. Alloys Compd.*, 855, 157334–12.

8. Anatychuk L.I. (1979). *Termoelementy i termoelectricheskiie ustroistva. Spravochnik.* [*Thermoelements and thermoelectric devices*. *Reference book*]. Kyiv: Naukova dumka [in Russian].
9. Romaka V.V., Romaka L.P., Krayovskyy V.Ya., Stadnyk Yu.V. (2015). *Stanidy ridkisnozemelnykh ta perekhidnykh metaliv* [*Stannides of rare earth and transition metals*] Lviv: Lvivska Polytechnika [in Ukrainian].
10. Romaka V.A., Stadnyk Yu.V., Krayovskyy V.Ya., Romaka L.P., Guk O.P., Romaka V.V., Mykyuchuk M.M., Horyn A.M. (2020). *Novitni termochutlyvi materialy ta peretvoriuvachi temperatury* [*New thermosensitive materials and temperature converters*]. Lviv, Lvivska Polytechnika [in Ukrainian].
11. Roisnel T., Rodriguez-Carvajal J. (2001). WinPLOTR: a windows tool for powder diffraction patterns analysis. *Mater. Sci. Forum*, Proc. EPDIC7 378–381, 118–123.
12. Babak V.P., Shchepetov V.V. (2018). Wear resistance of amorphous-crystalline coatings with lubricants. *J. Friction and Wear*, 39(1), 38–43.
13. Akai H. (1989). Fast Korringa-Kohn-Rostoker coherent potential approximation and its application to FCC *Ni-Fe* systems. *J. Phys.: Condens. Matter*., 1, 8045–8063.
14. Moruzzi V.L., Janak J.F., Williams A.R. (1978). *Calculated electronic properties of metals.* NY: Pergamon Press.
15. Savrasov S.Y. (1996). Linear-response theory and lattice dynamics: A muffin-tin-orbital approach. *Phys. Rev. B*, 54(23), 16470–16486.
16. Momma K., Izumi F. (2008). VESTA: a three-dimensional visualization system for electronic and structural analysis. *J. Appl. Crystallogr*., 41, 653–658.
17. Shklovskii B.I. and Efros A.L. (1984). *Electronic properties of doped semiconductors* NY: Springer; (1979) Moscow: Nauka.
18. Mott N.F., Davis E.A. (1979). *Electron processes in non-crystalline materials.* Oxford: Clarendon Press.

Submitted 06.04.2021

**Ромака В.А.,** *док. тех. наук*, *професор*[1]
**Стадник Ю.В.,** *канд. хім. наук*[2]
**Ромака В.В.,** *док. тех. наук*,
*канд. хім. наук*, *професор*[3]
**Демченко П.Ю.,** *канд. хім. наук*[2]
**Ромака Л.П.,** *канд. хім. наук*[2]
**Пашкевич В. З.,** *канд. техн. наук*[1]
**Горинь А.М.,** *канд. хім. наук*[2]
**Гопернюк А. Я.,** *канд. техн. наук*[1]

[1]Національний університет "Львівська політехніка",
вул. С. Бандери, 12, Львів, 79013, Україна;
[2]Львівський національний університет ім. І. Франка,
вул. Кирила і Мефодія, 6, Львів, 79005, Україна;
[3]Technische Universität Dresden, Bergstrasse 66,
01069 Dresden, Germany

# ДОСЛІДЖЕННЯ ВЛАСТИВОСТЕЙ НОВОГО ТЕРМОЕЛЕКТРИЧНОГО МАТЕРІАЛУ $Lu_{1-x}Sc_xNiSb$

*Досліджено кристалічну та електронну структури, термодинамічні, кінетичні, енергетичні та магнітні властивості термоелектричного матеріалу $Lu_{1-x}Sc_xNiSb$ за температур T=80–400 K. У залежності від концентрації легуючого компоненту у твердому розчині $Lu_{1-x}Sc_xNiSb$ встановлено різні механізмами входження атомів Sc у матрицю напівпровідника, що приводить до різних швидкостей генерування структурних дефектів акцепторної та донорної природи. Співвідношення концентрацій наявних дефектів донорної та акцепторної природи визначає у $Lu_{1-x}Sc_xNiSb$ положення рівня Фермі $\varepsilon_F$ та механізми провідності. Досліджений твердий розчин $Lu_{1-x}Sc_xNiSb$ є перспективним термоелектричним матеріалом.*
**Ключові слова**: електронна структура, електроопір, коефіцієнт термо-ерс. *Бібл. 18, рис. 8.*

**Ромака В.А.,** *док. тех. наук*, *профессор*[1]
**Стаднык Ю.В.,** *канд. хим. наук*[2]
**Ромака В.В.,** *док. тех. наук*,
*канд. хим. наук*, *профессор*[3]
**Демченко П.Ю.,** *канд. хим. наук*[2]
**Ромака Л.П.,** *канд. хим. наук*[2]
**Пашкевич В. З.,** *канд. техн. наук*[1]
**Горынь А.М.,** *канд. хим. наук*[2]
**Гопернюк А. Я.,** *канд. техн. наук*[1]

[1]Национальный университет "Львовская политехника",
ул. С. Бандеры, 12, Львов, 79013, Украина,
*e-mail: vromaka@polynet.lviv.ua*;
[2]Львовский национальный университет имени Ивана Франко,
ул. Кирилла и Мефодия, 6, Львов, 79005, Украина,
*e-mail: lyubov.romaka@lnu.edu.ua*
[3]Technische Universität Dresden, Bergstrasse 66, 01069
Dresden, Германия

# ИССЛЕДОВАНИЕ СВОЙСТВ НОВОГО ТЕРМОЭЛЕКТРИЧЕСКОГО МАТЕРИАЛА $Lu_{1-x}Sc_xNiSb$

*Исследованы кристаллическая и электронная структуры, термодинамические, кинетические, энергетические и магнитные свойства термоэлектрического материала. $Lu_{1-x}Sc_xNiSb$при температуре T = 80-400 K. В зависимости от концентрации легирующего компонента в твердом растворе $Lu_{1-x}Sc_xNiSb$ установлены различные механизмы вхождения атомов Sc в матрицу полупроводника, что приводит к разным скоростям генерирования структурных дефектов акцепторной и донорной природы. Соотношение концентраций имеющихся дефектов донорной и акцепторной природы определяет положение уровня Ферми $\varepsilon_F$ и механизмы проводимости $Lu_{1-x}Sc_xNiSb$. Исследованный твердый раствор $Lu_{1-x}Sc_xNiSb$ является перспективным термоэлектрическим материалом. Библ. 18, рис. 8.*
**Ключевые слова**: электронная структура, электросопротивление, коэффициент термоЭДС.

## References

1. Karla I., Pierre J., Skolozdra R.V. (1998). Physical properties and giant magnetoresistance in *RNiSb* compounds. *J. Alloys Compd.*, 265, 42–48.
2. Romaka V.V., Romaka L., Horyn A., Rogl P., Stadnyk Yu., Melnychenko N., Orlovskyy M., Krayovskyy V. (2016). Peculiarities of thermoelectric half-Heusler phase formation in *Gd-Ni-Sb* and *Lu-Ni-Sb* ternary systems. *J. Solid State Chem.*, 239, 145–152.
3. Wolańska I., Synoradzki K., Ciesielski K., Załęski K., Skokowski P., Kaczorowski D. (2019). Enhanced thermoelectric power factor of half-Heusler solid solution $Sc_{1-x}Tm_xNiSb$ prepared by high-pressure high-temperature sintering method. *Materials Chemistry and Physics*, 227, 29–35.
4. Romaka V.A, Stadnyk Yu., Romaka L., Krayovskyy V., Horyn A., Klyzub P., Pashkevych V. (2020). Study of structural, electrokinetic and magnetic characteristics of the $Er_{1-x}Zr_xNiSb$ Semiconductor. *J. Phys. Chem. Sol. State*, 21(4), 689-694.
5. Romaka V.A., Stadnyk Yu.V., Romaka L.P., Pashkevych V.Z., Romaka V.V., Horyn A.M., Demchenko P.Yu. (2021). Study of structural, thermodynamic, energy, kinetic and magnetic properties of thermoelectric material $Lu_{1-x}Zr_xNiSb$. *J. Thermoelectricity*, 1, 32–50.
6. Romaka V.A, Stadnyk Yu., Romaka L., Krayovskyy V., Klyzub P., Pashkevych V., Horyn A., Garanyuk P. (2021). Synthesis and Electrical Transport Properties of $Er_{1-x}Sc_xNiSb$ Semiconducting Solid Solution. *J. Phys. Chem. Sol. State*, 22(1), 146-152.
7. Romaka V.V., Romaka L., Horyn A., Stadnyk Yu. (2021). Experimental and theoretical investigation of the *Y–Ni–Sb* and *Tm–Ni–Sb* systems, *J. Alloys Compd.*, 855, 157334–12.
8. Anatychuk L.I. (1979). *Termoelementy i termoelectricheskiie ustroistva. Spravochnik.* [*Thermoelements and thermoelectric devices*. *Reference book*]. Kyiv: Naukova dumka [in Russian].
9. Romaka V.V., Romaka L.P., Krayovskyy V.Ya., Stadnyk Yu.V. (2015). *Stanidy ridkisnozemelnykh ta perekhidnykh metaliv* [*Stannides of rare earth and transition metals*] Lviv: Lvivska Polytechnika [in Ukrainian].
10. Romaka V.A., Stadnyk Yu.V., Krayovskyy V.Ya., Romaka L.P., Guk O.P., Romaka V.V., Mykyuchuk M.M., Horyn A.M. (2020). *Novitni termochutlyvi materialy ta peretvoriuvachi temperatury* [*New thermosensitive materials and temperature converters*]. Lviv, Lvivska Polytechnika [in Ukrainian].
11. Roisnel T., Rodriguez-Carvajal J. (2001). WinPLOTR: a windows tool for powder diffraction patterns analysis. *Mater. Sci. Forum*, Proc. EPDIC7 378–381, 118–123.
12. Babak V.P., Shchepetov V.V. (2018). Wear resistance of amorphous-crystalline coatings with lubricants. *J. Friction and Wear*, 39(1), 38–43.
13. Akai H. (1989). Fast Korringa-Kohn-Rostoker coherent potential approximation and its application to FCC *Ni-Fe* systems. *J. Phys.: Condens. Matter.*, 1, 8045–8063.
14. Moruzzi V.L., Janak J.F., Williams A.R. (1978). *Calculated electronic properties of metals.* NY: Pergamon Press.
15. Savrasov S.Y. (1996). Linear-response theory and lattice dynamics: A muffin-tin-orbital approach. *Phys. Rev. B*, 54(23), 16470–16486.
16. Momma K., Izumi F. (2008). VESTA: a three-dimensional visualization system for electronic and structural analysis. *J. Appl. Crystallogr.*, 41, 653–658.
17. Shklovskii B.I. and Efros A.L. (1984). *Electronic properties of doped semiconductors* NY: Springer; (1979) Moscow: Nauka.
18. Mott N.F., Davis E.A. (1979). *Electron processes in non-crystalline materials.* Oxford: Clarendon Press.

Submitted 06.04.2021

**Manyk Orest M.,** *Dr. of Phys. and Math. Sciences, docent*[1]
**Manyk Tetiana O.,** *Dr. of Phys. and Math. Sciences*[2]
**Bilynskyi-Slotylo Volodymyr R.,** *Dr. of Phys. and Math. Sciences*[1]

[1]Yuriy Fedkovych Chernivtsi National University
2 Kotsiubynskyi str., Chernivtsi, 58012, Ukraine,
*e-mail: o.manyk@chnu.edu.ua*
[2]Yaroslav Dombrowski Military University of Technology,
2 gen. Sylwester Kaliski str., Warsaw 46, 00-908, Poland,
*e-mail: tetjana.manyk@wat.edu.pl*

# THEORETICAL MODELS OF ORDERED ALLOYS OF THERMOELECTRIC MATERIAL TERNARY SYSTEMS. 1. CHEMICAL BOND AND STATE DIAGRAMS OF *In-Cd-Sb*

*Using the developed comprehensive approach for building theoretical models of ordered alloys of ternary systems of thermoelectric materials, a diagram of the distribution of phase regions for equilibrium in the solid state and isothermal sections based on intermediate binary compounds In-Sb, Cd-Sb, In-Cd are constructed. Calculations of effective charges, effective radii, electron density redistribution, and dissociation energy of nonequivalent hybrid orbitals (NHOs) in the In-Cd-Sb system depending on interatomic distances are presented. The results of theoretical calculations can be used in the development of technology for new thermoelectric materials based on ternary In-Cd-Sb systems. Bibl. 13, Fig. 4, Tabl. 3.*

**Key words:** state diagrams, phase transitions, chemical bond, nonequivalent hybrid orbitals, dissociation energy.

## Introduction

The search for new promising thermoelectric materials is increasingly reduced to the need to study multicomponent systems. Several main features of such systems should be noted. First and foremost, it is the formation of solid phases of variable composition within which there is a continuous transition in chemical composition and a gradual transition from densely packed crystal lattices to layered structures with corresponding changes in physical properties.

The nature of the chemical bond in such compounds varies from metallic to ionic non-polar in layered sublattices. In turn, a change in the chemical bond of the aforementioned compounds is reflected in a change in the structure of the short-range order of the interatomic interaction, which, in turn, is associated with the peculiarities of the phase diagrams and phase transformations, both in the solid state and in melts.

However, it should be noted that there is no consistent theory of phase transformations from the standpoint of chemical bonding. In this regard, the task was to obtain theoretical schemes of state diagrams of ternary systems (for example, *In-Cd-Sb*) using state diagrams of double alloys and to calculate the necessary parameters using molecular models of microscopic theory. This approach allows us to generalize the experimentally obtained results for binary and intermediate quasi-binary state diagrams [1-4] in the case of ternary systems. In turn, this would make it possible to additionally use the capabilities of these state diagrams: information on the nature of the phases and phase composition of a substance depending on

temperature, pressure and concentration, volume, strength of electric and magnetic fields in the development of technologies for obtaining thermoelectric materials based on ternary compounds. The availability of such information makes it possible to approach the solution of the problem of a theoretical description of the processes of melting and crystallization of such systems.

## State diagrams

To solve this problem, it is necessary to generalize the results of experimental studies of binary state diagrams [3-7], physicochemical properties and theoretical studies of quantum regularities of the initial components [8, 9] when constructing state diagrams of ternary compounds. The developed theoretical approaches were tested on *In-Cd-Sb* ternary compounds. The choice was not accidental, because these compounds analyzed the effect of low-temperature element *In* on the formation of stable and metastable phases in ternary systems. The action of In was carried out by constructing intermediate quasi-binary isothermal sections *In-Cd-Sb* (*In-Cd, In-Sb, Cd-Sb*) and solving the inverse problem. Its essence is that when the analysis of a complex multicomponent system with intermediate compounds is impossible, the study of such systems should be carried out by dividing them into simpler, according to established rules and patterns [10]. The elements *In, Cd, Sb* and state diagrams of binary compounds *In-Cd, In-Sb, Cd-Sb* were selected as initial data. A triple state diagram of *In-Cd-Sb* should be constructed on the basis of the analyzed theoretical and experimental rules and regularities.

The presented work begins with the assumption that intermediate ternary compounds with the desired properties based on the elements *In, Cd, and Sb* exist and it is necessary to find the conditions for their production. Fig. 1 shows a diagram of the distribution of phase regions for equilibrium in the solid state of *Cd-In-Sb*. Fig. 2-4 show isothermal cross sections at temperatures: $t_2 = 200$ °C, $t_3 = 300$ °C, $t_4 = 400$ °C.

In Figs. 1-4 the following designations are introduced:

δ – solid phase based on intermediate ternary compound *In-Cd-Sb*;
α – solid solution based on *Cd*;
β – solid solution based on *In;*
γ – solid solution based on *Sb*;
*L* – liquid (liquid phase);
ε – solid solution based on intermediate binary compounds *Cd-In*;
ρ – solid solution based on *In-Sb*;
σ – solid solution based on *Cd-Sb.*

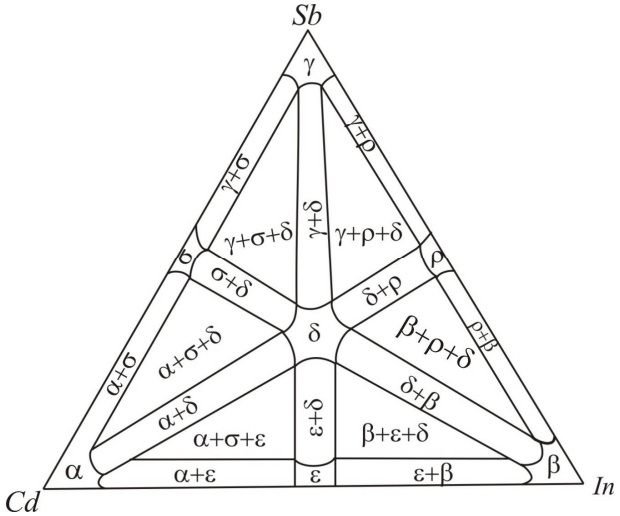


*Fig. 1. Distribution diagram of phase regions for equilibrium in the solid state of Cd-In-Sb*

According to Fig. 1, each quasi-double cross-section based on the ternary compound corresponds to a closed set of points and lines of compatible crystallizations of the two phases. These quasi-double cross-

sections divide the total three-component *In-Cd-Sb* system into six secondary ternary systems. It should be noted that in the presence of additional experimental data on intermediate quasi-double sections in the ternary system, the number of secondary ternary systems may be greater.

Fig. 2 shows the isothermal section at a temperature $t$ = 200 °C, which is lower than the melting point of *Cd* and *Sb*, but higher than the melting point of In. From Fig. 2, it can be concluded that a significant part of the section is occupied by liquid *L*. Present in Fig. 2 is a condom triangle with equilibrium phases $L + \alpha + \varepsilon$; $L + \beta + \varepsilon$. Two-phase equilibrium is realized by primary precipitates of $\sigma + \gamma$ crystals; $\rho + \gamma$, as well as ε – crystals (based on the *In-Cd* compound) and liquid.

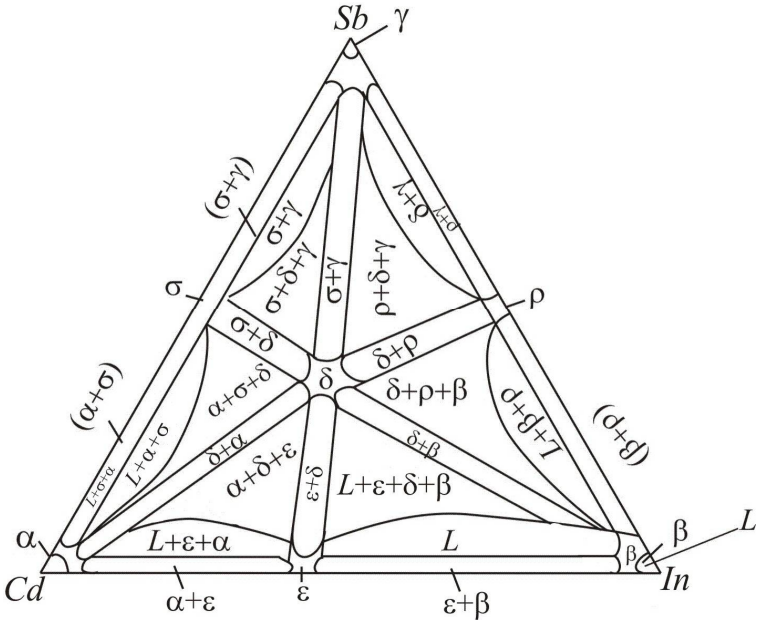


*Fig. 2. Isothermal section of Cd-In-Sb at t= 200°C*

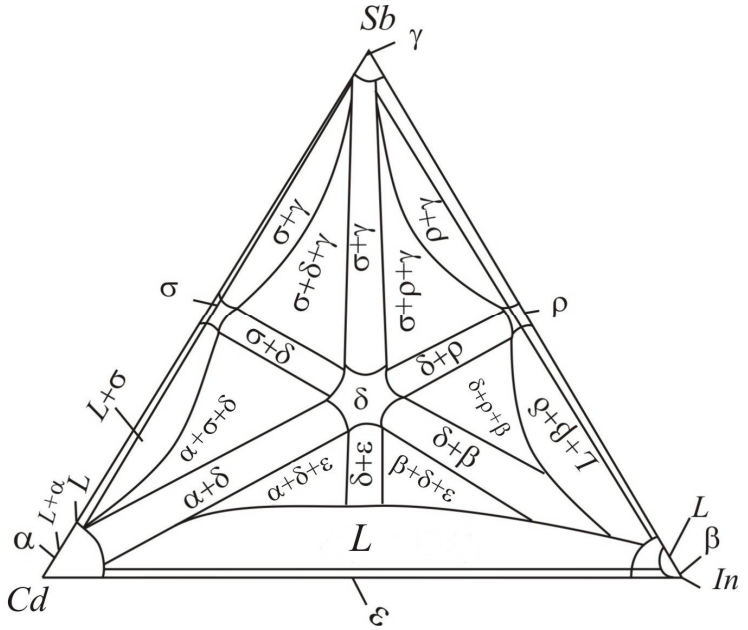


*Fig. 3.Isothermal section of Cd-In-Sb at t= 300°C*

Fig. 3 shows an isothermal section at $t$ = 300 °C, which is below the melting point of *Sb*, close to the

melting point of *Cd* and above the melting point of *In*. There are conode triangles with equilibrium phases $L + \alpha + \varepsilon$; $L + \beta + \varepsilon$; $\sigma + \delta + \gamma$; $\rho + \delta + \gamma$. The primary precipitates of *Cd* and *In* crystals and the intermediate binary compound *Cd-In* are in equilibrium with the liquid.

The third isothermal section corresponds to $t$ = 400 °C (see Fig. 4), which is higher than the melting point of *Cd* and *In* and below the melting point of *Sb*. Three-phase equilibria are represented by conode triangles $\alpha + \sigma + \delta$; $\gamma + \sigma + \delta$; $\gamma + \rho + \delta$; $\beta + \rho + \delta$, two-phase equilibria – by linear surfaces $\alpha + \sigma$; $\sigma + \gamma$; $\rho + \gamma$; $\rho + \beta$; $\delta + \rho$; $\delta + \gamma$; $\delta + \sigma$.

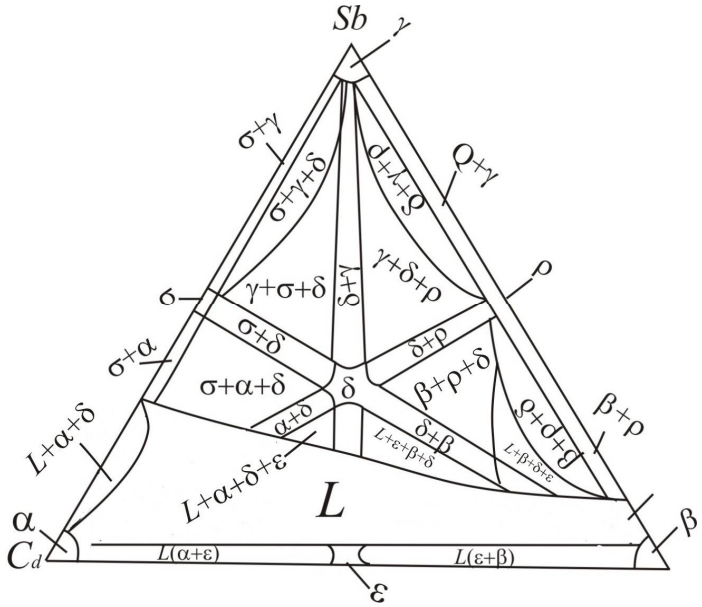


*Fig. 4.Isothermal section of Cd-In-Sb at t= 400 °C*

Thus, these isothermal sections make it possible to:

1. determine the quantitative ratios of coexisting phases and their concentrations;
2. establish the limits of phase equilibrium in the liquid-crystal regions (melting diagram), as well as the equilibrium of the phases associated with polymorphic transformations in the solid state;
3. distinguish state diagrams corresponding to a continuous series of solid solutions with points of equal concentrations where liquidus and solidus touch (the composition of both phases at these points is the same);
4. separate the boundaries of eutectic-type state diagrams, when the components are mixed in all ratios in the liquid state, from diagrams with limited solubility in the solid phase of the peritectic type;
5. predict cases of incongruent melting, when the chemical compound during melting decomposes into solid and liquid phases, the composition of which differs from the composition of the original compound.

However, isothermal sections do not indicate the temperature points of the phase transitions. In such cases, for multicomponent systems, methods are used that combine analytical and topological approaches with calculations of the energy of interaction of components in both phases, which increases the role of theoretical calculations in constructing state diagrams of ternary systems.

It should also be borne in mind that the theoretical analysis of numerous empirical dependencies is associated with a revision of views on the problem of interatomic interaction, as well as with the emergence of qualitatively new concepts, which are not always the result of the development of existing theories, but generally deny some of them.

## Theoretical models of ordered alloys and chemical bond

The simplest relations reflecting the quantum regularities of the structure and interatomic interaction of binary compounds were given in [8, 9]. They were obtained by postulating the linear dependence of the number of electrons on the outer shell of the atom on the logarithm of its Fermi radius $R_u$. The relationship between the tangent of the angle of inclination $tg\alpha = \frac{\Delta \lg R_u}{\Delta n}$ and the electronegativities does not allow changing compared values arbitrarily.

A good agreement of the experimental data gives the following dependence:

$$\lg R_u^x = \lg R_{uA}^{(o)} - xtg\alpha_A, \tag{1}$$

where $R_{uA}^{(o)}$ is the radius of the atom in the unexcited state and $x$ is valence.

Since equation (1) describes the change in $R_u$ of A i B atoms with a change in the number of electrons in the orbits of each, then, assuming the equality of the absolute values of the charges of interacting atoms, dependence (1) takes the form of a system of equations:

$$\lg R_{uA}^{+x} = \lg R_{uA}^{(o)} - xtg\alpha_A, \tag{2}$$

$$\lg R_{uB}^{-x} = \lg R_{uB}^{(o)} + xtg\alpha_B, \tag{3}$$

$$d_1 = R_{uA}^{+x} + R_{uB}^{-x}, \tag{4}$$

$d$ is the sum of ionic radii equal to the interatomic distance.

The system of equations (2) - (4) considers the geometric conditions of contact of spherical electron densities with different levels of density at the boundary. Therefore, additional criteria are needed to translate system (2) - (4) into the formalism of quantum chemistry, taking into account the fine structure of the chemical bond. For this, it is necessary to analyze the dependence of interatomic distances on effective charges. The analysis results showed that at an arbitrary point, apart from $d_1 = d_{min}$, the charge density at the ion boundary is different. The formation of the AB bond is accompanied by the transition of electrons to other directions of interatomic interaction, that is, the bond becomes donor. In this case, the escape of electrons ($+\Delta q$) or their localization ($-\Delta q$) in the given direction of the bond equally changes the values of the charges that this pair has at $d_1 = d_{min}$. With this approach, the system of equations (2) - (4) turns into a system that allows the theoretical part to be matched with the experimental one and was solved with a known $d_1$. Thus, as a result of taking into account the quantum interpretation of the empirical material, the expression for the energy of chemical bonds takes the form:

$$D_{A-B}^{(i)} = \frac{c_1\left(R_{uA}^{o} + R_{uB}^{o}\right)}{\left(tg\alpha_A + tg\alpha_B\right)}\left(\frac{c_2 d_i}{d_1^2 - R_{uA}R_{uB}} - \frac{1}{d_i}\right), \tag{5}$$

where $R_{uA(B)}^{o}$ and $tg\alpha_{A(B)}$ are coefficients of equations (2) - (4) for atoms $A$ and $B$, and $R_{uA}$ and $R_{uB}$ are effective radii of their ions, in $A$-$B$ bonds of length $d_i$; $i$ is the number of nonequivalent interatomic distances in compound; $c_1$ and $c_2$ are constants, $c_1$ is coefficient reflecting the relationship between the dimensional and energy characteristics of the interatomic interaction (in the case of using non-systemic units, when the distance is measured in angstroms, $c_1$ is measured in electron volts) and $c_2$ is a coefficient depending

on the type of crystal structure and chemical bond and is chosen dimensionless.

The equations presented were used to calculate the effective charges, effective radii, and dissociation energies of nonequivalent chemical bonds described by nonequivalent hybrid orbitals in melts of cadmium and indium antimonides. The peculiarity of the chemical bond in crystals is that each *Cd* atom in its immediate environment has three *Sb* atoms and one *Cd*, and each *Sb* atom has three nearest *Cd* atoms and one *Sb* atom. Altogether five NHO families, differing both in the interatomic distances and the composition of components ($\varphi_1$, $\varphi_2$, $\varphi_3$ correspond to *Cd-Sb* bonds of different length, as well as $\varphi_4$ (*Sb-Sb*) i $\varphi_5$ (*Cd-Cd*). The structure of In-Sb was similarly evaluated. The results of calculations of the coefficients of equations (2) - (4) of the initial components are given in Table. 1. Effective charges, effective radii and dissociation energies of NGOs in *CdSb* and *InSb* crystals are given in Tables 2 and 3. In this case, the values of the coefficients $c_1$ and $c_2$ in the first approximation are chosen equal to one.

*Table 1*

*Coefficients of equations (2) - (4) of the initial components*

| Z | Element | $R_u^o(\text{Å})$ | tgα |
|---|---|---|---|
| 48 | *Cd* | 1.51 | 0.097 |
| 49 | *In* | 1.66 | 0.106 |
| 51 | *Sb* | 1.45 | 0.074 |

*Table 2*

*Effective charges, effective radii and dissociation energies of CdSb NHOs*

| Parameters | *Cd-Sb* | | | *Sb-Sb* | *Cd-Cd* |
|---|---|---|---|---|---|
| | $\varphi_1$ | $\varphi_2$ | $\varphi_3$ | $\varphi_4$ | $\varphi_5$ |
| $d_j^{\text{екси}}(\text{Å})$ | 2.8400 | 2.9100 | 2.8100 | 2.8100 | 2.9900 |
| $d_j^{\text{теор}}(\text{Å})$ | 2.8390 | 2.9102 | 2.8102 | 2.810 | 2.9846 |
| $R_u^{Cd}(\text{Å})$ | 1.4406 | 1.4813 | 1.4239 | - | 1.4947 |
| $R_u^{Sb}(\text{Å})$ | 1.3990 | 1.4290 | 1.3860 | 1.405 | - |
| $\Delta q\,(\varphi_j)$ | 0.2100 | 0.0860 | 0.2630 | 0.185 | 0.0500 |
| $D^i$ (eB) | 2.0300 | 1.9800 | 2.0500 | 2.3180 | 1.734 |

*Таблиця 3*

*Effective charges, effective radii and dissociation energies of InSb NHOs*

| Parameters | *InSb* |
|---|---|
| | $\varphi_1$ |
| $d_j^{екcп}$(Å) | 2.7973 |
| $d_j^{meop}$(Å) | 2.797 |
| $R_u^{In}$(Å) | 1.1839 |
| $R_u^{Sb}$(Å) | 1.6137 |
| $\Delta q\ (\varphi_j)$ | 0.385 |
| $D^i$ (eB) | 1.9893 |

## Discussion of results

Analysis of the results obtained has shown that the algorithm of distribution of phase regions of equilibrium of ternary systems in solid state and the refinements introduced by constructing isothermal cross-sections and calculating the energy of interatomic interaction of the initial components depending on the interatomic distances are in good agreement with the results of studies of thermal rearrangements of atoms when forming the short-range order of chemical bond which is responsible for the appearance of stable and metastable phases in the melts of ternary systems presented in [11 – 13].

The results presented in the article expand the technological possibilities of obtaining new materials by taking into account the peculiarities of the fine structure of the chemical bond, triple phase diagrams, eutectic-peritectic and exothermic and endothermic reactions during the formation of short-range order in melts of *In-Cd-Sb* ternary systems.

A diagram of the distribution of phase regions in the solid state and isothermal sections have been constructed, which refine the dynamics of the formation of short-range order of chemical bonds in ternary systems of *In-Cd-Sb* melts.

## Conclusions

1. A diagram of the distribution of phase regions in the solid state and isothermal sections have been constructed, which refine the dynamics of the formation of short-range order of chemical bonds in ternary systems of *In-Cd-Sb* melts.
2. A method for calculating chemical bonding parameters in ternary *In-Cd-Sb* systems is proposed.
3. Calculations of effective radii and dissociation energies in ternary *In-Cd-Sb* systems are performed.
4. The obtained theoretical results are consistent with the results of calculations of the parameters of chemical bond, using the methods of microscopic theory and the results of studies of thermal rearrangement of atoms in melts, and can also be used in the development of technological modes for obtaining new materials based on *In-Cd-Sb* for use in thermoelectricity.

## References

1. Anatychuk L.I. (1979). *Termoelementy i termoelektricheskiie ustroistva: Spravochnik [Thermoelements and thermoelectric devices: Handbook]*. Kyiv: Naukova dumka (in Russian).
2. Lazarev V.B., Shevchenko V.Ya., Grinberg Ya.Kh., Sobolev V.V. (1978). *Poluprovodnikovyie soiedineniia gruppy $A^{II}$ $B^{V}$ [Semiconductor compounds of $A^{II}$ $B^{V}$ group]*. Moscow: Nauka (in Russian).
3. Khansen M., Anderko K. (1962). *Struktura dvoinykh splavov T.1, 2 [Structure of double alloys. Vol.1, 2]*. Moscow: Metalurgizdat (in Russian).
4. Chang Y.A., Chen S., Zhang F., Yan X., Xie F., Schmid-Fetzer R., Oates W.A. (2004). Phase diagram calculation: past, present and future. *Progress in Materials Science*, 49(3-4), 313-345.
5. Ghasemi Masoomeh, Zanolli Zeila, Stankovski Martin, Johansson Jonas. (2015). Size- and shape-dependent phase diagram of In-Sb nano-alloys. *Nanoscale*, 7(41), 17387-17396.
6. Liu Ya., Tedenac Jean-Claudeac (2009). Thermodynamic modeling of the Cd–Sb–Zn ternary system. *Calphad*, 33(4), 684-694.
7. Snugovsky L., Perovic D. D., Rutter J. W. (2000). Experimental study of Bi–Cd–In phase diagram using conventional methods plus quenching and "solidification path" techniques. *Materials Science and Technology*, 16(9), 968-978.
8. Manik O.M. (1999). *Bahatofactornyi pidkhid v teoretychnomu materialoznavstvi [Multi-factor approach in theoretical material science]*. Ukraine. Chernivtsi: Prut, 432 (in Ukrainian).
9. Manik O.M., Manik T.O., Bilynskyi-Slotylo V.R. (2018). Theoretical models of cadmium antimonide ordering alloys. *J.Thermoelectricity*, 4, 14-28.
10. Dremliuzhenko S.G. (2002). *Sistemy na osnove CdSb: diagrammy sostoianiia, polucheniie i svoistva splavov. Spravochnik [CdSb-based systems: diagrams of state, preparation and properties of alloys. Handbook]*. Chernivtsi: Ruta [in Russian].
11. Psarev V.I. (1997). Thermal rearrangement of atoms in Cd-Sb melts. *Russian Journal of Physical Chemistry*, 21(6), 1022-1059.
12. Belotskij D.P., Manik O.N. (1996).On the relationship between thermoelectric materials melts properties and structures and the state diagrams. 1. *J. Thermoelectricity*, 1, 21-47.
13. Belotskij D.P., Manik O.N. (1996). On the relationship of electronic properties and structures of melts to the diagrams of state in the thermoelectric material. 2. Phase changes and electronic properties of melts, *J. Thermoelectricity*, 2, 23-57.

Submitted 14.04.2021

**Маник О.М.,** *канд. фіз.-мат. наук*, *доцент*[1]
**Маник Т.О.,** *канд. фіз.-мат. наук*[2]
**Білинський-Слотило В.Р.,** *канд. фіз.-мат. наук*[1]

[1]Чернівецький національний університет
імені Юрія Федьковича, вул. Коцюбинського 2,
Чернівці, 58012, Україна, *e-mail: o.manyk@chnu.edu.ua,*
*e-mail: slotulo@gmail.com*
[2]Військово-технічний університет
ім. Ярослава Домбровського, вул. ген. Сільвестра Каліського, 2,
Варшава 46, 00-908, Польща, *e-mail: tetjana.manyk@wat.edu.pl*

# ТЕОРЕТИЧНІ МОДЕЛІ УПОРЯДКОВУВАНИХ СПЛАВІВ ПОТРІЙНИХ СИСТЕМ ТЕРМОЕЛЕКТРИЧНИХ МАТЕРІАЛІВ. 1. ХІМІЧНИЙ ЗВ'ЗОК ТА ДІАГРАМИ СТАНУ *In-Cd-Sb*

*Використовуючи розроблений комплексний підхід для побудови теоретичних моделей упорядковуваних сплавів потрійних систем термоелектричних матеріалів побудовано схему розподілу фазових областей для рівноваги у твердому стані та ізотермічні перерізи на основі проміжних бінарних сполук In-Sb, Cd-Sb, In-Cd. Представлено розрахунки ефективних зарядів, ефективних радіусів, перерозподілу електронної густини та енергії дисоціації нееквівалентних гібридних орбіталей (НГО) в системі In-Cd-Sb в залежності від міжатомних віддалей. Результати теоретичних розрахунків можуть бути використані при розробці технології одержання нових термоелектричних матеріалів на основі потрійних систем In-Cd-Sb. Бібл. 13, рис. 4, табл. 3.*
**Ключові слова:** діаграми станів, фазові переходи, хімічний зв'язок, нееквівалентні гібридні орбіталі, енергія дисоціації.

**Маник О.Н.,** *канд. физ.-мат. наук, доцент*[1]
**Маник Т.О.** *канд. физ.-мат. наук*[2]
**Билинский-Слотило В.Р.,** *канд. физ.-мат. наук*[1]

[1]Черновицкий национальный университет
имени Юрия Федьковича, ул. Коцюбинского 2, Черновцы,
58012, Украина, *e-mail:o.manyk@chnu.edu.ua,*
*e-mail: slotulo@gmail.com*
[2]Военно-технический университет
им. Ярослава Домбровского, ул. ген. Сильвестра Калисского, 2,
Варшава 46, 00-908, Польша, *e-mail:tetjana.manyk@wat.edu.pl*

# ТЕОРЕТИЧЕСКИЕ МОДЕЛИ УПРАВЛЯЕМЫХ СПЛАВОВТРОЙНЫХ СИСТЕМ ТЕРМОЭЛЕКТРИЧЕСКИХ МАТЕРИАЛОВ. 1. ХИМИЧЕСКАЯ СВЯЗЬ И ДИАГРАММЫ СОСТОЯНИЯ *In-Cd-Sb*

*Используя разработанный комплексный подход для построения теоретических моделей упорядочиваемых сплавов тройных систем термоэлектрических материалов построена схема распределения фазовых областей для равновесия в твердом состоянии и изотермические сечения на основе промежуточных бинарных соединений In-Sb, Cd-Sb, In-Cd. Представлены расчеты эффективных зарядов, эффективных радиусов, перераспределения электронной плотности и энергии диссоциации неэквивалентных гибридных орбиталей (НГО) в системе In-Cd-Sb в зависимости от межатомных расстояний. Результаты теоретических расчетов могут использоваться при разработке технологии получения новых термоэлектрических материалов на основе тройных систем In-Cd-Sb. Библ. 13, рис. 4, табл. 3.*
**Ключевые слова:** диаграммы состояний, фазовые переходы, химическая связь, неэквивалентные гибридные орбитали, энергия диссоциации.

## References

1. Anatychuk L.I. (1979). *Termoelementy i termoelektricheskiie ustroistva: Spravochnik [Thermoelements and thermoelectric devices: Handbook]*. Kyiv: Naukova dumka (in Russian).
2. Lazarev V.B., Shevchenko V.Ya., Grinberg Ya.Kh., Sobolev V.V. (1978). *Poluprovodnikovyie soiedineniia gruppy $A^{II} B^{V}$ [Semiconductor compounds of $A^{II} B^{V}$ group]*. Moscow: Nauka (in Russian).
3. Khansen M., Anderko K. (1962). *Struktura dvoinykh splavov T.1, 2 [Structure of double alloys. Vol.1, 2]*. Moscow: Metalurgizdat (in Russian).
4. Chang Y.A., Chen S., Zhang F., Yan X., Xie F., Schmid-Fetzer R., Oates W.A. (2004). Phase diagram calculation: past, present and future. *Progress in Materials Science*, 49(3-4), 313-345.
5. Ghasemi Masoomeh, Zanolli Zeila, Stankovski Martin, Johansson Jonas. (2015). Size- and shape-dependent phase diagram of In-Sb nano-alloys. *Nanoscale*, 7(41), 17387-17396.
6. Liu Ya., Tedenac Jean-Claudeac (2009). Thermodynamic modeling of the Cd–Sb–Zn ternary system. *Calphad*, 33(4), 684-694.
7. Snugovsky L., Perovic D. D., Rutter J. W. (2000). Experimental study of Bi–Cd–In phase diagram using conventional methods plus quenching and "solidification path" techniques. *Materials Science and Technology*, 16(9), 968-978.
8. Manik O.M. (1999). *Bahatofactornyi pidkhid v teoretychnomu materialoznavstvi [Multi-factor approach in theoretical material science]*. Ukraine. Chernivtsi: Prut, 432 (in Ukrainian).
9. Manik O.M., Manik T.O., Bilynskyi-Slotylo V.R. (2018). Theoretical models of cadmium antimonide ordering alloys. *J.Thermoelectricity*, 4, 14-28.
10. Dremliuzhenko S.G. (2002). *Sistemy na osnove CdSb: diagrammy sostoianiia, polucheniie i svoistva splavov. Spravochnik [CdSb-based systems: diagrams of state, preparation and properties of alloys. Handbook]*. Chernivtsi: Ruta [in Russian].
11. Psarev V.I. (1997). Thermal rearrangement of atoms in Cd-Sb melts. *Russian Journal of Physical Chemistry*, 21(6), 1022-1059.
12. Belotskij D.P., Manik O.N. (1996).On the relationship between thermoelectric materials melts properties and structures and the state diagrams. 1. *J. Thermoelectricity*, 1, 21-47.
13. Belotskij D.P., Manik O.N. (1996). On the relationship of electronic properties and structures of melts to the diagrams of state in the thermoelectric material. 2. Phase changes and electronic properties of melts, *J. Thermoelectricity*, 2, 23-57.

Submitted 14.04.2021

**Kolobrodov V.G.,** *doc. techn. sciens, professor*
**Tymchyk G.S.,** *doc. techn. sciences, professor*
**Mykytenko V.I.,** *doc. techn. sciens, docent*
**Kolobrodov M.S.**

National Technical University of Ukraine
"Igor Sikorsky Kyiv Polytechnic Institute"
37 Peremohy Ave., Kyiv, 03056, Ukraine
*e-mail: deanpb@kpi.ua*

# TEST OBJECT FOR AUTOMATED MEASUREMENT OF CHARACTERISTICS OF POLARIZING THERMAL IMAGERS

*The growing popularity of increasing the efficiency of remote surveillance by analyzing the degree of polarization of optical radiation in the infrared spectrum requires the development of theoretical and practical methods for determining the characteristics of a new class of optoelectronic devices - polarizing thermal imagers. In contrast to the calculation methods, the issues of practical implementation of measuring benches are currently insufficiently studied. This paper proposes and analyzes options for the structure of test objects for experimental studies of polarizing thermal imagers. A metal plate is considered, which can tilt relative to the line of sight, as well as a spherical metal surface that does not require additional mechanical drives. In the former case, the degree of polarization, ellipticity, and polarization angle are varied by changing its angular orientation in the vertical and horizontal planes. The spherical surface forms a photometric body, in which the radiation of concentric zones has a certain constant degree of polarization. Such test objects provide measurements of the noise equivalent temperature difference NETD and the minimum resolvable temperature difference MRTD of polarizing thermal imagers for different polarization states of the input radiation, which is characterized by the intensity, degree of polarization, ellipticity and polarization angle. Bibl. 17, Figs. 9.*

***Key words:*** *polarizing thermal imager, test object, spatial resolution, temperature resolution, measuring bench*

## Introduction

Thermal imaging surveillance systems are widely used in various fields of science and technology [1-3]. Thermal imagers can be particularly effective in the study of thermoelectric effects, which are understood as a set of physical phenomena due to the relationship between thermal and electrical processes in metals and semiconductors [4]. Thermoelectric phenomena include the Seebeck, Peltier and Thomson effects. To evaluate the efficiency of thermoelectric converters, there is a need for non-contact measurement of the static and dynamic temperature state of the converters [5].

The principle of operation of classical thermal imagers is based on the conversion of the brightness (intensity) of the radiation of the surveillance object and the background of the plane of objects into an adequate distribution of the brightness of the image of the target environment (TE) on the display screen. The limiting characteristics of such thermal imagers are determined by the radiation contrast of the TE. In recent years, developers have been actively trying to use the polarization properties of the radiation of TE

elements to significantly improve these characteristics. As a rule, radiation from the target is partially polarized, while radiation from the background is natural [3,6]. Thus, under certain conditions, polarimetric images demonstrate a significant increase in the signal from the object and suppression of background noise.

The main characteristics of polarized radiation are intensity, degree of polarization, azimuth and ellipticity of polarization [7-9]. To measure these characteristics in the infrared (IR) region of the spectrum, polarizing thermal imagers (PT) are used. At the same time, the main characteristic of any classical thermal imager is the energy resolution, which is determined by the threshold radiation contrast of the surveillance object located against the background.

To determine and measure the energy (temperature) resolution, test objects specified by the relevant standards or methods are used. There is a considerable body of monographs and papers devoted to the calculation and measurement of the energy resolution of classical thermal imagers [2, 10–12]. At the same time, there is practically no scientific and technical information on the choice of test object for modeling and measuring the main characteristics of PT. A rather important factor in the experimental determination of the characteristics of the PT at the present stage is also the possibility of automating this process, for example, in conditions of large-scale production.

## Problem statement

The purpose of this paper is to substantiate the choice of a test object and develop methods for measuring the characteristics of polarizing thermal imagers. These measuring instruments must take into account the current standards for modern thermal imaging and be amenable to automation of measurement processes.

## The main characteristics of thermal imagers

The generalized characteristics of thermal imagers are spatial and thermal resolution, which determine the quality of thermal imaging and temperature sensitivity. To measure the temperature sensitivity, the noise equivalent temperature difference *NETD* is used [2,10].

## Polarization parameters of partially polarized radiation

Test object must assure measurement of the noise equivalent temperature difference *NETD* and minimum resolvable temperature difference *MRTD* for different polarization states of output radiation which is characterized by the intensity $I_0$, polarization degree $P$, ellipticity $\chi$ and polarization angle $\theta$ (Fig. 1).

The process of obtaining elliptically polarized light has been considered in monographs [13–15]. The generalized equation of this type of polarization can be represented as:

$$\frac{x^2}{a^2}+\frac{y^2}{b^2}-2\frac{x}{a}\frac{y}{b}\cos\Delta\varphi=\sin^2\Delta\varphi, \qquad (1)$$

where $\Delta\varphi$ is phase difference between linearly polarized in mutually perpendicular planes components $E_{01}$ and $E_{e1}$ of partially polarized radiation, $x = E_0$; $a = E_{01}$; $y = E_e$; $b = E_{e1}$ are ellipse parameters.

Eq.(1) is the equation of an ellipse arbitrarily oriented relative to the optical axis 00 of the crystal (phase plate) (Fig.1). The orientation of the ellipse is determined by the polarization angle $\theta$, and the shape of the ellipse is determined by the angle of ellipticity $\chi$. Depending on these angles, elliptically polarized light is converted into linearly polarized light, as well as circularly polarized light with rotation of the resulting vector $\vec{E}_r = \vec{E}_o + \vec{E}_e = \vec{x} + \vec{y}$ to the right or left.

In the general case, the ellipse (1) is located inside a rectangle of size $2E_{01} \times 2E_{e1}$ and touches its contour at four points (Fig. 1). If the third term in Eq.(1) is zero, then the axes of the ellipse are parallel to the χ and *y* axes.

The polarization angle $\theta$ is the angle between the main axis of the ellipse and the horizontal axis *x*, which is determined by the components of the electric field of light:

$$tg2\theta = \frac{2E_{0x}E_{0y}\cos\Delta\varphi}{E_{0x}^2 + E_{0y}^2}, \text{ де } 0 < \theta < \pi. \quad (2)$$

The angle of ellipticity χ is given by the ratio of the lengths of the minor and major axes of the ellipse:

$$tg\chi = \frac{\pm b}{a}, \text{ де } -\pi/2 < \chi < \pi/2 \quad (3)$$

The angle of ellipticity χ is also determined by the components of the electric field of light:

$$tg2\chi = \frac{2E_{0x}E_{0y}\cos\Delta\varphi}{E_{0x}^2 + E_{0y}^2}, \text{ де } 0 < \theta < \pi. \quad (4)$$

## Polarization of thermal radiation

Studies of the laws of thermal radiation of heated objects indicate that metal surfaces have a higher degree of radiation polarization compared to dielectric and transparent surfaces. The greatest degree of polarization is observed in the radiation of polished surfaces when observed at a large angle relative to the normal to the surface. This is due to the laws of refraction of radiation at the "metal - air" boundary.

According to Kirchhoff's law, the spectral emissivity $\varepsilon(\lambda)$ of the surface of the observed object, which is in a state of temperature equilibrium, is equal to the absorption coefficient $\alpha(\lambda)$ and is related to the reflection coefficient $R(\lambda)$ by the relation:

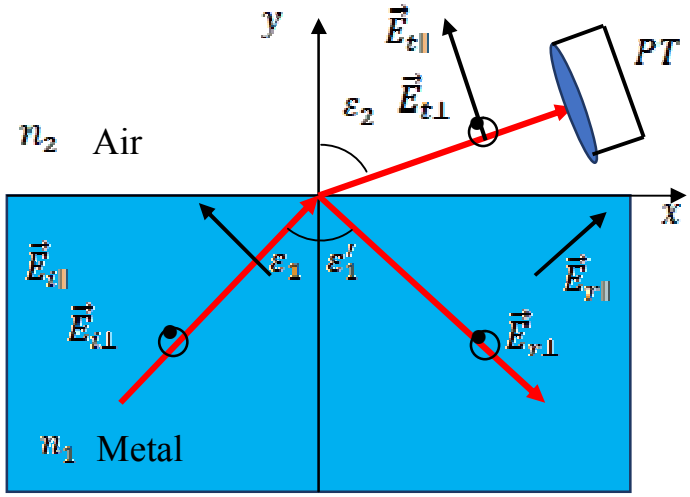


*Fig. 2. Radiation and reflection of light incident at an inclined angle ε_1 from metal to the "metal - air" boundary*

$$\varepsilon(\lambda) = \alpha(\lambda) = 1 - R(\lambda). \tag{7}$$

The amplitude of thermal radiation $E_t$ at the "metal-air" boundary is partially polarized, where the parallel component $E_{t\parallel}$ is greater than the perpendicular component $E_{t\perp}$ (Fig. 2). The axis of sight (observation) of PT is located in the $xy$ plane of observation.

Using Kirchhoff's law (7) and Fresnel's formulae for partial energy reflection coefficients $R_\parallel$ and $R_\perp$ [15, 16], we obtain formulae for calculating the parallel and perpendicular components of (partial) radiation coefficients

$$\varepsilon_\parallel = \left|\frac{E_{t_\parallel}}{E_{i_\parallel}}\right|^2 = \frac{4n_1\cos\varepsilon_2}{\cos\varepsilon_2 + 2n_1\cos\varepsilon_2 + n_1^2 + \kappa_1^2}, \tag{8}$$

$$\varepsilon_\perp = \left|\frac{E_{t_\perp}}{E_{i_\perp}}\right|^2 = \frac{4n_1\cos\varepsilon_2}{\left(n_1^2 + \kappa_1^2\right)\cos\varepsilon_2 + 2n_1\cos\varepsilon_2 + 1}, \tag{9}$$

where $n_c = n_1 - j\kappa_1$ is a complex refractive index of metal; $\varepsilon_2$ is refracting (viewing) angle. The resulting emissivity is the average of the parallel and perpendicular components

$$\varepsilon = \frac{1}{2}\left(\varepsilon_\parallel + \varepsilon_\perp\right). \tag{10}$$

The degree of polarization of radiation is defined as

$$DOP(\varepsilon_v) = \frac{\varepsilon_\perp(\varepsilon_v) - \varepsilon_\parallel(\varepsilon_v)}{\varepsilon_\perp(\varepsilon_v) + \varepsilon_\parallel(\varepsilon_v)}, \tag{11}$$

where $\varepsilon_v = \varepsilon_2$ is viewing angle.

The dependences of partial emissivity factors $\varepsilon_\parallel(\varepsilon_v)$ and $\varepsilon_\perp(\varepsilon_v)$ and the degree of polarization DOP($\varepsilon_v$) at the "aluminum-air" boundary on the viewing angle $\varepsilon_v$ are shown in Figs. 3 and 4. For the radiation of the aluminum surface, the perpendicular component is larger than the parallel component. The perpendicular component increases with increase in viewing angle to a maximum value of about 0.92, and then decreases at large angles. The perpendicular component decreases monotonically with increase in angle $\varepsilon_v$. The overall emissivity factor $\varepsilon$ increases slightly with increase in angle $\varepsilon_v$. The degree of polarization with increase in viewing angle increases to a maximum value of 92% at $\varepsilon v \approx 90°$. When constructing plots to take into account the roughness and oxidation of the surface of the aluminum plate, the complex refractive index $n_c = 4.45 - j3.3$ was used.

On the contrary, for the "dielectric-air" boundary, the partial components of the emissivity factor decrease with increase in viewing angle. The overall emissivity factor decreases with increase in viewing angle in proportion to COS$\varepsilon_v$. The degree of polarization of the surface radiation also increases with increase in the angle $\varepsilon_v$, but has a smaller value compared to the radiation of the surface of metals.

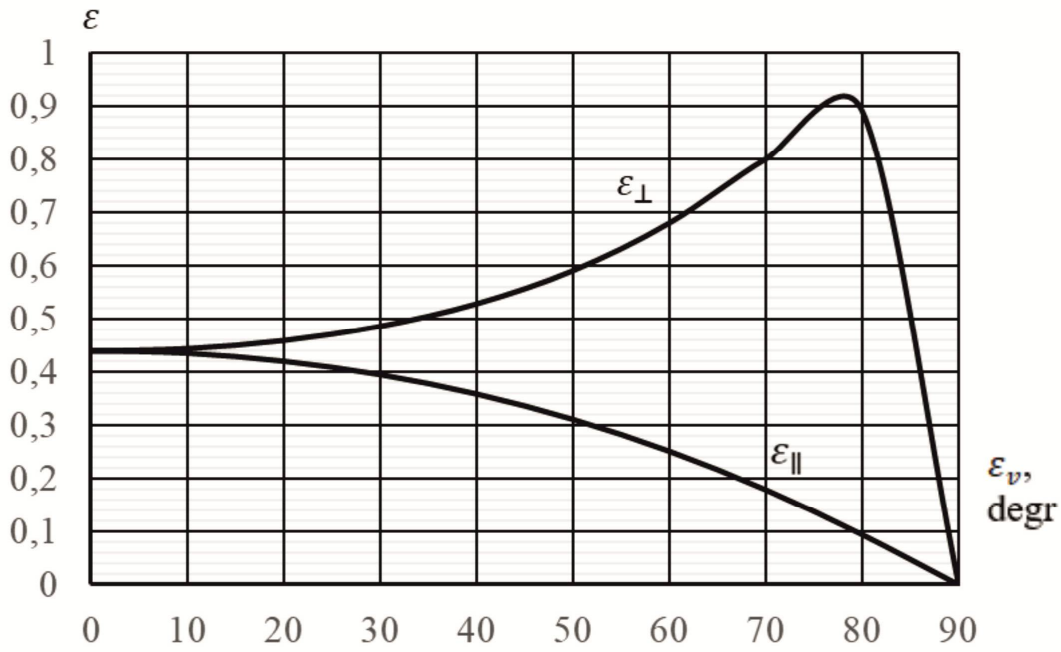


*Fig. 3. Dependences of partial emissivity factors of the aluminum surface on the angle $\varepsilon_v$ at $n_c = 4{,}45 - j3.3$*

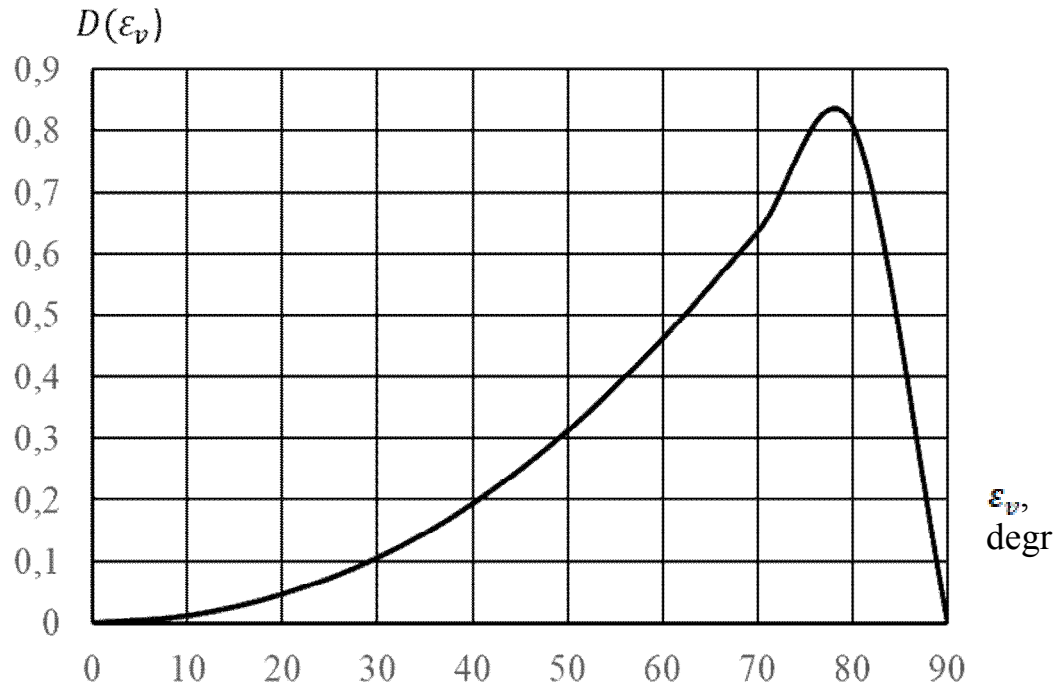


*Fig. 4. The dependence of the degree of polarization of the radiation of the aluminum surface on the viewing angle $\varepsilon$ at $n_c = 4{,}45 - j3.3$*

Thus, the analysis of the laws of thermal radiation of the metal surface shows the following:

1. The radiation is partially polarized, which is due to the difference in emissivity factors for linearly polarized light in surveillance plane $\varepsilon_{\parallel}$ and the plane $\varepsilon_{\perp}$ perpendicular to it,
2. The parallel component of linearly polarized radiation $E_{\parallel}(\varepsilon_v)$ in surveillance plane with increase in viewing angle monotonically decreases from 0.44 at $\varepsilon_v = 0°$ to zero at $\varepsilon_v = 90°$.
3. The perpendicular component of linearly polarized radiation $E_{\perp}(\varepsilon_v)$ in surveillance plane with increase in viewing angle $\varepsilon_v$ increases from 0.44 to maximum value 0.92 at $\varepsilon_v \approx 80°$, and then decreases to zero at at $\varepsilon_v = 90°$..
4. The degree of polarization DOP($\varepsilon_v$) of radiation of aluminum surface with increase in viewing angle $\varepsilon_v$ increases from zero to maximum value 0.83 at $\varepsilon_v \approx 80°$ and decreases to zero at $\varepsilon_v = 90°$.
5. For small viewing angles $\varepsilon_v < 30°$, which is characteristic of typical surveillance cases, the degree of polarization does not exceed 10%, and the resulting emissivity factor is $\approx \varepsilon_{\parallel} \approx \varepsilon_{\perp} = 0{,}438$

## Selection of test object

For experimental studies of classical thermal imagers and measurement of their characteristics, test objects are used, which are located on a uniform background [9,10]. The schematic of a setup for measuring the characteristics of PT is shown in Fig.5. The schematic of a setup for measuring the characteristics of the PT is shown in Fig. 5. The background emitter 1, the test object 2, and the studied polarizing thermal imager 3 are successively located on the optical bench [17].

As a background, it is proposed to use a metal (aluminum) plate covered with black lacquer, which has an emissivity factor close to one. Therefore, such a plate will be considered as a completely black body, the surface of which radiates according to Lambert's law. The rear surface of the background plate is covered with thermoplastic. There is a heater between the thermoplastic and the aluminum plate, and thermocouples for temperature measurement in the four corners of the plate. This ensures a uniform temperature background.

The heater allows changing the surface temperature of the plate in a given range. The plate is located perpendicular to the optical axis of the PT. In this case, the radiation entering the PT from the background, will be unpolarized, i.e. Pb ≈ 0 (Fig. 4). This is characteristic of most natural background sources of IR radiation.

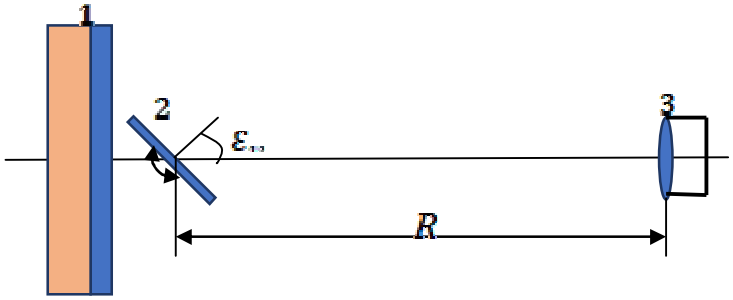


*Fig. 5. Schematic of the method for measuring the NETD of a polarizing thermal imager (in the horizontal plane): 1 - background emitter; 2 – test object; 3 - polarizing thermal imager*

As test object 2, it is proposed to use a rectangular plate, the Foucault gauge or a spherical surface made of aluminum with a complex refractive index $n_c = n - j\kappa$, which are located perpendicular to the optical axis of the PT.

To measure the *NETD*, we will use a rectangular plate that can rotate about the vertical axis by the viewing angle $\varepsilon_v$ relative to the optical axis of the PT in the horizontal plane. By changing the angle $\varepsilon_v$, a change in the degree of polarization $P(\varepsilon_v)$ of the radiation entering the PT is achieved (Fig. 4). The test object rotates about the vertical axis in the range from 0º to 80º. The temperature of the plate is equal to the ambient temperature and is measured by temperature sensors.

The change of the polarization angle θ is achieved by tilting (reversing) the plate relative to the vertical plane of the optical system (Fig. 6).

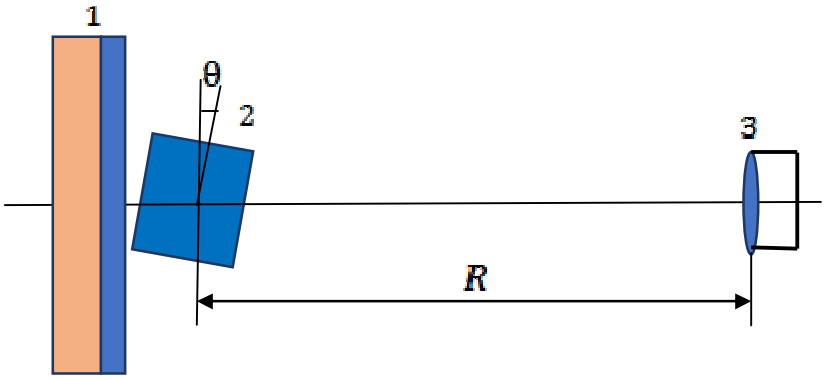


*Fig. 6. Schematic of the method for measuring the NETD of a polarizing thermal imager at different polarization angles θ (in the vertical plane): 1 – background emitter; 2 – test object; 3 - polarizing thermal imager*

The technical implementation of the test object turns can be quite simple and allows automating the measurement process.

To study the dependence of the *NETD* on the degree of polarization, it is proposed to use a hemisphere made of aluminum. A certain point on the hemisphere surface will correspond to a variable angle $\varepsilon_v$ between the beam entering the PT and the normal to the surface, i.e. each point of the hemispheric image has its own degree of polarization (Fig. 7).

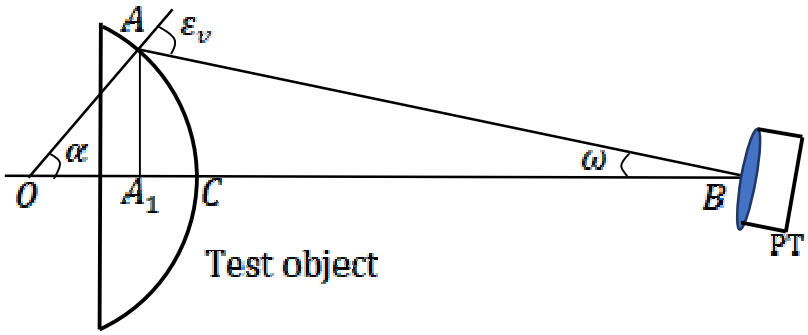


*Fig. 7. Schematic for measuring PT characteristics using a test object with a spherical surface.*

Let us determine the dependence of the viewing angle $\varepsilon_v$ of the surface of test object on the deviation angle $\omega$ of the PT optical axis from the horizontal plane using Fig. 7. From the triangle *ABO* we have $\varepsilon_v = \alpha + \omega \rightarrow \alpha = \varepsilon_v - \omega$. From the triangles $AA_1O$ and $AA_1B$ we get

$$AA_1 = AO\sin\alpha = A_1Btg\omega, \quad , \tag{12}$$

where $AO = r_{th}$ is radius of the spherical surface of test object; $A_1B = BC + CA_1 = R + CA_1$, where $BC = R$ is the distance from PT to test object.

From the triangle $AA_1O$ we have $OA_1 = r_{th}cos\alpha$. Then $CA_1 = OC - OA_1 = r_{th}(1\text{-}cos\alpha)$. Let us substitute the obtained relations to Eq.(12)

$$r_{th}\sin\alpha = \left(R + CA_1\right)tg\omega = \left[R + r_{th}\left(1 - \cos\alpha\right)\right]tg\omega$$

We write the obtained transcendental equation in the form

$$\sin\alpha = \left[R_n + \left(1 - \cos\alpha\right)\right]tg\omega\,, \tag{13}$$

where $Rn = R/r_{th}$ is the normalized distance from the PT to the test object.

The solution of Eq. (13) are the dependences of the viewing angle $\varepsilon_v = \alpha + \omega$ on the change in the direction $\omega$ of the optical axis of thermal imager for different values of the normalized distance from the PT to the test object $R_n$, which are shown in Fig.8.

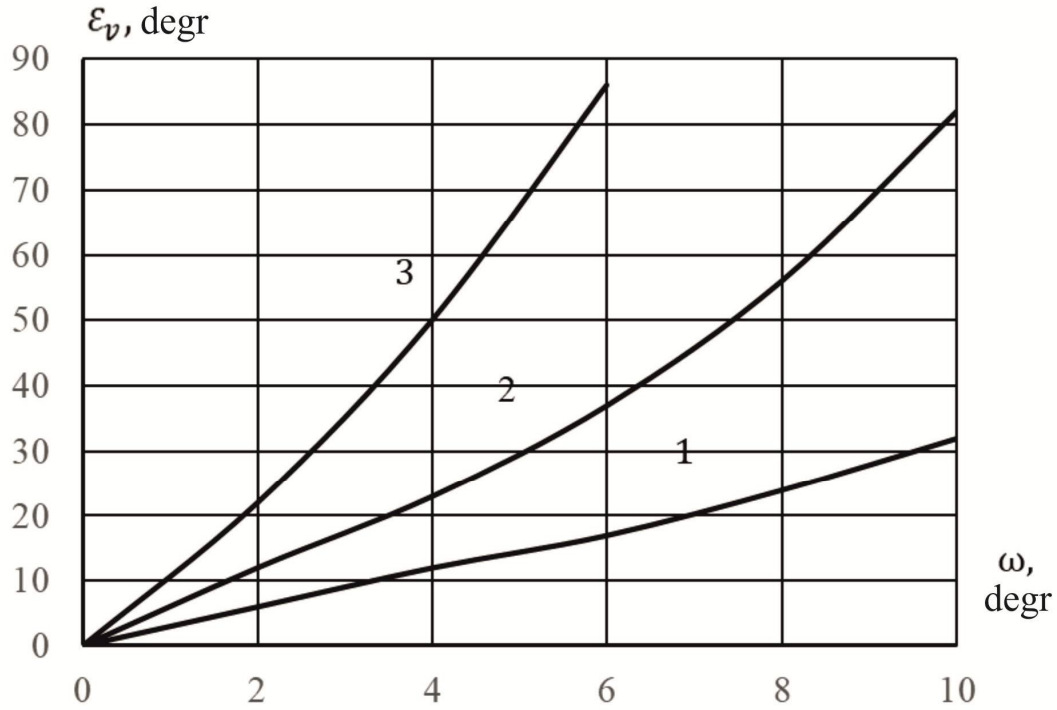


*Fig. 8. Dependence of the thermal imager viewing angle $\varepsilon_v$ of the test object spherical surface on the deviation angle $\omega$ of the PT optical axis from the horizontal plane for different values of the normalized distance from the PT to the test object $R/r_{th}$: 1–2; 2–5; 3–10*

The emitter in the form of a spherical surface can be used to form particles of polarized radiation with different degrees of polarization. The degree of polarization will be determined by formula (11), the plot of which is shown in Fig. 4. The angular position ω of a point on the surface of a sphere, which corresponds to a certain degree of polarization, is found from the relation $DOP(\omega) = DOP(\varepsilon_v - \alpha)$.

The dependence of the deviation angle ω of the PT optical axis on the angle $\varepsilon_v$ is determined from Eq. (13), or the plots shown in Fig. 8. In turn, the degree of polarization DOP(ω) is found from the plot shown in Fig. 4. The calculated dependence DOP(ω) is given in Fig. 9.

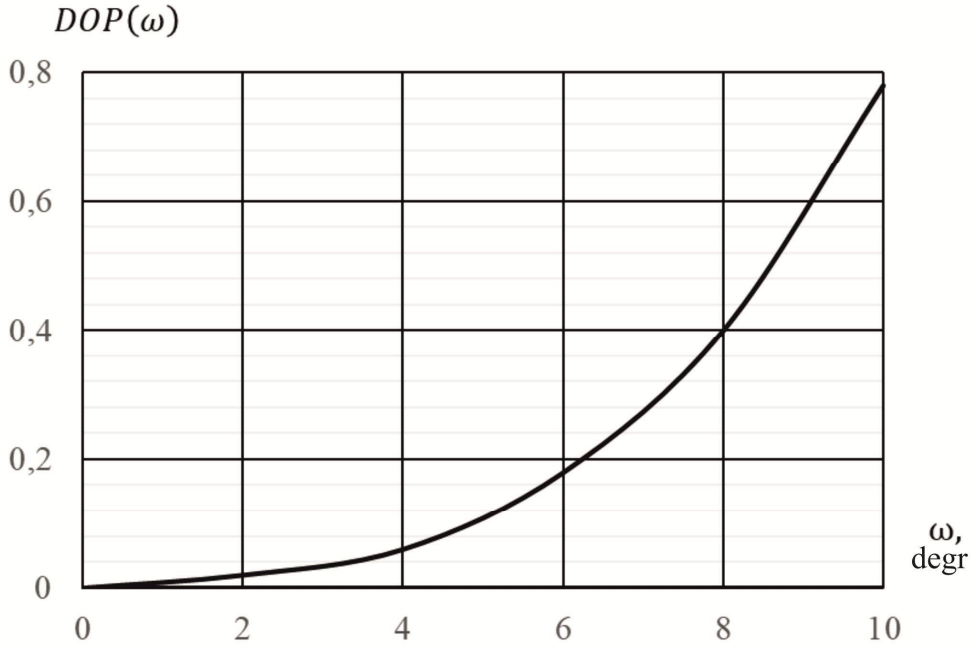


*Fig. 9. Dependence of the degree of polarization DOP (ω) of the spherical surface radiation on the angle of deviation ω of the PT optical axis for the normalized distance from the PT to the test object $R/r_{th} = 5$*

The analysis of the obtained dependence indicates the following:

1. If the optical axis of the PT coincides with the optical axis of the experimental setup, i.e. when ω = 0, the degree of radiation polarization in the centre of the image of the test object is zero.

2. With a deviation of the optical axis of PT from the optical axis of the setup by the angle ω, the degree of polarization increases from zero to the maximum value 0.83 for the normalized distance from the test object $R/r_{th} = 5$.

To measure the minimum resolving temperature difference of PT, it is reasonable to use in the schematic shown in Fig.5 the test object in the form of a four-mark Foucault gauge [6,7].

## Conclusions

1. A feature of the test object for measuring polarization characteristics is the ability to generate partially polarized IR radiation with the given intensity, temperature contrast, polarization degree, ellipticity and polarization angle.
2. Physical models of the test object are proposed in the form of a rectangular metal plate for measuring *NETD*, a metal plate in the form of the Foucault gauge for measuring *MRTD* and a metal spherical surface.

3. The plates allow one to change the degree of polarization, ellipticity and polarization angle by changing their angular orientation in the vertical and horizontal planes.
4. A spherical surface makes it possible to obtain an image of such a surface, the concentric zones of which are formed by radiation having a certain constant degree of polarization.

## References

1. Peri´c Dragana, Livada Branko, Peri´c Miroslav and Vuji´ Saša (2019). Thermal imager range: predictions, expectations, and reality. *Sensors*, 19, 3313.
2. Schuster Norbert, Kolobrodov Valentin G. (2004). *Infrarotthermographie*. Zweite, überarbeitete und erweiterte Ausgabe. Berlin: WILEY-VCH.
3. Vollmer Michael and Mollman Klaus-Peter (2018). *Infrared thermal imaging. Fundamentals, research and applications*. 2nd ed. Weinheim: Wiley – VCH.
4. Anatychuk L.I. (2020). Efficiency criterion of thermoelectric energy converters using waste heat. *J.Thermoelectricity*, 4, 59-63.
5. Anatychuk L.I., Vikhor L.M., Kotsur M.P., Kobylianskyi R.R., Kadenyuk T.Ya. (2016). Optimal control of time dependence of cooling temperature in thermoelectric devices. *J.Thermoelectricity*, 5, 5-11.
6. Vollmer M., Karstadt S., Mollmann K.-P., Pinno F. (2001). *Identification and suppression of thermal imaging. InfraMation Proceedings.* Brandenburg: University of Applied Sciences. Brandenburg. – ITC 104 A.
7. Goldstein D.H. (2011). *Polarized light*. Third edition. London New York: CRC Press is an imprint of Taylor & Francis Group.
8. Gurton K.P., Yuffa A.J., Videen G.W. (2014). Enhanced facial recognition for thermal imagery using polarimetric imaging. *Optical Society of America*, 39(13), 3857–3859.
9. Zhang Y., Shi Z.G., Qiu T.W. (2017). Infrared small target detection method based on decomposition of polarization information. *Journal of Electronic Imaging*, 33004, № 1.
10. Chrzanowski K. (2010). *Testing thermal imagers. Practical guidebook*. Military University of Technology, 00-908 Warsaw, Poland.
11. Kaplan Herbert. (2007). *Practical applications of infrared thermal sensing and imaging equipment*. 3d ed. Washington: SPIE Press.
12. Chyzh I., Kolobrodov V., Molodyk A., Mykytenko V., Tymchyk G., Romaniuk R., Kisała P., Kalizhanova A., Yeraliyeva B. (2020). Energy resolution of dual-channel opto-electronic surveillance system. *SPIE Proceedings*, 11581, Photonics Applications in Astronomy, Communications, Industry, and High Energy Physics Experiments 2020; 115810K.
13. Chipman Russell A., Tiffany Lam Wai-Sze, Young Garam (2019). *Polarized light and optical systems*. Taylor & Francis, CRC Press.
14. Collett Edward (2005). *Field guide to polarized light*. Washington: SPIE Press.
15. Born M., Wolf E. (2002). *Principles of optics*. 7th ed. Cambridge: Cambridge University.
16. Kolobrodov, V.G. Polarization model of thermal contrast observation objects / Kolobrodov, V.G., Mykytenko, V.I., Tymchyk, G.S. // Journal of thermoelectricity. - 2020, 2020(1). – P. 36–49.
17. Short N. J., Yuffa A.J., Videen G. and Hu S. (2016). Effects of surface materials on polarimetric thermal measurements: applications to face recognition. *Applied Optic*, 55 (19), 5226–5233.

Submitted 29.04.2021

**Колобродов В.Г.,** *докт. техн. наук, професор*
**Тимчик Г.С.,** *докт. техн. наук, професор*
**Микитенко В.І.,** *докт. техн. наук, доцент*
**Колобродов М.С.**

Національний технічний університет України
«Київський політехнічний інститут імені Ігоря Сікорського»
проспект Перемоги, 37, Київ, 03056, Україна
*e-mail: deanpb@kpi.ua*

# ТЕСТ-ОБ'ЄКТ ДЛЯ АВТОМАТИЗОВАНОГО ВИМІРЮВАННЯ ХАРАКТЕРИСТИК ПОЛЯРИЗАЦІЙНИХ ТЕПЛОВІЗОРІВ

*Зростаюча популярність підвищення ефективності дистанційних спостережень за рахунок аналізу ступеню поляризації оптичного випромінювання в інфрачервоному діапазоні спектру вимагає розроблення теоретичних і практичних методів визначення характеристик нового класу оптико-електронних приладів – поляризаційних тепловізорів. На відміну від розрахункових методів питання практичної реалізації вимірювальних стендів наразі опрацьовані недостатньо. В даній статті запропоновано і проаналізовано варіанти структури тест-об'єктів для експериментальних досліджень поляризаційних тепловізорів. Розглянуто металеву пластину, що може нахилятись відносно лінії візування, а також сферичну металеву поверхню, яка не потребує додаткових механічних приводів. В першому випадку ступінь поляризації, еліптичність і поляризаційний кут варіюються шляхом зміни її кутової орієнтації у вертикальній і горизонтальній площині. Сферична поверхня формує фотометричне тіло, в якому випромінювання концентричних зон має певну постійну ступінь поляризації. Такі тест-об'єкти забезпечують вимірювання еквівалентної шуму різниці температур і мінімальної роздільної різниці температур поляризаційних тепловізорів для різних станів поляризації вхідного випромінювання, яке характеризується інтенсивністю, ступенем поляризації, еліптичністю і поляризаційним кутом. Бібл. 17, рис. 9.*

**Ключові слова:** поляризаційний тепловізор, тест-об'єкт, просторове розділення, температурне розділення, вимірювальний стенд

**Колобродов В.Г.**, *докт. техн. наук, професор*
**Тимчик Г.С.**, *докт. техн. наук, професор*
**Микитенко В.И.**, *докт. техн. наук, доцент*
**Колобродов М.С.**

Национальный технический университет Украины
"Киевский политехнический институт имени Игоря Сикорского»,
проспект Победы, 37, Киев, 03056, Украина, *e-mail: deanpb@kpi.ua*

# ТЕСТ-ОБЪЕКТ ДЛЯ АВТОМАТИЗИРОВАННОГО ИЗМЕРЕНИЯ ХАРАКТЕРИСТИК ПОЛЯРИЗАЦИОННЫХ ТЕПЛОВИЗОРОВ

*Возрастающая популярность повышения эффективности дистанционных наблюдений за счет анализа степени поляризации оптического излучения в инфракрасном диапазоне спектра требует разработки теоретических и практических методов определения характеристик нового класса оптико-электронных приборов – поляризационных тепловизоров. В отличие от расчетных методов вопросы практической реализации измерительных стендов в настоящее время проработаны недостаточно. В данной статье предложены и проанализированы варианты структуры тест-объектов дляэкспериментальных исследований поляризационных тепловизоров Рассмотрена металлическая пластина, которая может наклоняться относительно линии визирования, а также сферическую металлическую поверхность, не требующая дополнительных механических приводов.В первом случаестепень поляризации, эллиптичность и поляризационный уголварьируютсяпутём изменения ее угловой ориентации в вертикальной и горизонтальной плоскости. Сферическая поверхность формирует фотометрическое тело, в котором излучение концентрических зон имеет определенную постоянную степень поляризации. Такие тест-объекты обеспечивают измерение эквивалентного шума разности температур и минимального раздельного различия температур поляризационных тепловизоров для разных состояний поляризации входного излучения, характеризующееся интенсивностью, степенью поляризации, эллиптичностью и поляризационным углом. Библ. 17, рис. 9.*

**Ключевые слова:** поляризационный тепловизор, тест-объект,пространственное разделение,температурное разделение, измерительный стенд

## References

1. Peri´c Dragana, Livada Branko, Peri´c Miroslav and Vuji´ Saša (2019). Thermal imager range: predictions, expectations, and reality. *Sensors*, 19, 3313.
2. Schuster Norbert, Kolobrodov Valentin G. (2004). *Infrarotthermographie*. Zweite, überarbeitete und erweiterte Ausgabe. Berlin: WILEY-VCH.
3. Vollmer Michael and Mollman Klaus-Peter (2018). *Infrared thermal imaging. Fundamentals, research and applications*. 2nd ed. Weinheim: Wiley – VCH.
4. Anatychuk L.I. (2020). Efficiency criterion of thermoelectric energy converters using waste heat. *J.Thermoelectricity*, 4, 59-63.
5. Anatychuk L.I., Vikhor L.M., Kotsur M.P., Kobylianskyi R.R., Kadenyuk T.Ya. (2016). Optimal control of time dependence of cooling temperature in thermoelectric devices. *J.Thermoelectricity*, 5, 5-11.
6. Vollmer M., Karstadt S., Mollmann K.-P., Pinno F. (2001). *Identification and suppression of thermal imaging. InfraMation Proceedings.* Brandenburg: University of Applied Sciences. Brandenburg. – ITC 104 A.
7. Goldstein D.H. (2011). *Polarized light*. Third edition. London New York: CRC Press is an imprint of Taylor & Francis Group.
8. Gurton K.P., Yuffa A.J., Videen G.W. (2014). Enhanced facial recognition for thermal imagery using polarimetric imaging. *Optical Society of America*, 39(13), 3857–3859.

9. Zhang Y., Shi Z.G., Qiu T.W. (2017). Infrared small target detection method based on decomposition of polarization information. *Journal of Electronic Imaging*, 33004, № 1.
10. Chrzanowski K. (2010). *Testing thermal imagers. Practical guidebook*. Military University of Technology, 00-908 Warsaw, Poland.
11. Kaplan Herbert. (2007). *Practical applications of infrared thermal sensing and imaging equipment*. 3d ed. Washington: SPIE Press.
12. Chyzh I., Kolobrodov V., Molodyk A., Mykytenko V., Tymchyk G., Romaniuk R., Kisała P., Kalizhanova A., Yeraliyeva B. (2020). Energy resolution of dual-channel opto-electronic surveillance system. *SPIE Proceedings*, 11581, Photonics Applications in Astronomy, Communications, Industry, and High Energy Physics Experiments 2020; 115810K.
13. Chipman Russell A., Tiffany Lam Wai-Sze, Young Garam (2019). *Polarized light and optical systems*. Taylor & Francis, CRC Press.
14. Collett Edward (2005). *Field guide to polarized light*. Washington: SPIE Press.
15. Born M., Wolf E. (2002). *Principles of optics*. 7th ed. Cambridge: Cambridge University.
16. Kolobrodov, V.G. Polarization model of thermal contrast observation objects / Kolobrodov, V.G., Mykytenko, V.I., Tymchyk, G.S. // Journal of thermoelectricity. - 2020, 2020(1). – P. 36–49.
17. Short N. J., Yuffa A.J., Videen G. and Hu S. (2016). Effects of surface materials on polarimetric thermal measurements: applications to face recognition. *Applied Optic*, 55 (19), 5226–5233.

Submitted 29.04.2021

**L.I. Anatychuk,** *acad. National Academy of Sciences of Ukraine*[1,2]
**L.M. Vikhor,** *doc. phys.-mat. Sciences*[1]
**Kotsur M.P.** *cand. phys.-mat. Sciences*[1,2]
**R.V. Kuz,** *cand. phys.-mat. Sciences*[1,2]
**R.G. Cherkez**, *doc. phys.-mat. Sciences, Acting professor*[1,2]

[1]Institute of Thermoelectricity of the NAS and MES of Ukraine,
1 Nauky str., Chernivtsi, 58029, Ukraine,
*e-mail: anatych@gmail.com*;
[2]Yu.Fedkovych Chernivtsi National University,
2, Kotsiubynskyi str., Chernivtsi, 58012, Ukraine

# COMPARATIVE ANALYSIS OD THERMOELECTRIC ENERGY CONVERTERS WITH PERMEABLE AND SOLID THERMOELEMENTS

*The paper describes methods for calculating the optimal parameters of two models of a thermoelectric converter in the mode of electrical energy generation, namely, a sectional converter with the heat carrier movement along the heat-absorbing junctions of thermoelements and a converter of permeable thermoelements, in which the heat carrier passes through channels located along the height of the thermoelement legs. The energy and economic indicators of such models are calculated and their comparative analysis is carried out. Bibl. 32, Fig. 10, Table. 1.*

**Key words:** sectional thermoelectric converter, permeable thermoelement, permeable thermoelectric converter, thermoelectric generator

## Introduction

In the modern world, two thirds of the thermal energy obtained from fuel combustion is not used, but released into the environment [1,2]. Only with the exhaust gases of vehicles 30 - 35% of heat is lost, which makes it impossible to save resources and preserve the environment. Thermal waste generated in technological processes, during the incineration of waste, during the operation of turbines, internal combustion engines and other heat engines can be utilized and converted into electricity by direct thermoelectric energy conversion. In [3], it was noted that about 90% of thermal waste has a temperature of up to 300 °C. This determines the relevance of the development and creation of thermoelectric generators (TEG), designed for this temperature level.

Compared to mechanical and other heat recovery technologies, thermoelectric generators have a number of undeniable advantages, such as compactness, quiet operation, reliability, durability and environmental friendliness. TEGs have no moving parts and do not require costly maintenance due to wear or corrosion of parts. Papers [4 – 20] describe examples of the practical application of TEG for generating electricity from waste heat from industrial furnaces [5 – 10], gas turbines [11 – 13], and internal combustion engines on vehicles [2, 14 – 20].

In the generator, thermal energy is transferred to the thermopile by the flow of the heat carrier (gas or liquid). The schematic of the thermoelectric converter (TEC) of the heat carrier energy is shown in Fig. 1a. The generators use two models of converters, which differ in the thermoelectric modules used in them. In the first model, the heat carrier is passed through a heat exchanger located in direct thermal contact with the heat-absorbing surface of classical thermoelectric modules, the thermoelements of which are made of solid materials (Fig. 1b). The heat carrier energy can be used more efficiently if additional heat exchangers and thermoelectric modules operating at lower temperatures are used. For this option, the thermopile consists of several sections of modules located in the direction of the heat carrier movement. The temperature of the heat exchanger base, and, hence, of the heat-absorbing junctions of thermoelements of each subsequent section will be lower than the previous one. In [3, 21], it was shown that the TEC model with several sections is more efficient than a single-section one and allows increasing the generated electric power.

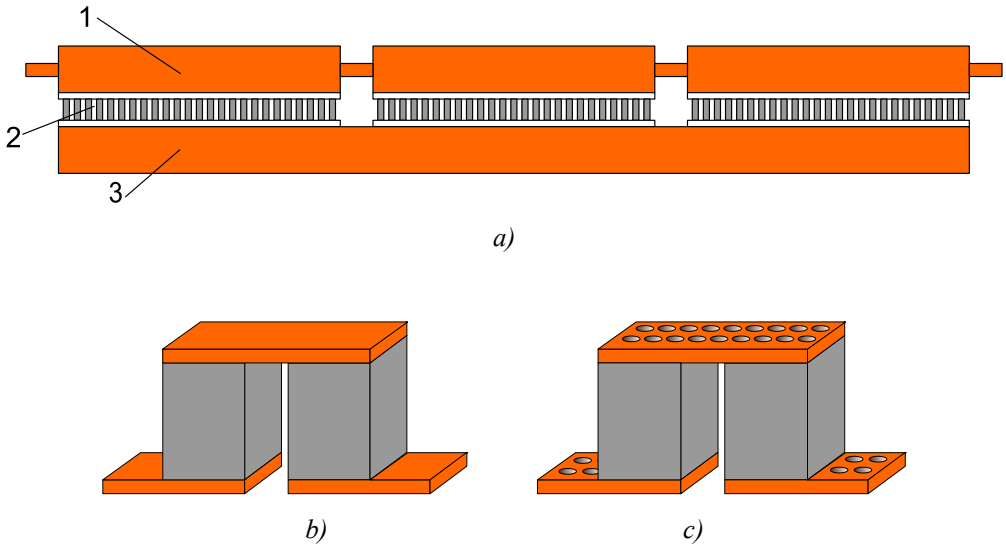


*Fig. 1. a) Schematic of a thermoelectric energy converter. 1 – heat exchanger, 2 – thermoelectric module, 3 – thermostat; b) thermoelement of solid materials; c) permeable thermoelement.*

In the second TEC model, modules of permeable thermoelements (Fig.1c) are used, which have pores or channels, located along the height of the legs along which the heat carrier moves. Heat transfer takes place not only in the area of junctions, but also in the bulk of thermoelectric legs. For the first time a method of increasing the efficiency of thermoelectric energy conversion using permeable thermoelements was described in the patent [22]. In [1, 23 – 27], it is proposed to use porous structures for such thermoelements. The theoretical analysis carried out in [1] showed that porous thermoelements, in comparison with solid ones, significantly improve the parameters of the generator. From the conclusions of theoretical studies of the indicators of channel permeable TEC, carried out in [28 – 30] by methods of optimal control theory, it follows that their efficiency increases by a factor of 1.2 – 1.4 compared to classical modules made of solid materials.

Hence, a question arises as to which of the TEC models, sectional or permeable, is more rational. Therefore, the purpose of this work was to carry out a comparative analysis of the energy and economic indicators of the sectional and permeable TEC and to establish which of the models is more effective for practical use, in particular in systems for utilizing thermal waste.

## Method of calculating the parameters of sectional TEC

The schematic of sectional TEC is shown in Fig. 2. In the general case, the TEC contains N sections located along the direction of the heat carrier flow. Each section consists of a heat exchanger through which the heat carrier moves, classical thermoelectric modules made of thermoelements of solid materials. We assume that the temperature T0 of the heat-generating surfaces of thermoelectric modules is kept constant.

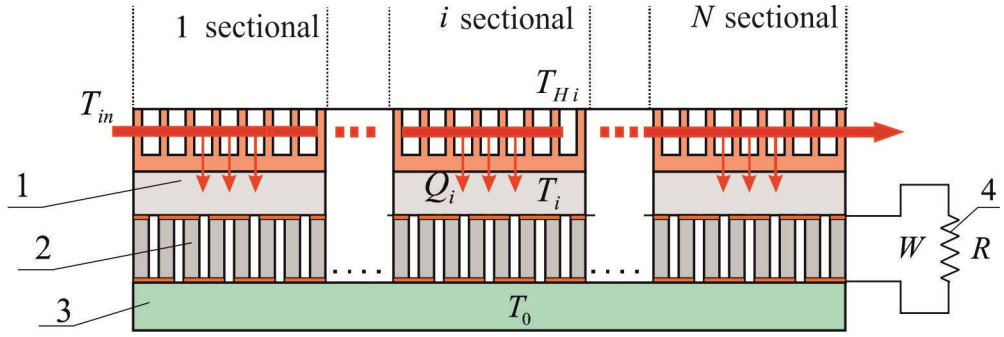


*Fig. 2. Schematic of N-sectional TEC. 1 – heat exchanger, 2 – thermoelectric modules, 3 – thermostat, 4 – matched electric load.*

The task is to evaluate the optimal parameters of each section, which ensure the maximum efficiency of the TEC in the generator mode at a given temperature $T_{in}$ of the heat carrier at the inlet to the heat exchanger and the mass flow rate $m$ of the heat carrier.

The efficiency of TEC is determined as follows:

$$\eta = \frac{W}{G(T_{in} - T_0)}\ , \tag{1}$$

where $G = c_p m$ is total heat capacity of the heat carrier, $c_p$ is its specific heat, $W$ is total power generated by TEC. Taking into account that, according to the conditions of the problem, $T_0$ and $T_{in}$ are given, the maximum value of η corresponds to the maximum power $W$:

$$W = \sum_{i=1}^{N} W_i\ , \tag{2}$$

where $W_i$ is the power of the $i$-th section of TEC.

The following approximations are used to solve the problem.

1. In the steady state, the temperature of the heat exchanger base of the $i$-th section does not depend on the coordinates and is equal to the temperature $T_i$ of the heat-absorbing surface of the modules of the $i$-th section.

2. Stirring in the flow of heat carrier is quite intense and the average temperature of the heat carrier at the outlet of the $i$-th heat exchanger is equal to the temperature of the heat carrier at the inlet to the $(i + 1)$-th heat exchanger, i.e.

$$T_{in\,i+1} = T_{Hi}\ . \tag{3}$$

3. The Seebeck coefficient α, the resistivity ρ and the thermal conductivity κ are temperature independent and have the same value for *n*- and *p*-type legs.

4. The heat transfer coefficient $\alpha_T$ of the heat carrier and its heat capacity $c_p$ are temperature independent.

5. Heat loss to the environment is neglected.

According to these assumptions, the power of the heat transferred by the heat carrier of the *i*-th section is determined as follows

$$Q_i = G(T_{in\,i} - T_{H\,i}) \tag{4}$$

and is equal to the thermal power of convective heat exchange with the heat carrier in the *i*-th heat exchanger, i.e.

$$Q_i = \alpha_T K S_{TEi} (T_{H\,i} - T_i)\,, \tag{5}$$

where $K = S_{Hi} / S_{TEi}$ is the ratio between the area of the heat exchanger base $S_{Hi}$ and the total cross-sectional area $S_{TEi}$ of thermoelement legs in the *i*-th section.

The electric power generated by the thermopile of the *i*-th section is determined from the ratio

$$W_i = \eta_i (T_i, T_0) Q_i = \eta_i (T_i, T_0) G(T_{H\,i-1} - T_{H\,i})\,, \tag{6}$$

which takes into account condition (3) and notation $T_{H\,0} = T_{in}$. In this expression, $\eta_i (T_i, T_0)$ is the maximum value of the efficiency of the thermopile of the *i*-th section, determined by formula [31]

$$\eta_i (T_i, T_0) = \frac{T_i - T_0}{T_i} \frac{M - 1}{M + T_0 / T_i}\,, \tag{7}$$

where $M = \sqrt{1 + 0.5 Z (T_i + T_0)}$, $Z = \dfrac{\alpha^2}{\rho\kappa}$. The heat balance condition is fulfilled on the heat-absorbing surface of the *i*-th thermopile, namely

$$Q_i = Q_{h\,i}\,, \tag{8}$$

where $Q_{h\,i}$ is the heating capacity of the *i*-th thermopile, which in the maximum efficiency mode satisfies the relation [31]

$$Q_{h\,i} (T_i, T_0) = \frac{\kappa S_{TEi}}{L} \frac{ZM (T_i M + T_0)(T_i - T_0)}{(M+1)^2 (M-1)}\,, \tag{9}$$

where $L$ is the height of thermoelement legs. Then, from the heat balance condition (8), the expression for the heat carrier temperature $T_{H\,i}$ is obtained:

$$T_{H\,i} = T_i + \frac{\kappa}{\alpha_T K L} \frac{ZM (T_i M + T_0)(T_i - T_0)}{(M+1)^2 (M-1)}\,. \tag{10}$$

Using expressions (6), (7), (10), by formula (2) the total power of TEC is determined as a function of temperatures of heat-absorbing junctions of thermoelements of all sections: $W = W(T_1, ..., T_N)$. Computer methods are used to find the optimal sequence of the temperatures of the junctions $T_i$ and, accordingly, the

temperatures of the heat carrier $T_{Hi}$ in the heat exchangers, at which the power $W$, and hence the efficiency of the TEC, acquire maximum values.

Subsequently, for optimal temperature distributions $T_i$ and $T_{Hi}$ the power values of each section $W_i$ ( (6) are found, and from the ratio

$$\rho\frac{L}{S_{TEi}}=\frac{\alpha^2(T_i-T_0)^2}{4W_i} \tag{11}$$

the total cross-sectional area $S_{TEi}$ of the thermoelement legs of each section is calculated under conditions of a given leg height $L$. The volume of thermoelectric material is determined by the formula $V=L\sum_{i=1}^{N}S_{TEi}$ .

## Method of calculating the parameters of a permeable TEC

The permeable TEC is formed by series-connected permeable modules of thermoelements with channels in the connecting plates and legs directed along the height of the legs. The model of a permeable thermoelement is shown in Fig. 3.

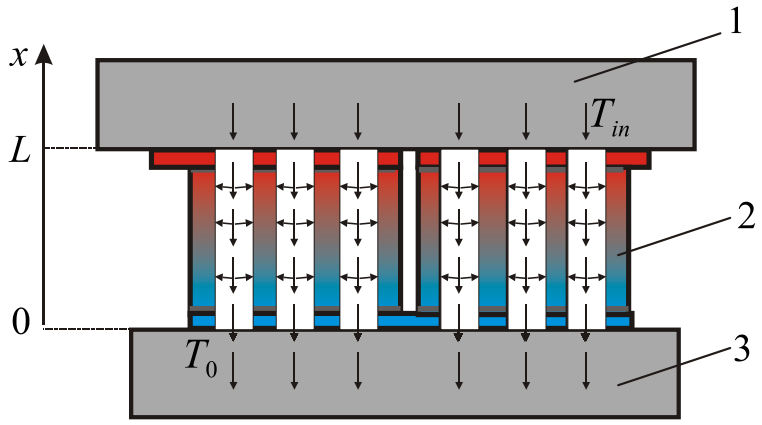


*Fig. 3. Model of a permeable thermoelement. 1 – heat carrier container, 2 – thermoelement with channels for heat carrier, 3 – thermostat*

As with the previous model of sectional TEC, we assume that the parameters of thermoelectric materials are temperature independent and their value is the same for n- and p-legs. The lateral surfaces of the legs are adiabatically isolated. The temperature $T_0$ of the heat-generating junctions of permeable thermoelements is kept constant. The heat carrier moves along the channels, gives off heat to the volume of thermoelement legs and cools down.

Similar to the sectional TEC, the task is to find the optimal parameters of the permeable TEC that provide the maximum efficiency at a given temperature $T_{in}$ of the heat carrier at the inlet to the channels and the heat carrier flow rate $m$. The efficiency of a TEC is characterized by the efficiency of its individual permeable thermoelement, determined by the formula

$$\eta=\frac{W_{TE}}{c_p m_{TE}(T_{in}-T_0)}\ , \tag{12}$$

where $m_{TE}$ is heat carrier flow rate for thermoelement, $W_{TE}$ is power generated by thermoelement.

To calculate the efficiency, it is necessary to solve a stationary boundary-value problem describing the temperature and heat flux distributions in the thermoelement legs and the heat carrier flow. In the one-dimensional approximation, the system of differential equations of this problem has the form [30]

$$\begin{aligned}
&\frac{dT}{dx} = -\frac{\alpha j}{\kappa} T - \frac{j}{\kappa} q, \\
&\frac{dq}{dx} = \frac{\alpha^2 j}{\kappa} T + \frac{\alpha j}{\kappa} q + j\rho + \frac{\alpha_e}{jS}(t - T), \\
&\frac{dt}{dx} = \frac{\alpha_e}{c_p m_{TE}}(t - T),
\end{aligned} \tag{13}$$

where the following notation is used: T is temperature of the thermoelement, t is temperature of the heat carrier in the channels, $q = \frac{1}{j}\left(\alpha j T - \kappa \frac{dT}{dx}\right)$ is specific heat flux in the thermoelement legs, S is cross-sectional area of the thermoelement leg material, $j = I/S$ is current density in the thermoelement legs, $\alpha_e = \alpha_T P_c N_c$, $\square_T$ is heat transfer coefficient in the channels, $N_c$ is the number of channels in the thermoelement legs, $P_c$ is the perimeter of the channel.

The boundary conditions of the problem for the system of equations (13):

$$T(0) = T_0, \quad t(L) = T_{in}, \quad q(L) = 0. \tag{14}$$

The electric power generated by the permeable thermoelement is calculated by the formula

$$W_{TE} = Q_h - Q_0, \tag{15}$$

where $Q_h = c_p m_{TE}(T_{in} - t(0))$ is power of heat absorbed in the channels of permeable thermoelement, $Q_0 = q(0)jS$ is the heat given off by the heat-releasing thermoelement surface to the environment.

Therefore, according to expressions (12) and (15), the maximum efficiency of permeable TEC under conditions of determined geometry and size of thermoelements is achieved if the heat carrier flow rate $m_{TE}$ in the channels and current densities j in the thermoelement legs take optimal values. The optimization problem lies in finding the maximum efficiency (12) of the permeable thermoelement, under the conditions of constraints imposed on the thermoelement by the boundary value problem (13) – (14). This problem is solved by the methods of optimal control theory using the Pontryagin maximum principle [32]. Optimality conditions and examples of solving such a problem are given in [29, 30]. The problem is solved with the help of computer tools.

The results of solving the problem are the optimal values of the electrical power $W_{TE}$ and the heat carrier flow rate $m_{TE}$ for the thermoelement, which ensure maximum efficiency. The number of series-connected thermoelements $N_{TE}$ in the generator thermopile to ensure the specified heat carrier consumption $m$, the total power $W$ and the volume of the thermoelectric material $V$ are calculated by the formulae

$$N_{TE} = m/m_{TE}, \quad W = W_{TE} N_{TE}, \quad V = N_{TE} LS. \tag{16}$$

Thus, the methods for calculating and optimizing the parameters of the sectional and permeable TEC are fundamentally different. The sectional model requires optimization of the generator thermopile as a whole, and in the permeable model it is sufficient to optimize the parameters of a separate thermoelement.

This feature is explained by the fact that due to the difference in the flow patterns of the heat carrier in these TEC models, solid thermoelements in different sections operate in different temperature conditions, and permeable thermoelements - in the same. Accordingly, there is a need for a correct comparison of the theoretical results of optimization of the sectional and permeable TEC in order to identify a more rational model of the converter for its further practical implementation.

## Results of calculating the parameters of sectional and permeable TEC and their comparison

To compare two TEC models made of $Bi_2Te_3$-based materials, the maximum efficiency, the generated power and the corresponding values of thermoelectric material consumption and its unit cost were calculated. The calculations were carried out at the same for both models given values of the heat carrier flow rate and its temperature at the inlet to the TEP heat exchanger. The initial data for the calculation are presented in Table 1.

TEC indicators depend on the intensity of heat transfer, characterized by the heat transfer coefficient $\alpha_T$ and the heat transfer area. The coefficient $\alpha_T$ was chosen the same for both TEC models. As for the heat exchange area, for the sectional model it depends on the ratio between the area of the heat exchanger base and the total cross-sectional area of thermoelectric legs in the sections, characterized by the coefficient $K$. For a permeable TEC, the heat exchange area depends on the number of channels of a given diameter located on an area S = 1 $cm^2$ of the thermoelectric material. Therefore, for calculating the optimal TEC indicators, the heat exchange area cannot be a predetermined value. Therefore, the parameters of the sectional TEC were calculated for two options, namely, for the rational case of heat exchange with the coefficient $K$ = 3.5 and for the "ideal" case when the temperature of the heat-absorbing junctions of thermoelements is considered equal to the temperature of the heat carrier in the heat exchanger, i.e. heat transfer does not affect the TEC parameters. For the permeable converter model, the calculations were performed for the TEC with a different number of channels.

*Table 1*

*Values of quantities used to calculated TEC parameters*

| Quantity | Value |
|---|---|
| Seebeck coefficient □, μV/K | 230 |
| Resistivity □, Ohm□cm | $1.25 \cdot 10^{-3}$ |
| Thermal conductivity □, W/cm□K | 0.015 |
| Coefficient of heat exchange □$_T$, W/ $cm^2$□K | 0.015 |
| Specific heat of heat carrier (gas $CO_2$) $c_p$, J/(g□K) | 1000 |
| Heat carrier flow rate $m$, g/s | $1.15 \cdot 10^{-3}$ |
| Heat carrier temperature at the inlet to heat exchanger $T_{in}$, □C | 100 – 300 |
| Temperature of heat-releasing surface of TEC $T_0$, □C | 50 |

The results of calculating the parameters of two TEC models are shown in Fig. 4-10. First of all, it was necessary to determine the rational number of sections for a sectional TEC and the rational height of the legs for a permeable TEC.

Fig. 4 shows the dependences of the maximum efficiency on the number of sections $N$ of the converter and the height of the legs $L$ of permeable thermoelements. The calculations were carried out at a heat carrier inlet temperature $T_{in} = 300$ °C, for a sectional TEC with a leg height of 1 cm, $K = 3.5$ and for a permeable TEC with 25 channels per 1 cm$^2$ of material area. With an increase in the number of sections or the height of the permeable legs, the efficiency for both TEC models grows and tends to the same value, in this case up to $\eta_{max} = 4$ %. This is due to the increase in the area of heat transfer, which allows more complete use of the thermal power of the heat carrier, which for both models in this case is $Q_{heat} = c_p m(T_{in} - T_0) = 287.5$ W. For a sectional TEC, it is advisable to use $3-4$ sections, and for a permeable TEC, the height of legs up to 2 cm is rational. It is clear that a further increase in the number of sections or height does not significantly increase the efficiency, but drastically increases the thermoelectric material consumption.

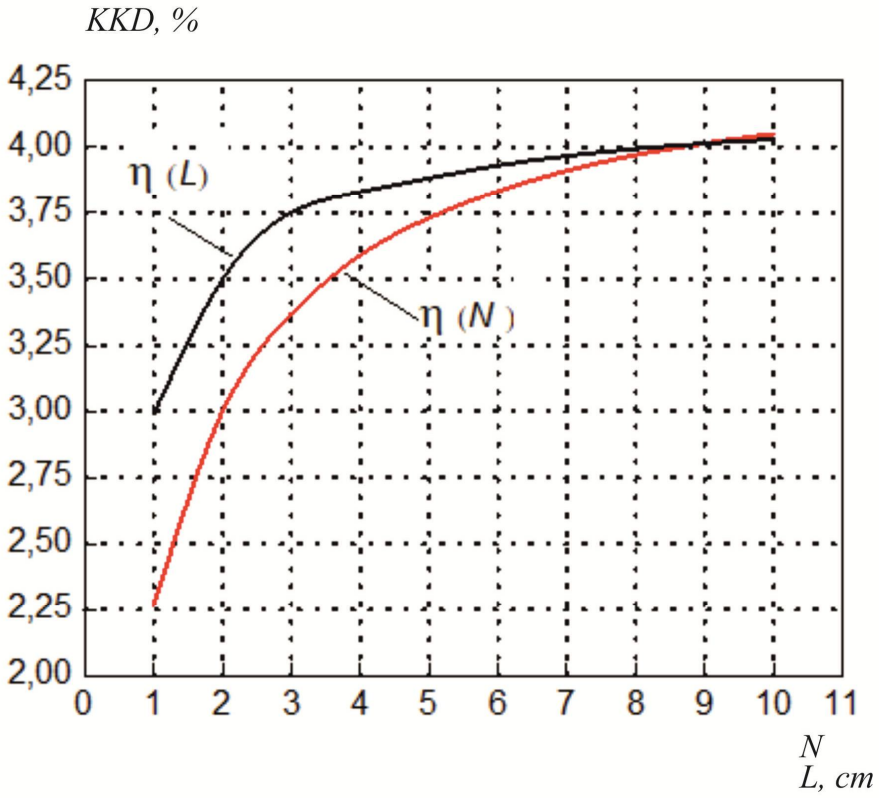


*Fig. 4. η(N) – the efficiency of sectional TEC versus the number of sections N. η(L) – the efficiency of permeable TEC versus the height L of thermoelement legs.*

Fig. 5 shows the dependence of the efficiency of a sectional TEC with a different number of sections on temperature $T_{in}$ of the heat carrier at the inlet to the heat exchanger. The calculations were made taking into account the heat transfer between the heat carrier and the heat-absorbing surface of the TEC (solid lines) and for the "ideal" case in the approximation when heat transfer is not taken into account (dashed lines), that is, the heat transfer coefficient $\alpha_T \to \infty$.

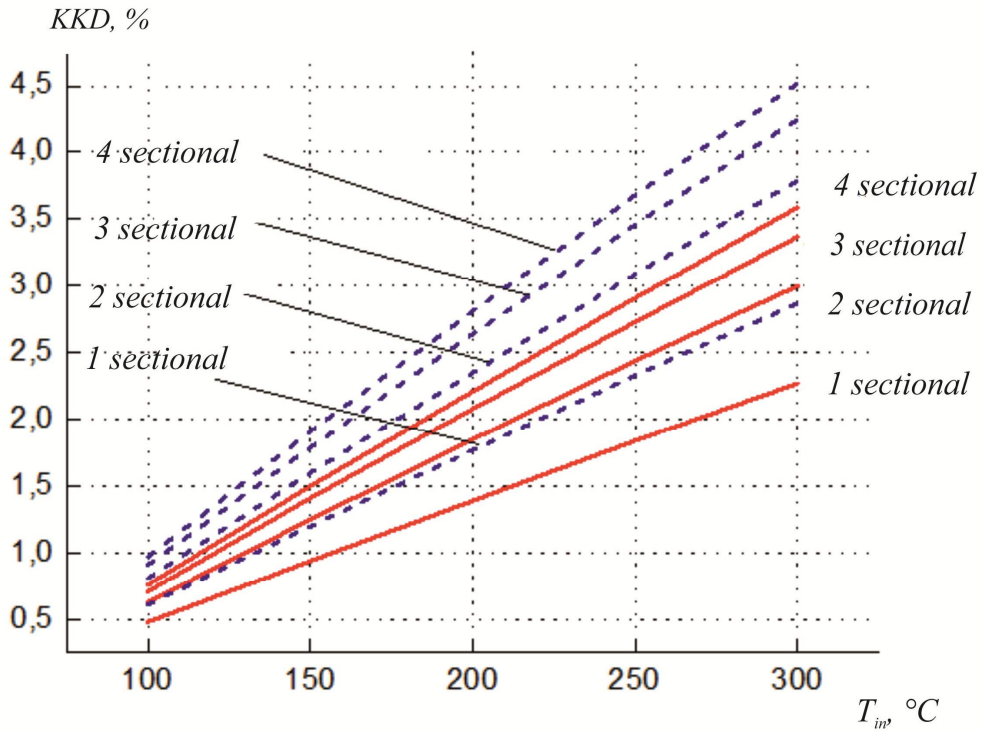


*Fig. 5. The efficiency of sectional TEC with regard to heat exchange (solid lines) and without heat exchange (dashed lines). The height of thermoelement legs is 1 cm.*

The efficiency depends on the number of sections. These results emphasize the conclusion that the most rational model is a three-section TEC. A further increase in the number of sections does not lead to a significant increase in the efficiency of thermal energy conversion.

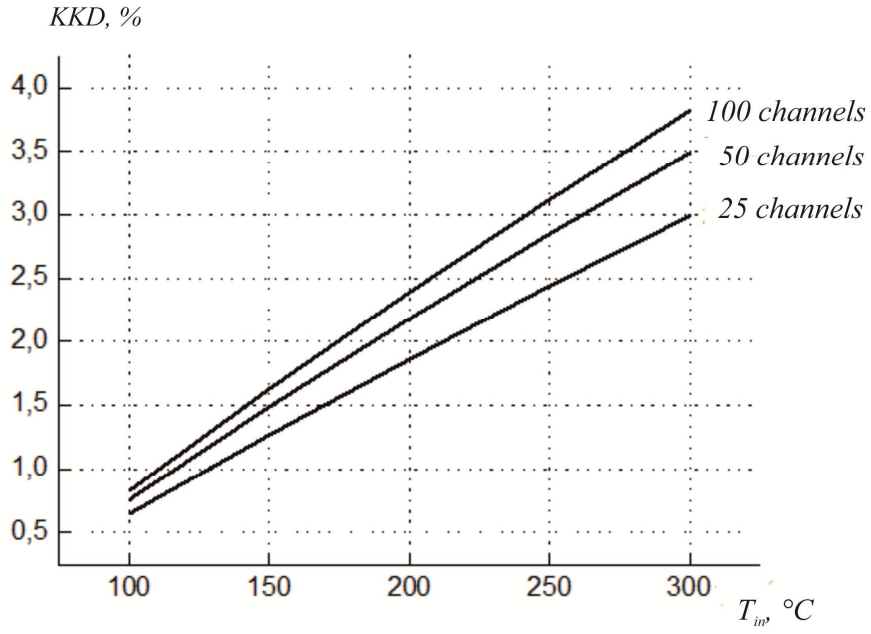


*Fig. 6. The efficiency of permeable TEC with a different number of channels on 1 cm$^2$ of thermoelectric material area.*

Fig. 6 shows the dependence of the efficiency on the temperature $T_{in}$ of the heat carrier at the inlet to a permeable TEC with a leg height of 1 cm and a different number of channels per 1 cm$^2$ of the thermoelectric material area (channel diameter 1 mm). From comparison of these results with the data for the permeable TEC in Fig. 6 it follows that for $T_{in}$ = 300 °C the efficiency of permeable thermoelements 1 cm high with 50 channels and 2 cm high with 25 channels are practically the same. Consequently, in a permeable TEC, it is advisable to increase the area of heat exchange with the heat carrier by increasing the number of channels, rather than increasing the height of the legs, because this will not lead to an increase in the volume of the thermoelectric material.

For comparison, Fig. 7 shows the dependence of the efficiency of the heat carrier temperature at the inlet to the heat exchanger for sectional (solid lines) and permeable (dashed lines) TEC. The efficiency values of the most rational TEC designs, namely a three-section TEC and a permeable TEC with 50 channels per 1 cm$^2$, do not differ significantly. At a heat carrier temperature $T_{in}$ =300 °C, the efficiency of these TEC options reaches 3.5%.

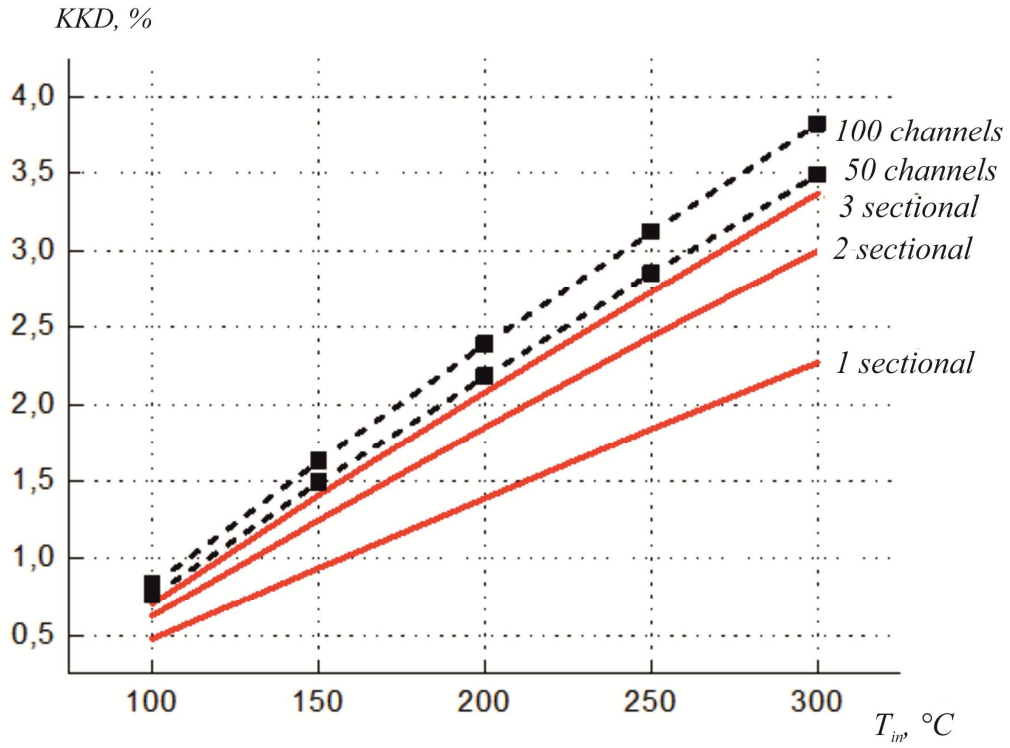


*Fig. 7. Comparison of the efficiency of sectional and permeable TEC.*

The efficiency of permeable TEC increases if you increase the number of channels for the heat carrier. Under these conditions, the area of heat exchange between the heat carrier and the thermoelectric material is enlarged, which increases the efficiency. The rational number of channels is from 50 to 100. Further increase in the number of channels does not significantly increase the efficiency.

To increase the efficiency of sectional TEC, it is advisable to improve the heat transfer system between the heat carrier and the hot surface of the thermopile in order to improve the convective heat transfer between the heat carrier and the heat exchanger. Under these conditions, the efficiency increases and approaches the value of the efficiency in the ideal case when heat transfer does not affect the efficiency (Fig. 5).

Fig. 8 shows the results of calculating the maximum electrical power for different designs of TEC. At a heat carrier temperature of 300 °C, the power of a 3-section TEC and a permeable TEC with 50 channels per 1 $cm^2$ is about 10 W.

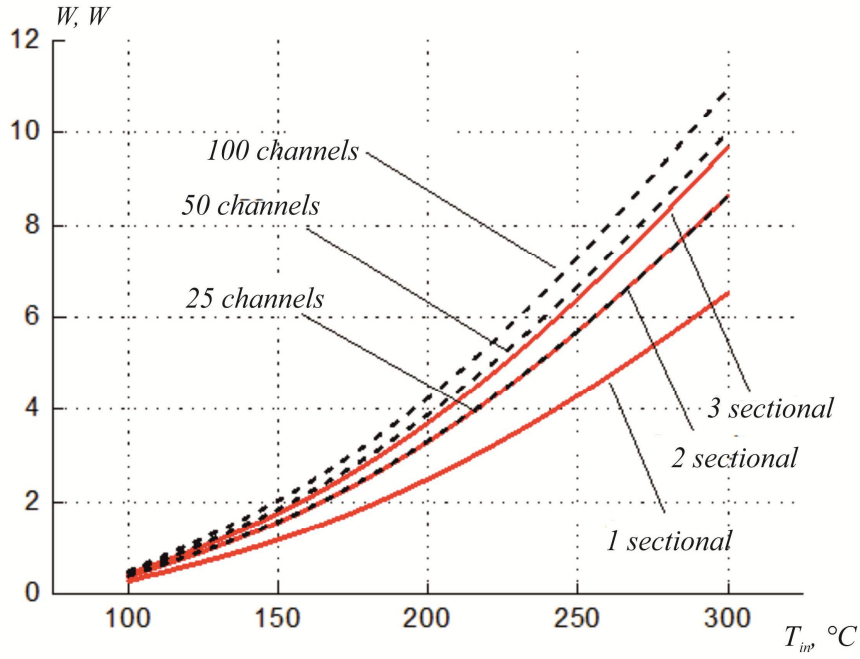


*Fig. 8. Maximum electric power of sectional and permeable TEC.*

To compare the economic performance of the two TEC models, the volume of thermoelectric material, its consumption and the unit cost of obtaining 1 W of electricity were calculated. The results are shown in Fig. 9, 10.

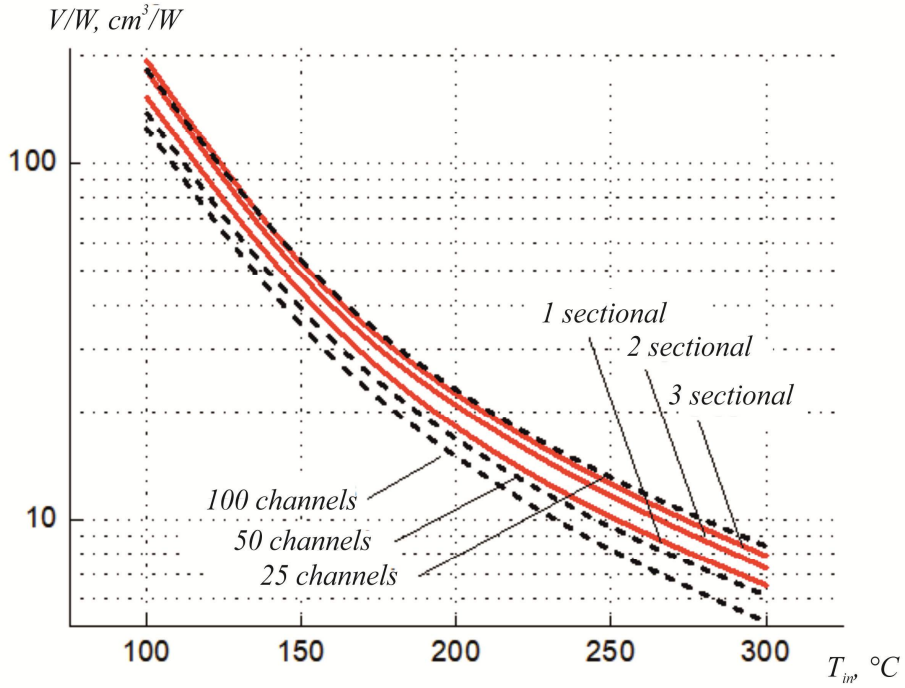


*Fig. 9. Consumption of thermoelectric material for sectional and permeable TEC per 1 W of generated electric energy.*

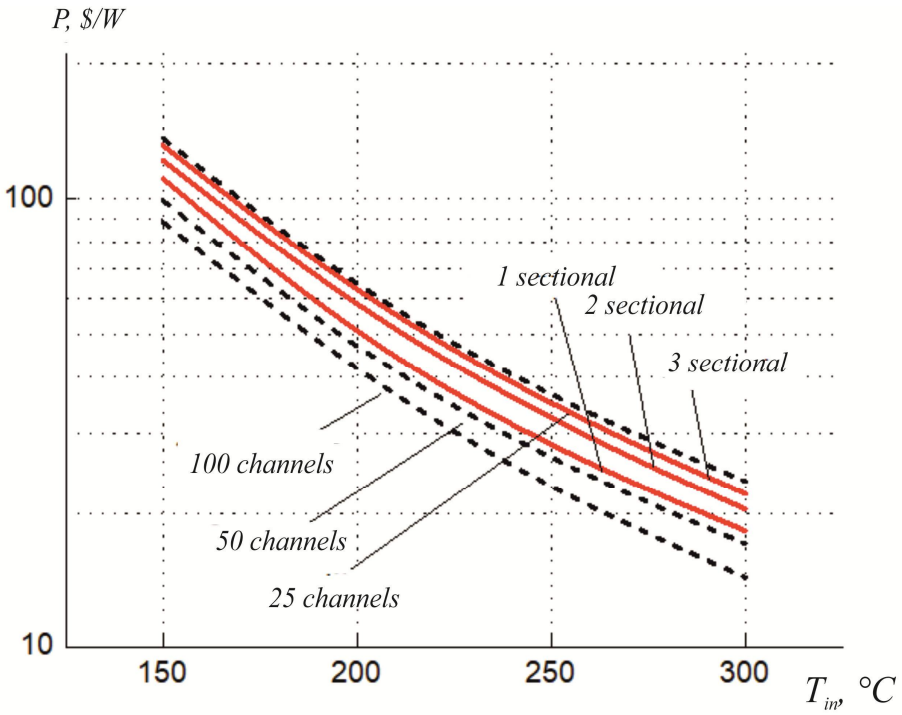


*Fig. 10. Unit cost of material for sectional and permeable TEC.*

According to these parameters, a permeable TEC which has from 50 to 100 channels per 1 см$^2$ in the legs of thermoelements is more efficient. Material consumption and unit cost for such a TEC is 25 - 35% less compared to a three-section converter.

Note that the economic characteristics of TEC significantly depend on the temperature of the heat carrier at the inlet to the heat exchanger. With a rise in temperature from 100 °C to 300 °C, the material consumption and the unit cost of both sectional and permeable TEC decrease by a factor of 25.

## Conclusions

The calculation and comparison of the parameters of sectional and permeable TEC allow the following conclusions:

1. In the ideal case, when the heat exchange area between the heat carrier and the thermoelectric material increases infinitely, the efficiency of a sectional thermoelement made of classical thermoelements of solid materials and a converter made of permeable thermoelements will be the same.

2. The most rational real models are a 3-section TEC of classical thermoelements and a permeable TEC, which has 50 channels per 1 cm$^2$ of thermoelectric material. The efficiency of these TECs is not much different.

3. In terms of economic indicators, a TEC made of permeable thermoelements is a better model, for which the consumption of thermoelectric material and the unit cost of 1 W of electricity can be 25 - 35% less than that of a sectional TEC.

4. Further research is needed on the effect of an increase in the heat exchange area in permeable modules and a decrease in the height of the legs of thermoelements made of solid materials in classical modules for each section on the energy and economic indicators of TEC.

## References

1. Cui, Y.J., Wang B.L., Wang K.F., Zheng L. (2019). Power output evaluation of a porous annular thermoelectric generator for waste heat harvesting. *International Journal of Heat and Mass Transfer*, 137, 979–989.
2. Kuz R.V. (2019). Thermoelectric generators for transport means: analysis of practical achievements. *J.Thermoelectricity*, 6, 1–10.
3. Anatychuk L.I., Kuz R.V. (2020). Efficiency of thermoelectric recuperators for rational temperatures of heat sources. *J.Thermoelectricity*, 4, 1–13.
4. Ismail Basel I., Ahmed Wael H. (2009). Thermoelectric power generation using waste-heat energy as an alternative green technology. *Recent Patents on Electrical Engineering*, 27-39.
5. Kuroki T., Kabeya K., Makino K., Kajihara T., Kaibe H., Hachiuma H., Matsuno H.(2014). Thermoelectric generation using heat in steal works. *Journal of Electronic Materials*.
6. Anatychuk L.I., Jenn-Dong Hwang, Lysko V.V. (2013). Thermoelectric heat recuperators for cement kilns. *J.Thermoelectricity*, 5, 39-45.
7. Kajikawa T. (2011). Advances in thermoelectric power generation technology in Japan. *J. Thermoelectricity*, 3, 5–19.
8. Montecucco A., Siviter J., Knox A.R. (2015). A combined heat and power system for solid-fuel stoves using thermoelectric generator. The 7th International Conference on Applied Energy – ICAE2015. *Energy Procedia*, 75, 597 – 602.
9. Gou X., Xiao H., Yang S. (2010). Modeling, experimental study and optimization on low-temperature waste heat thermoelectric generator system. *Appl. Energy*, 87, 3131–3136.
10. Villar A., Arribas J. (2012). Waste-to-energy technologies in continuous process industries. *Clean Techn Environ Policy*, 14, 29-39.
11. Yodovard P, Khedari J, Hirunlabh J. (2001). The potential of waste heat thermoelectric power generation from diesel cycle and gas turbine cogeneration plants. *Energy Sources*, 23, 213-224.
12. Karri M.A., Thacher E.F., Helenbrook B.T. (2011). Exhaust energy conversion by thermoelectric generator: two case studies. *Energy Convers. Manag*., 52, 1596–1611.
13. Anatychuk L.I., Morozov V.I., Mitin V.P., Prybyla A.V. (2012). Thermoelectric recuperator for gas turbines. *31-th International and 10-th European Conference on Thermoelectrics (Aalborg, Denmark, 2012)*.
14. In B.D., Kim H.L., Son J.W. (2015). The study of a thermoelectric generator with various thermal conditions of exhaust gas from a diesel engine. *Int. J. Heat Mass Transfer*, 86, 667–680.
15. Orr B., Akbarzadeh A., Mochizuki M., Singh R. (2016).A review of car waste heat recovery systems utilising thermoelectric generators and heat pipes. *Appl. Therm. Eng*., 101, 490–495.
16. X. Liu Y. D. Deng W. S. Wang C., Su Q. (2015). Experimental investigation of exhaust thermoelectric system and application for vehicle. *J. of Electronic Materials*, 44(6), 2203–2210.
17. Meng Jing-Hui, Wang Xiao-Dong, Chen Wei-Hsin (2016). Performance investigation and design optimization of a thermoelectric generator applied in automobile exhaust waste heat recovery. *Energy Convers. Manag*,120, 71–80.
18. Zhang Yanliang, Cleary Martin, Wang Xiaowei, Kempf Nicholas, Schoensee Luke, Yang Jian, Joshib Giri, Medac Lakshmikanth (2015). High-temperature and high-power-density nanostructured thermoelectric generator for automotive waste heat recovery. *Energy Convers. Manag*. 105, 946–950.
19. Kim S., Won B., Rhi S., Kim S.H., Yoo J. (2011). Thermoelectric power generation system for future hybrid vehicles using hot exhaust gas. *J. of Electronic Materials*, 40 (5).
20. Bosch Henry. (2016). From modules to a generator: An integrated heat exchanger concept for car applications of a thermoelectric generator. *J. of Electronic Materials*, 45(3).

21. Anatychuk L.I., Kuz R.V., Prybyla A.V. (2014). Efficiency improvement of sectional thermoelectric heat recuperators. *J.Thermoelectricity*, 6, 77–88.
22. *USSR Author's Certificate 162578* (1964). I.V.Zorin. Method for improving the efficiency of thermoelectric generator [in Russian].
23. Eura T., Komine T., Hasegava Y., Takata A., Katsuki F., Katoh M., Nakao K., Utsumi K.(2001). Research and development on a thermoelectric power generating system using low-calorie exhaust gas *(20th ICT, 2001, 409-412*).
24. Reddy E.S., Noudem J.G., Goupil C. (2007). Open porous foam oxide thermoelectric elements for hot gases and liquid environments. *Energy Convers. Manage*. 48, 1251–1254.
25. Cui Y.J., Wang B.L., Wang, K.F., et al. (2018). Fracture mechanics analysis of delamination buckling of a porous ceramic foam coating from elastic substrates. *Ceram. Int*. 44, 17986–17991.
26. Nithyanandam K., Mahajan R.L. (2018). Evaluation of metal foam based thermoelectric generators for automobile waste heat recovery. *J. Heat Mass Transfer*, 122, 877–883.
27. Koumoto K., Funahashi R., Guilmeau E., et al. (2013). Thermoelectric ceramics for energy harvesting. *J. Am. Ceram. Soc*. 96, 1–23.
28. Cherkez R. G. (2012). Energy possibilities of permeable generator thermoelements based on segmented legs. *AIP Conf. Proc*. 1449 (443), 439-442.
29. Cherkez R.G., Pozhar E.V., Zhukova A.S., Khrykov V.K. (2019). Influence of the number of channels on the efficiency of permeable thermoelements of *Bi-Te-Se-Sb* based materials. *J.Thermoelectricity*, 3, 58–63.
30. Anatychuk L.I., Cherkez R.G. (2003). Permeable thermoelement in electric energy generation mode. *J.Thermoelectricity*, 2003, 2, 35–45.
31. Burshtein A.I. (1964). *Semiconductor thermoelectric devices*. London: Temple Press.
32. Pontryagin L.S., Boltianskii V.G., Gamkrelidze R.V., Mishchenko E.F. (1976). *Matematicheskaia teoriia optimalnykh protsessov [Mathematical theory of optimal processes]*. Moscow: Nauka [in Russian].

Submitted 19.05.2021

**Анатичук Л.І.** *акад. НАН України*[1,2],
**Вихор Л.М** *докт. фіз.мат. наук*[1]
**Коцур М.П.** *канд. фіз.мат. наук*[1,2]
**Кузь Р.В.** *канд. фіз.мат. наук*[1,2]
**Черкез Р.Г.** *док. фіз.-мат. наук, в.о. професора*[1,2]

[1]Інститут термоелектрики НАН і МОН України,
вул. Науки, 1, Чернівці, 58029, Україна,
*e-mail: anatych@gmail.com*;
[2]Чернівецький національний університет
імені Юрія Федьковича, вул. Коцюбинського 2,
Чернівці, 58012, Україна

## ПОРІВНЯЛЬНИЙ АНАЛІЗ ТЕРМОЕЛЕКТРИЧНИХ ПЕРЕТВОРЮВАЧІВ ЕНЕРГІЇ З ПРОНИКНИМИ ТА

## УЦІЛЬНИМИ ТЕРМОЕЛЕМЕНТАМИ

*В роботі описані методи розрахунку оптимальних параметрів двох моделей термоелектричного перетворювача в режимі генерації електричної енергії, а саме секційного перетворювача з рухом теплоносія вздовж теплопоглинальних спаїв термоелементів і перетворювача з проникних термоелементів, в якому теплоносій проходить по каналам, розташованим вздовж висоти віток термоелементів. Розраховані енергетичні та економічні показники таких моделей і проведено їх порівняльний аналіз. Бібл. 32, рис. 10, табл. 1.*

**Ключові слова:** секційний термоелектричний перетворювач, проникний термоелемент, проникний термоелектричний перетворювач, термоелектричний генератор

**Анатычук Л.И.** *акад. НАН Украини*[1,2]
**Вихор Л.Н** *докт. физ.мат. наук*[1]
**Коцур М.П.** *канд. физ.мат. наук*[1,2]
**Кузь Р.В.** *канд. физ.мат. наук*[1,2]
**Черкез Р.Г.** *док. физ.-мат. наук, и.о. професора*[1,2]

[1]Институт термоэлектричества НАН и МОН Украины, ул. Науки, 1, Черновцы, 58029, Украина, *e–mail: anatych@gmail.com;*
[2]Черновицкий национальный университет им. Юрия Федьковича, ул. Коцюбинского, 2, Черновцы, 58012, Украина

## СРАВНИТЕЛЬНЫЙ АНАЛИЗ ТЕРМОЭЛЕКТРИЧЕСКИХ ПРЕОБРАЗОВАТЕЛЕЙ ЭНЕРГИИ С ПРОНИЦАЕМЫМИ И СПЛОШНЫМИ ТЕРМОЭЛЕМЕНТАМИ

*В работе описаны методы расчета оптимальных параметров двух моделей термоэлектрического преобразователя в режиме генерации электрической энергии, а именно секционного преобразователя с движением теплоносителя вдоль теплопоглощающих спаев термоэлементов и преобразователя из проницаемых термоэлементов, в котором теплоноситель проходит по каналам, расположенным вдоль высоты. Рассчитаны энергетические и экономические показатели таких моделей и проведен их сравнительный анализ. Библ. 32, рис. 10, табл. 1.*

**Ключевые слова:** секционный термоэлектрический преобразователь, проницаемый термоэлемент, проницаемый термоэлектрический преобразователь, термоэлектрический генератор

## References

1. Cui, Y.J., Wang B.L., Wang K.F., Zheng L. (2019). Power output evaluation of a porous annular thermoelectric generator for waste heat harvesting. *International Journal of Heat and Mass Transfer*, 137, 979–989.
2. Kuz R.V. (2019). Thermoelectric generators for transport means: analysis of practical achievements. *J.Thermoelectricity*, 6, 1–10.
3. Anatychuk L.I., Kuz R.V. (2020). Efficiency of thermoelectric recuperators for rational temperatures of heat sources. *J.Thermoelectricity*, 4, 1–13.
4. Ismail Basel I., Ahmed Wael H. (2009). Thermoelectric power generation using waste-heat energy as an alternative green technology. *Recent Patents on Electrical Engineering*, 27-39.

*5.* Kuroki T., Kabeya K., Makino K., Kajihara T., Kaibe H., Hachiuma H., Matsuno H.(2014). Thermoelectric generation using heat in steal works. *Journal of Electronic Materials.*
6. Anatychuk L.I., Jenn-Dong Hwang, Lysko V.V. (2013). Thermoelectric heat recuperators for cement kilns. *J.Thermoelectricity*, 5, 39-45.
7. Kajikawa T. (2011). Advances in thermoelectric power generation technology in Japan. *J. Thermoelectricity*, 3, 5–19.
8. Montecucco A., Siviter J., Knox A.R. (2015). A combined heat and power system for solid-fuel stoves using thermoelectric generator. The 7th International Conference on Applied Energy – ICAE2015. *Energy Procedia*, 75, 597 – 602.
9. Gou X., Xiao H., Yang S. (2010). Modeling, experimental study and optimization on low-temperature waste heat thermoelectric generator system. *Appl. Energy*, 87, 3131–3136.
10. Villar A., Arribas J. (2012). Waste-to-energy technologies in continuous process industries. *Clean Techn Environ Policy*, 14, 29-39.
11. Yodovard P, Khedari J, Hirunlabh J. (2001). The potential of waste heat thermoelectric power generation from diesel cycle and gas turbine cogeneration plants. *Energy Sources*, 23, 213-224.
12. Karri M.A., Thacher E.F., Helenbrook B.T. (2011). Exhaust energy conversion by thermoelectric generator: two case studies. *Energy Convers. Manag*., 52, 1596–1611.
13. Anatychuk L.I., Morozov V.I., Mitin V.P., Prybyla A.V. (2012). Thermoelectric recuperator for gas turbines. *31-th International and 10-th European Conference on Thermoelectrics (Aalborg, Denmark, 2012).*
14. In B.D., Kim H.L., Son J.W. (2015). The study of a thermoelectric generator with various thermal conditions of exhaust gas from a diesel engine. *Int. J. Heat Mass Transfer*, 86, 667–680.
15. Orr B., Akbarzadeh A., Mochizuki M., Singh R. (2016).A review of car waste heat recovery systems utilising thermoelectric generators and heat pipes. *Appl. Therm. Eng*., 101, 490–495.
16. X. Liu Y. D. Deng W. S. Wang C., Su Q. (2015). Experimental investigation of exhaust thermoelectric system and application for vehicle. *J. of Electronic Materials*, 44(6), 2203–2210.
17. Meng Jing-Hui, Wang Xiao-Dong, Chen Wei-Hsin (2016). Performance investigation and design optimization of a thermoelectric generator applied in automobile exhaust waste heat recovery. *Energy Convers. Manag*,120, 71–80.
18. Zhang Yanliang, Cleary Martin, Wang Xiaowei, Kempf Nicholas, Schoensee Luke, Yang Jian, Joshib Giri, Medac Lakshmikanth (2015). High-temperature and high-power-density nanostructured thermoelectric generator for automotive waste heat recovery. *Energy Convers. Manag*. 105, 946–950.
19. Kim S., Won B., Rhi S., Kim S.H., Yoo J. (2011). Thermoelectric power generation system for future hybrid vehicles using hot exhaust gas. *J. of Electronic Materials*, 40 (5).
20. Bosch Henry. (2016). From modules to a generator: An integrated heat exchanger concept for car applications of a thermoelectric generator. *J. of Electronic Materials*, 45(3).
21. Anatychuk L.I., Kuz R.V., Prybyla A.V. (2014). Efficiency improvement of sectional thermoelectric heat recuperators. *J.Thermoelectricity*, 6, 77–88.
22. *USSR Author's Certificate 162578* (1964). I.V.Zorin. Method for improving the efficiency of thermo-electric generator [in Russian].
23. Eura T., Komine T., Hasegava Y., Takata A., Katsuki F., Katoh M., Nakao K., Utsumi K.(2001). Research and development on a thermoelectric power generating system using low-calorie exhaust gas *(20th ICT, 2001, 409-412*).
24. Reddy E.S., Noudem J.G., Goupil C. (2007). Open porous foam oxide thermoelectric elements for hot gases and liquid environments. *Energy Convers. Manage*. 48, 1251–1254.
25. Cui Y.J., Wang B.L., Wang, K.F., et al. (2018). Fracture mechanics analysis of delamination buckling

of a porous ceramic foam coating from elastic substrates. *Ceram. Int*. 44, 17986–17991.
26. Nithyanandam K., Mahajan R.L. (2018). Evaluation of metal foam based thermoelectric generators for automobile waste heat recovery. *J. Heat Mass Transfer*, 122, 877–883.
27. Koumoto K., Funahashi R., Guilmeau E., et al. (2013). Thermoelectric ceramics for energy harvesting. *J. Am. Ceram. Soc*. 96, 1–23.
28. Cherkez R. G. (2012). Energy possibilities of permeable generator thermoelements based on segmented legs. *AIP Conf. Proc*. 1449 (443), 439-442.
29. Cherkez R.G., Pozhar E.V., Zhukova A.S., Khrykov V.K. (2019). Influence of the number of channels on the efficiency of permeable thermoelements of *Bi-Te-Se-Sb* based materials. *J.Thermoelectricity*, 3, 58–63.
30. Anatychuk L.I., Cherkez R.G. (2003). Permeable thermoelement in electric energy generation mode. *J.Thermoelectricity*, 2003, 2, 35–45.
31. Burshtein A.I. (1964). *Semiconductor thermoelectric devices*. London: Temple Press.
32. Pontryagin L.S., Boltianskii V.G., Gamkrelidze R.V., Mishchenko E.F. (1976). *Matematicheskaia teoriia optimalnykh protsessov [Mathematical theory of optimal processes]*. Moscow: Nauka [in Russian].

Submitted 19.05.2021

*Anatychuk L.I..*

**Anatychuk L.I.,** *acad. National Academy of Sciences of Ukraine*[1,2]
**Lysko V.V.,** *cand. phys.-math. sciences*[1,2]

[1]Institute of Thermoelectricity of the NAS and MES of Ukraine, 1 Nauky str., Chernivtsi, 58029, Ukraine, *e-mail: anatych@gmail.com*;
[2]Yu.Fedkovych Chernivtsi National University, 2, Kotsiubynskyi str., Chernivtsi, 58012, Ukraine

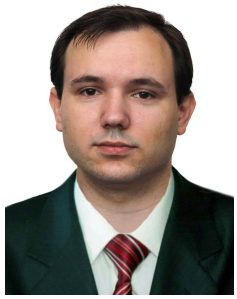

*Lysko V.V.*

# DETERMINATION OF THE TEMPERATURE DEPENDENCES OF THERMOELECTRIC PARAMETERS OF MATERIALS USED IN GENERATOR THERMOELECTRIC MODULES WITH A RISE IN TEMPERATURE DIFFERENCE

*A method is proposed for determining the thermoelectric parameters of materials used in generator thermoelectric modules in the case when the cold side of module is thermostated, and the temperature difference across the module gradually increases due to a rise in the hot side temperature with the help of an electric heater. A detailed physical model of this method is considered and the results of estimating possible values of measurement errors are presented.*

**Key words:** measurement, electric conductivity, thermoEMF, thermal conductivity, figure of merit, thermoelectric module.

## Introduction

Further progress in thermoelectricity largely depends on the quality of thermoelectric material, which is determined by the figure of merit Z of the material and on which the efficiency of thermoelectric power converters depends, namely the efficiency of generators, the maximum temperature difference and coefficient of performance of coolers, and the heating coefficient of heaters. In this case, the most effective are experimental methods of material optimization, which are reduced to creating a set of samples of materials of different composition and with different concentrations of impurities, measuring their electrical conductivity, thermoEMF, thermal conductivity and determining the figure of merit Z. In this procedure, the correct measurement of these material parameters plays a decisive role. Preliminary studies carried out at the Institute of Thermoelectricity of the National Academy of Sciences and the Ministry of Education and Science of Ukraine made it possible to develop methods and create equipment for accurate determination of the properties of thermoelectric materials by the absolute method, the accuracy of which exceeds the accuracy of world analogues by a factor of 3-5.

The task of creating measuring equipment for studying the parameters of materials used in ready-made thermoelectric power converters remains important. This information is necessary both for optimizing the thermoelectric material for its specific applications, and for improving the design of the thermoelectric converters themselves, improving the technology for creating connecting junctions, and also expanding the possibilities for quality control of the finished product. The most suitable for solving this problem is the absolute method for measuring the parameters of generator thermoelectric modules and

equipment ALTEC-10002 based on it [8]. At the Institute of Thermoelectricity, a method for determining the thermoelectric parameters of the module leg material when measuring its parameters by the absolute method is developed, a detailed physical model of this method is considered and the results of estimating possible error values are given. However, practical implementation of this method encounters difficulties due to the fact that for measurements it is required to create a small temperature difference (about 10 °C) at temperatures of both sides of the module up to 500–600 °C.

*The purpose of this work* is to create a method for determining the thermoelectric parameters of materials used in the generator thermoelectric modules for the case when the cold side of module is thermostated, and the temperature difference on the module gradually increases due to a rise in the hot side temperature.

## Description of the method for determining the σ, α, κ, *Z* of the legs material when measuring parameters of a generator thermoelectric module

The method for determining the average values σ, α, κ, Z of the legs material making up the module is as follows:

– determination of electrical conductivity σ by the measured value of the AC resistance of the module and the known design of the module;

– determination of the Seebeck coefficient α by the measured values of module EMF and temperature difference between the heater and the heat sink (with regard to corrections);

– determination of thermal conductivity κ according to the measured values of heat flow through the module (using a heat meter) and the temperature difference between the heater and the heat sink (taking into account corrections and minimizing heat loss).

The average values of electrical conductivity, thermoEMF, thermal conductivity and figure of merit of the material of thermoelectric module legs are determined by the formulae

$$\sigma = \frac{1}{R_M / 2N} \frac{h_1}{a_1 \cdot b_1}, \tag{1}$$

$$\alpha = \frac{E / 2N}{(T_{h_0} - T_{x_0})}, \tag{2}$$

$$\kappa = \frac{Q / 2N}{(T_{h_0} - T_{x_0})} \frac{h_1}{a_1 \cdot b_1}, \tag{3}$$

$$Z = \frac{\alpha^2 \sigma}{\kappa}, \tag{4}$$

where $R_M$ is module resistance measured on alternating current; $a_1 \times b_1$ is the cross-section of legs; $h_1$ is the height of legs; $N$ is the number of pairs; $E$ is the EMF of module; $Th_0$ is the temperature on the heat-leveling plate located on the hot side of module; $Tc_0$ is the temperature on heat meter located on the cold side of module; $Q$ is heat flow through the module measured by heat meter.

In Fig. 1: $Q$ is heat released by heater 11; $Q_1$ is heat transferred from heater 11 to the "hot" side of module 5; $Q_2$ is heat transferred from heat leveling plate 6 to shield 7 by convection; $Q_3$ is heat transferred from heat leveling plate 6 to shield 7 by radiation; $Q_4$, $Q_{10}$ is heat transferred from heater 11 to shield 7 through heater wires; $Q_5$, $Q_9$ is heat transferred from heater 11 to shield 7 through potential heater wires; $Q_6$

is heat transferred from heater 11 to shield 7 through the module clamp; $Q_7$ is heat transferred from heater 11 to shield 7 by convection; $Q_8$ is heat transferred from heater 11 to shield 7 by radiation; $Q_{11}$ is heat transferred from heat leveling plate 6 to shield 7 through wires of thermocouple 21; $Q_{12}$ is heat transferred from module 5 to shield 7 by convection; $Q_{13}$ is heat transferred from module 5 to shield 7 by radiation; $Q_{14}$, $Q_{19}$ is heat transferred from module 5 to shield 7 through module wires 4 and 23; $Q_{15}$ is heat transferred from heat meter 2 to shield 7 through wires of thermocouple 25; $Q_{16}$ is heat transferred from the "cold" side of module 5 to heat meter 2; $Q_{17}$ is heat transferred from heat meter 2 to shield 7 by convection; $Q_{18}$ is heat transferred from heat meter 2 to shield 7 by radiation.

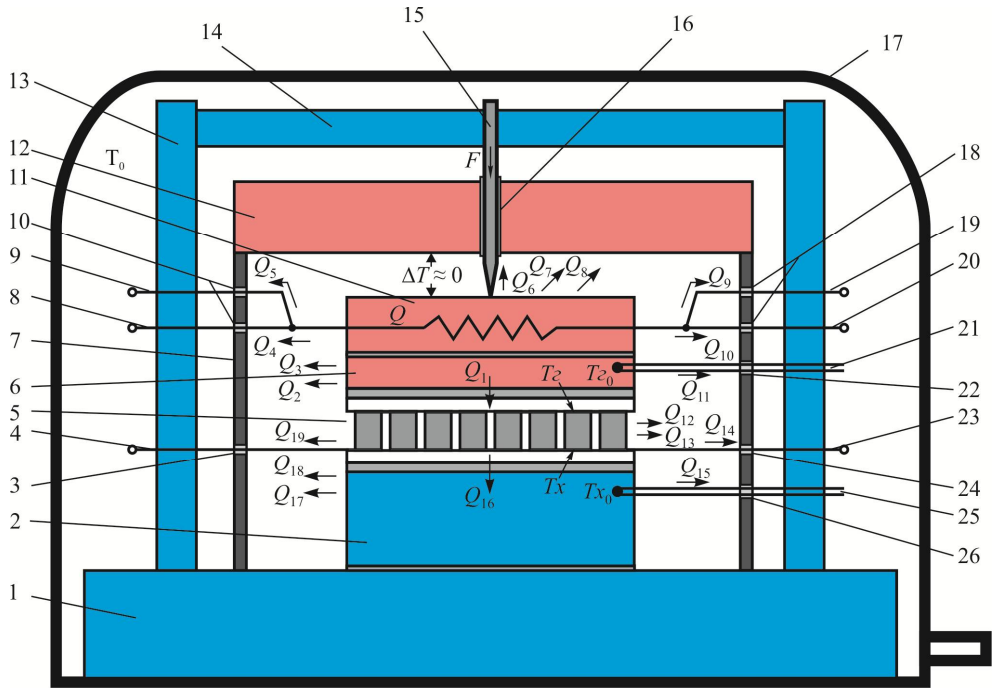


*Fig. 1. Schematic for determining the thermoelectric parameters of materials when measuring the parameters of generator thermoelectric modules using thermal switches and radiation shield: 1 – device for providing the required "cold" temperature of module; 2 – heat meter; 3, 10, 16, 18, 22, 24, 26 – thermal switches; 4, 23 – module wires; 5 – module; 6 – heat leveling plate; 7 – gradient radiation shield; 8, 20 – heater wires; 9, 19 – potential heater wires; 11 – module heater; 12 – shield heater; 13 – clamping mechanism racks; 14 – clamping bar; 15 – clamping screw; 17 – bell jar; 21, 25 – thermocouples.*

In this case, due to the temperature dependence of the thermoelectric parameters of material, measurements should be carried out at small temperature differences. Therefore, to apply this technique on equipment for measuring generator modules, in which temperatures can be in the range of $T_c$ = 30 - 90 °C, $T_h$ = 30 - 600 °C, additional operations are required to determine the parameters of materials with a rise in temperature difference.

In general, *the method for determining the average values σ, α, κ, Z of the legs material with a rise in temperature difference* will include the following steps.

1. Accurate measurements of σ, α, κ, $Z$ with temperature difference up to 10 K in the temperature range of the cold module side $T_c$ = 30 – 90 °C (for instance: $T_c$ = 30 °C, $T_h$ = 40 °C).

2. Determination of σ, α, κ, $Z$ at temperature differences greater than 10 K.

2.1. Determination of thermal conductivity κ.

To determine the thermal conductivity at each subsequent value of the temperature difference, the value of thermal conductivity obtained from the results of previous measurements is used. It allows dividing the thermal resistance $K_T$ of the leg into two parts (Fig. 2): thermal resistance $K_T^{N-1}$ of the leg section from $x = 0$ to $x = L^{N-1}$, where the temperature difference is equal to the difference of the previous investigated point – $(Th^{N-1} - Tc)$;

- thermal resistance $K_T^{N}$ of the leg section from $x = L^{N-1}$ to $x = L^{N} = L_{total.}$, where the temperature difference is equal to $(Th^{N} - Th^{N-1}) \approx 10$ K.

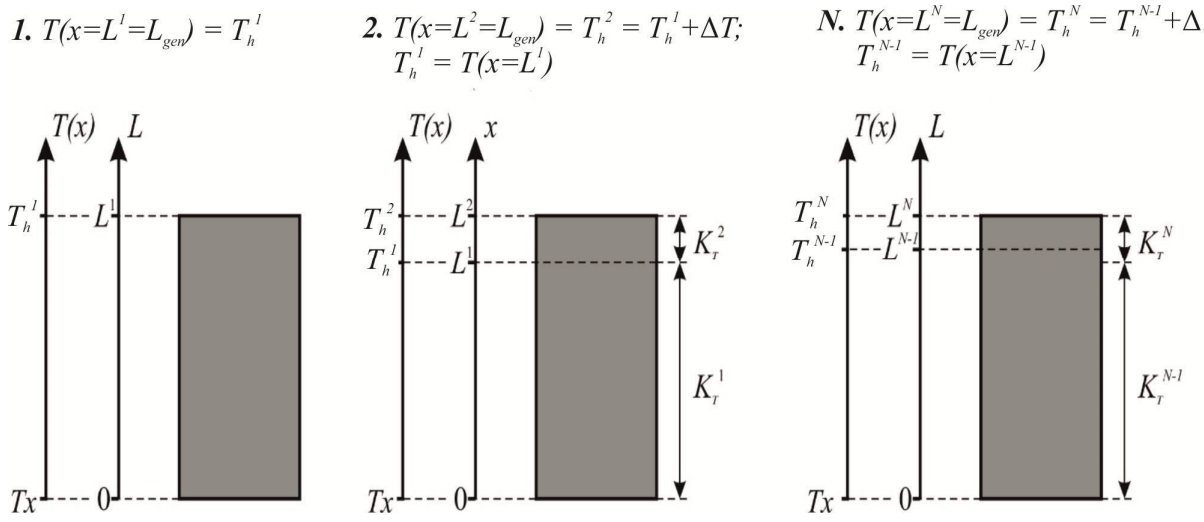


*Fig. 2. Procedure for determining the thermal conductivity of the legs material with a rise in temperature difference*

Then the value of thermal conductivity at temperature $(Th^{N} + Th^{N-1})/2$ will be determined by the formula

$$\kappa\left(\frac{Tc^{N} + Tc^{N-1}}{2}\right) = \frac{L_{total.}}{a_1 \cdot b_1} \frac{Q^{N} - Q^{N-1}}{\left(Tc^{N} - T_0\right) - \left(Tc^{N-1} - T_0\right)}, \tag{5}$$

2.2. Determination of the Seebeck coefficient α.

$$\alpha\left(\frac{Tc^{N} + Tc^{N-1}}{2}\right) = \frac{E^{N} - E^{N-1}}{\left(Tc^{N} - T_0\right) - \left(Tc^{N-1} - T_0\right)}, \tag{6}$$

2.3. Determination of electrical conductivity σ.

Electrical conductivity can be determined according to the procedure described in paragraph 2.1 for thermal conductivity, using electric resistance $R$ instead of thermal resistance $K_T$.

$$\sigma\left(\frac{Tc^{N} + Tc^{N-1}}{2}\right) = \frac{L_{total.}}{a_1 \cdot b_1} \frac{1 - \frac{Q^{N-1}}{Q^{N}}}{R^{N} - R^{N-1} \cdot \frac{Q^{N-1}}{Q^{N}}}, \tag{7}$$

2.4. Determination of the figure of merit Z.

The figure of merit of the leg material is determined by the classical ratio

$$Z(T) = \frac{\alpha^2(T) \cdot \sigma(T)}{\kappa(T)}. \quad (8)$$

where:

$$\alpha(T) = A_0 + A_1 \cdot T + A_2 \cdot T^2 + \ldots + A_n \cdot T^n, \quad (9)$$

$$\sigma(T) = B_0 + B_1 \cdot T + B_2 \cdot T^2 + \ldots + B_n \cdot T^n, \quad (10)$$

$$\kappa(T) = C_0 + C_1 \cdot T + C_2 \cdot T^2 + \ldots + C_n \cdot T^n, \quad (11)$$

where $A_i$, $B_i$, $C_i$, are coefficients of polynomials, $n$ is polynomial degree.

## Results of estimation of possible errors of the proposed method

To test the proposed method for determining the temperature dependences of the thermoelectric parameters of materials used in generator thermoelectric modules with a rise in temperature difference, a computer experiment was carried out in the COMSOL Multiphysics application package. To do this, a computer model of thermoelectric generator module Altec-1061 was created with the following parameters: number of pairs – 56; leg height – 3 mm; leg cross section – 1.8 mm x 4.2 mm; ceramics thickness – 0.65 mm; ceramics area – 40 mm × 40 mm; interconnect thickness – 0.25 mm.

The temperature dependences of the thermoelectric properties of module legs material based on Bi-Te are given by polynomials

$$\alpha(T) = 178.25 + 0.6507 \cdot T - (3.9 \times 10^{-3}) \cdot T^2 + (5 \times 10^{-6}) \cdot T^3, \quad (12)$$

$$\sigma(T) = 1356.2 - 6.1067 \cdot T + (1.38 \times 10^{-2}) \cdot T^2 - (7 \times 10^{-6}) \cdot T^3, \quad (13)$$

$$\kappa(T) = 1.4987 + (2 \times 10^{-4}) \cdot T - (8 \times 10^{-6}) \cdot T^2 + (7 \times 10^{-8}) \cdot T^3, \quad (14)$$

$$Z(T) = \frac{\alpha^2(T) \cdot \sigma(T)}{\kappa(T)}. \quad (15)$$

The cold side of the module was thermostated at a temperature $Tc$ = 30 °C. The temperature of the hot side gradually increased, starting from $Th$ = 40 °C with a step of 10 °C and at each subsequent step according to the computer simulations of temperature and electric potential distributions found in the module, the average values σ, α, κ, $Z$ of legs material were calculated by formulae (5) - (8) of the procedure described in paragraph 1.

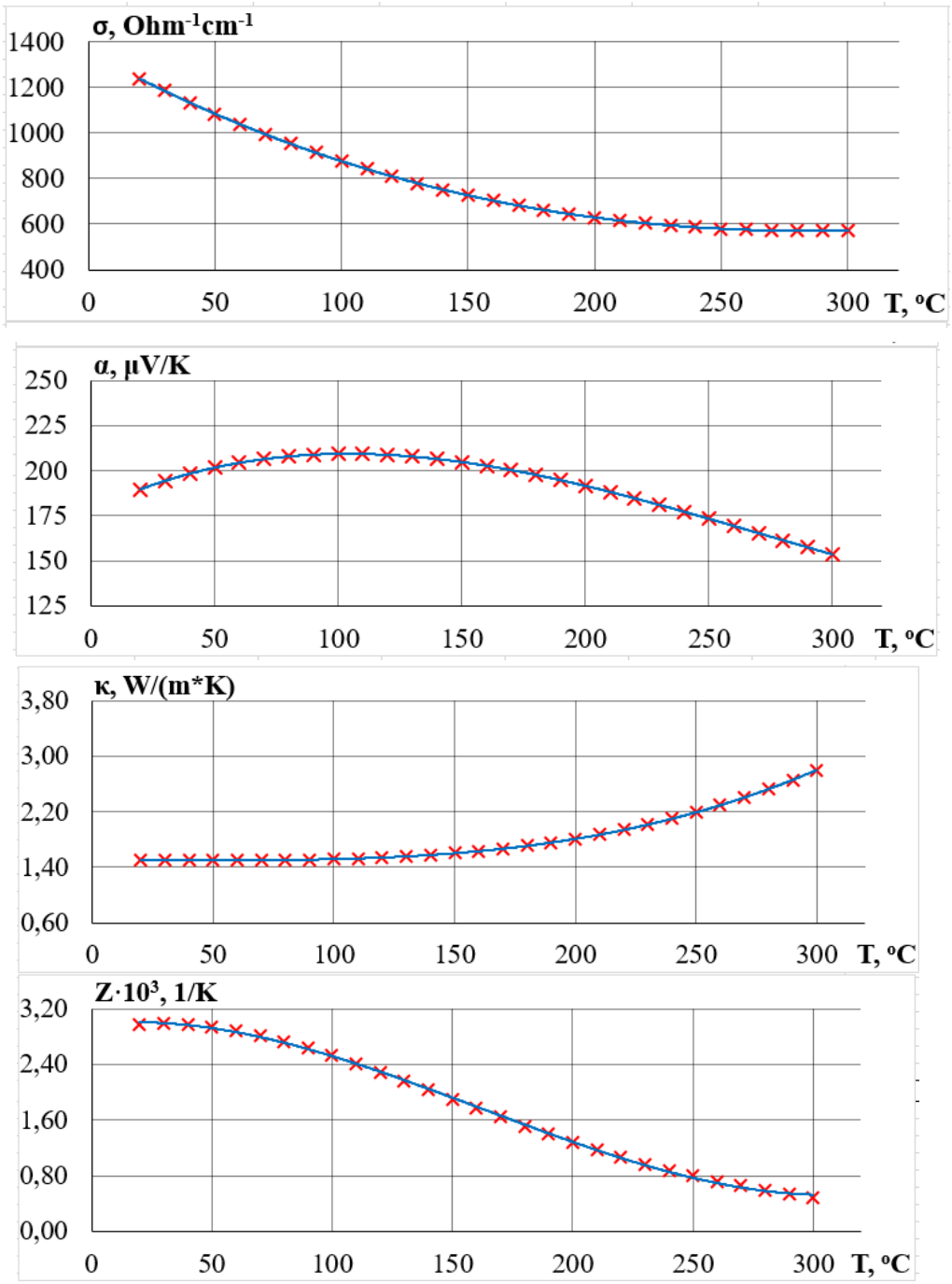


*Fig. 3. Temperature dependences of the thermoelectric properties of Bi-Te based material (the lines indicate the dependences constructed using polynomials (5)-(8), the marks "x" are the results obtained by a computer experiment using the proposed measurement technique).*

Fig. 3 compares the temperature dependences of the thermoelectric properties of module legs material obtained by a computer experiment in COMSOL Multiphysics using the proposed measurement method and given by polynomials (12) - (15). According to the results of computer simulations, the errors in determining the σ, α, κ, *Z* of legs material with a rise in temperature difference by the proposed method do not exceed 2-3%. The proposed method is easier to implement and is the basis for the modernization of "ALTEC-10002" equipment for measuring the parameters of thermoelectric generator modules.

## Conclusions

1. A method is proposed for determining the temperature dependences of the thermoelectric properties of the legs material of generator thermoelectric module when measuring its parameters by the absolute method. A detailed physical model of this method is considered and an estimate of possible errors is made.
2. Computer experiment has been used to confirm the possibility of determining the thermoelectric parameters of materials used in generator thermoelectric modules in the case when the cold module side is thermostated, and the temperature difference on the module gradually increases due to a rise in its hot side temperature. In so doing, the errors in determining the σ, α, κ, *Z* of legs material do not exceed 2-3%.

## References

1. Anatychuk L.I., Lysko V.V. (2012). Investigation of the effect of radiation on the precision of thermal conductivity measurement by the absolute method. *J.Thermoelectricity*, 1, 67-76.
2. Anatychuk L.I., Havrylyuk N.V., Lysko V.V. (2012). Methods and equipment for quality control of thermoelectric materials. *J. Electronic Materials*, 41(6), 1680-1685.
3. Anatychuk L.I., Lysko V.V. (2012). Modified Harman's method. *AIP Conf. Proc*., 1449, 373-376.
4. Anatychuk L.I., Lysko V.V. (2014). On improvement of the accuracy and speed in the process of measuring characteristics of thermoelectric materials. *J. Electronic Materials*, 43 (10), 3863-3869.
5. Anatychuk L.I., Havryliuk M.V., Lysko V.V. (2015). Absolute method for measuring of thermoelectric properties of materials. *Materials Today: Proceedings*, 2, 737 – 743.
6. Anatychuk L.I., Lysko V.V. (2014). Methods for assuring high quality electric and thermal contacts when measuring parameters of thermoelectric materials. *J.Thermoelectricity*, 4, 83-90.
7. *Patent for utility model № 127473* (2018). L.I. Anatychuk, M.V.Havryliuk, V.V. Lysko. Automated device for determining electric conductivity, thermal conductivity, thermoEMF and figure of merit of thermoelectric materials [in Ukrainian].
8. Anatychuk L.I., Havryliuk M.V. (2011). Procedure and equipment for measuring parameters of thermoelectric generator modules. *J. Electronic Materials*, 40(5), 1292 - 1297.

Submitted 06.05.2021

**Анатичук Л.І.** *акад. НАН України*
**Лисько В.В.** *канд. фіз.-мат. наук*

[1]Інститут термоелектрики НАН і МОН України,
вул. Науки, 1, Чернівці, 58029, Україна,
*e-mail: anatych@gmail.com*;
[2]Чернівецький національний університет
імені Юрія Федьковича, вул. Коцюбинського 2,
Чернівці, 58012, Україна

## ВИЗНАЧЕННЯ ТЕМПЕРАТУРНИХ ЗАЛЕЖНОСТЕЙ ТЕРМОЕЛЕКТРИЧНИХ ПАРАМЕТРІВ МАТЕРІАЛІВ У СКЛАДІ ГЕНЕРАТОРНИХТЕРМОЕЛЕКТРИЧНИХ МОДУЛІВ ПРИ ЗРОСТАЮЧОМУ ПЕРЕПАДІ ТЕМПЕРАТУР

*Запропоновано методику визначення термоелектричних параметрів матеріалів у складі*

*генераторних термоелектричних модулів у випадку, коли холодна сторона модуля є термостатованою, а перепад температури на модулі поступово зростає за рахунок підвищення температури гарячої сторони за допомогою електричного нагрівника. Розглянуто детальну фізичну модель цієї методики та наведено результати оцінки можливих величин похибок при вимірюваннях. Бібл. 8, рис. 3.*
**Ключові слова:** вимірювання, електропровідність, термоЕРС, теплопровідність, добротність, термоелектричний модуль.

**Анатичук Л.И.** *акад. НАН Украины*
**Лисько В.В.** *канд. физ.-мат. наук*

[1]Институт термоэлектричества НАН и МОН Украины, ул. Науки, 1, Черновцы, 58029, Украина, e-mail: anatych@gmail.com ;
[2]Черновицкий национальный университет им. Юрия Федьковича, ул. Коцюбинского, 2, Черновцы, 58012, Украина

## МЕТОДИКА ОПРЕДЕЛЕНИЯ ТЕРМОЭЛЕКТРИЧЕСКИХ ПАРАМЕТРОВ МАТЕРИАЛОВ В СОСТАВЕ ТЕРМОЭЛЕКТРИЧЕСКИХ МОДУЛЕЙ ОХЛАЖДЕНИЯ

*Предложена методика определения термоэлектрических параметров материалов в составе термоэлектрических модулей охлаждения. Рассмотрена подробная физическая модель этой методики и приведены результаты оценки возможных величин погрешностей. Исследована эффективность применения различных методов снижения погрешностей. Библ. 8, рис. 2, табл. 1.*
**Ключевые слова:** измерение, электропроводность, термоЭДС, теплопроводность, добротность, термоэлектрический модуль.

## References

1. Anatychuk L.I., Lysko V.V. (2012). Investigation of the effect of radiation on the precision of thermal conductivity measurement by the absolute method. *J.Thermoelectricity*, 1, 67-76.
2. Anatychuk L.I., Havrylyuk N.V., Lysko V.V. (2012). Methods and equipment for quality control of thermoelectric materials. *J. Electronic Materials*, 41(6), 1680-1685.
3. Anatychuk L.I., Lysko V.V. (2012). Modified Harman's method. *AIP Conf. Proc.*, 1449, 373-376.
4. Anatychuk L.I., Lysko V.V. (2014). On improvement of the accuracy and speed in the process of measuring characteristics of thermoelectric materials. *J. Electronic Materials*, 43 (10), 3863-3869.
5. Anatychuk L.I., Havryliuk M.V., Lysko V.V. (2015). Absolute method for measuring of thermoelectric properties of materials. *Materials Today: Proceedings*, 2, 737 – 743.
6. Anatychuk L.I., Lysko V.V. (2014). Methods for assuring high quality electric and thermal contacts when measuring parameters of thermoelectric materials. *J.Thermoelectricity*, 4, 83-90.
7. *Patent for utility model № 127473* (2018). L.I. Anatychuk, M.V.Havryliuk, V.V. Lysko. Automated device for determining electric conductivity, thermal conductivity, thermoEMF and figure of merit of thermoelectric materials [in Ukrainian].
8. Anatychuk L.I., Havryliuk M.V. (2011). Procedure and equipment for measuring parameters of thermoelectric generator modules. *J. Electronic Materials*, 40(5), 1292 - 1297.

Submitted 06.05.2021


*Anatychuk L.I.*

**Anatychuk L.I.,** *acad. National Academy of Sciences of Ukraine*[1,2]
**Lysko V.V.,** *cand. phys.-math. sciences*[1,2]

[1]Institute of Thermoelectricity of the NAS and MES of Ukraine, 1 Nauky str., Chernivtsi, 58029, Ukraine,
*e-mail: anatych@gmail.com*;
[2]Yu.Fedkovych Chernivtsi National University,
2, Kotsiubynskyi str., Chernivtsi, 58012, Ukraine

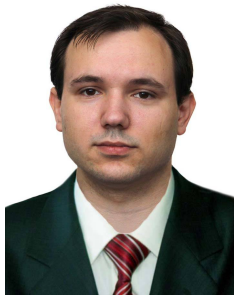
*Lysko V.V.*

# COMPUTER DESIGN OF A THERMOELECTRIC GENERATOR FOR HEAT AND ELECTRICITY SUPPLY TO HEAVY-DUTY VEHICLES

*The physical model of the thermoelectric generator for the autonomous system of pre-heating of high-power vehicles is considered. The design of heat exchangers of heat supply and exhaust systems, which allow to ensure the optimal mode of operation of thermoelectric modules, has been determined by computer design. The design of a thermoelectric generator with an electric power of up to 350 W has been developed, which will be enough to supply electric energy to preheaters with a thermal power of 25-30 kW. Such a system, taking into account the thermal energy of the thermoelectric generator, will be equivalent to more powerful preheaters (36 - 40 kW), but will not require the use of battery electricity. Bibl. 8, Fig. 9, Table. 1.*
**Key words:** starting heater, thermoelectric generator, physical model, computer simulation.

## Introduction

Operation of vehicles at low ambient temperatures requires the use of methods of preliminary thermal preparation of engines for start-up. The most common methods of preheat treatment of engines used for heavy-duty civil and military equipment include refuelling the engine cooling system and lubrication system with hot antifreeze and engine oil, the use of furnaces that heat the crankcase by direct flame, heating air filters by introducing filter heads for small amounts of fuel from a special electric glow plug, the use of heaters to heat the air entering the engine cylinders, etc. However, these methods of preheating engines are inefficient and time consuming. Therefore, pre-heaters are used more and more, which run on vehicle fuel and heat the engine coolant [1, 2]. An effective method of solving the problem of discharging the battery of vehicles during the operation of preheaters is the use of a thermoelectric generator that operates from the heat of the heater and provides autonomous power to its components [3 - 5]. Moreover, the electric energy excess of thermal generator can be used for battery charging and power supply to other equipment.

The Institute of Thermoelectricity has created an experimental sample of a thermoelectric preheater with a thermal power of 3.5 kW and a maximum electric power of 100 W for heating vehicles with an engine capacity of up to 4 liters [6, 7].

Preliminary analysis [8] shows the prospects for such uses to improve the operational capabilities of heavy-duty vehicles, including armoured vehicles.

The purpose of this work is to develop and optimize the design of a thermoelectric generator for the autonomous source of heat and electricity for heavy-duty vehicles.

## Physical model of a thermoelectric generator and its mathematical description

To find the optimal design of the generator, it is necessary to consider its physical model (Fig. 1). The model consists of five sections, each of which containing a hot heat exchanger, thermoelectric modules and a cold heat exchanger. The design of heat exchangers of each section must be optimized to achieve the optimal mode of operation of all thermoelectric modules. The model provides a separate heat source – air heater on diesel fuel. Heat is supplied to the hot heat exchanger of the generator due to forced convection of hot fuel combustion products moving in the heat exchanger channels. Heat removal from thermoelectric modules is carried out by a liquid coolant that is forcibly circulating in the system.

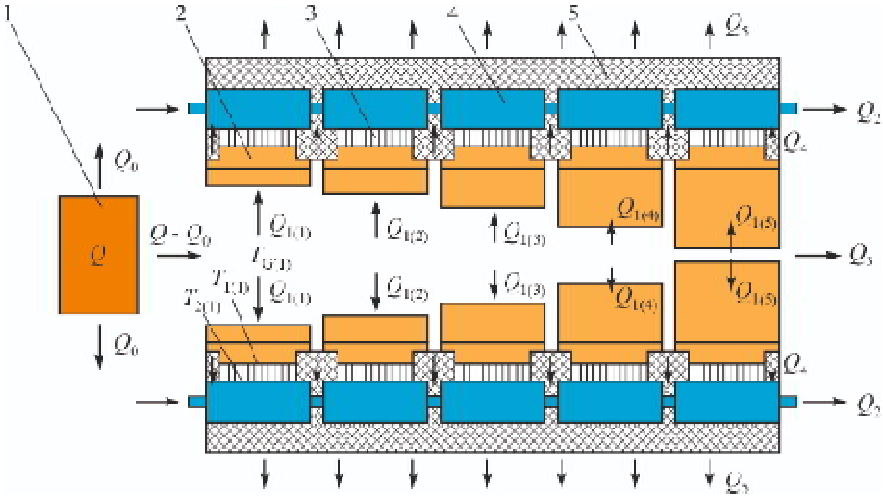


*Fig. 1. Physical model of a thermoelectric generator for heat and electricity source for armoured vehicles.: 1 – heat source; 2 – hot heat exchanger (radiator); 3 – thermopile; 4 – cold heat exchanger; 5 – thermal insulation*

The thermoelectric converter is composed of standard thermoelectric modules Altec - 1061 that are most suitable for creation of thermoelectric recuperators. The optimal temperature of the hot side of modules is about 280 - 300°C, and of the cold side – 30 - 50 °C.

The heat $Q_{1(i)}$ which comes to the hot heat exchanger of $i$-th section is passed by way of convection and radiation:

$$Q_{1(i)} = \alpha_{(i)} \cdot \left(T_{G(i)} - T_{r(i)}\right) \cdot S_{R(i)} + \varepsilon_{(i)} \cdot \sigma_0 \cdot \left( \varepsilon_G \cdot \left(\frac{T_{G(i)}}{100}\right)^4 - A_{r(i)} \cdot \left(\frac{T_{r(i)}}{100}\right)^4 \right) \cdot S_{R(i)}, \qquad (1)$$

where $\alpha_{(i)}$ is convective coefficient of heat exchange from the hot gas to heat receiving surface of the hot heat exchanger of the $i$-th section; $T_{G(i)}$ is the average gas temperature in the hot heat exchanger of the $i$-th section; $T_{r(i)}$ is the average temperature of the heat receiving surface of the hot heat exchanger of the $i$-th section; $S_{R(i)}$ is the area of heat receiving surface of the hot heat exchanger of the $i$-th section; $\varepsilon_{(i)} = (\varepsilon_{r(i)}+1)/2$ is the effective degree of blackness of the "hot gas-heat receiving surface" system of the hot heat exchanger of the $i$-th section; $\varepsilon_{r(i)}$ is the degree of blackness of the heat receiving surface of the hot heat exchanger of the $i$-th section; $\sigma_0$ is Stephan-Boltzmann constant; $\varepsilon_G$ is the degree of blackness of gas; $A_{r(i)}$ is the absorptivity of the heat receiving surface of the hot heat exchanger of the $i$-th section.

Heat $Q_2$ is removed from the cold side of thermoelectric modules with the flow of heat carrier which circulates in the cold liquid heat exchanger 4:

$$Q_2 = g_T \cdot c_{pT} \cdot \left(T_{вх} - T_{вих}\right), \qquad (2)$$

where $g_T$ is heat carrier consumption; $c_{pT}$ is heat capacity of heat carrier $T_{in}$, $T_{out}$ are temperatures of heat carrier at the inlet and outlet of system for cooling thermoelectric modules, respectively.

As long as the cold liquid heat exchangers are combined into one hydraulic loop with engine cooling system 5, the heat dissipated from the modules is used to preheat the engine.

The main losses of heat are determined as follows:

1) $Q_3$ – with reaction products (water $H_2O$, carbon dioxide $CO_2$ and nitrogen $N_2$):

$$Q_3 = C_c \cdot m_c \cdot \left(T_{G(вих.)} - T_0\right), \tag{3}$$

where $C_c$ is the average heat capacity of reaction products, $m_c$ is the mass of reaction products, $T_{G(out)}$ is the temperature of reaction products at the outlet from the generator.

2) $Q_4$ – on the thermal insulation:

$$Q_4 = \frac{\lambda S_{рг}}{L}(T_Б - T_0), \tag{4}$$

where $\lambda$ is thermal conductivity of insulation material; $S_{рг}$ is the surface area of the hot heat exchanger not occupied by thermopile; $L$ is the thickness of thermal insulation layer.

Thus, the heat balance equation for this physical model of thermoelectric generator can be written as:

$$\begin{cases} Q = Q_0 + \sum_{i=1}^{n} Q_{1(i)} + Q_3 + Q_5, \\ Q_6 = P + Q_2 + Q_4. \end{cases} \tag{5}$$

where $n$ is the number of sections in the hot heat exchanger of thermoelectric generator.

The relationship between the velocity $v$ and the hot gas temperature $T_G$ in the heat exchanger is determined by the formula:

$$v = 5 \cdot \left[ \frac{\frac{G_n}{T_G - T_0} - K_1}{K_2} + 1 \right] \cdot \frac{K(O_2) \cdot g_n}{\rho_{T0} \cdot \pi \cdot d^2 / 4}, \tag{3.36}$$

where $K(O_2)$ is coefficient that determines the amount of oxygen necessary for full combustion of fuel, $d$ is the diameter of combustion chamber; $K_1$ and $K_2$ are coefficients that determine the amount of carbon dioxide, water, nitrogen and air which formed as a result of full combustion of fuel and are derived with regard to specific values of gas volatility degrees $i$, Mendeleev-Klapeyron constant $R$ and gas molar mass $\mu$; $g_n$ is air consumption; $\rho_{T0}$ is air density at a given ambient temperature $T_0$.

The solution of the system of thermal balance equations (5) allows determining the main energy and structural parameters of the generator. It was implemented in the Comsol Multiphysics application package by finite-element method in two steps which aimed at determining:

– the effective geometry of the hot heat exchanger and optimal fuel consumption and air velocity $v$ to assure maximum operating temperature of thermopile hot junctions;

– the effective geometry of the cold heat exchanger and optimal heat carrier consumption to assure the necessary operating temperature of thermopile cold junctions.

The input data for the calculation of structural parameters of the heater hot heat exchanger are the dependences of electric power $P_{mod}$ and the efficiency $\eta_{mod}$ of the used thermoelectric generator modules of the type Altec-1061 (Fig. 2).

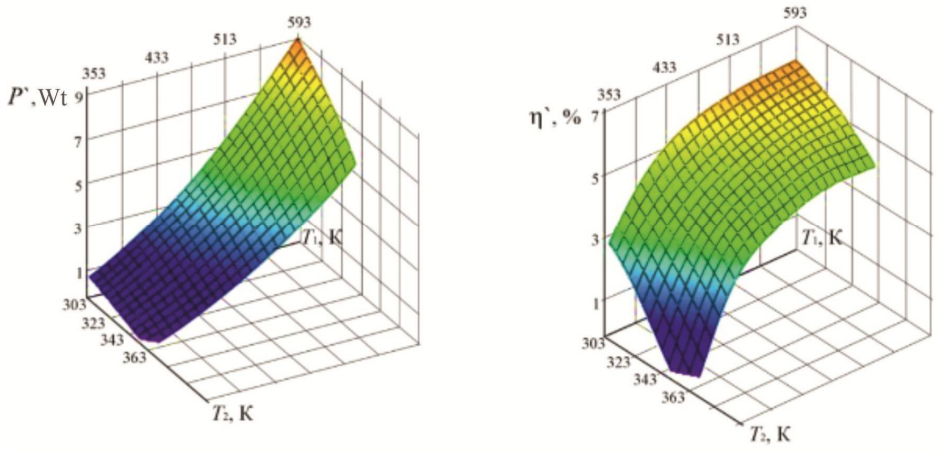


*a*) *b)*

*Fig. 2. Dependences of efficiency η (a) and electrical power P (b) of thermoelectric module of the type Altec-1061 on the hot $T_1$ and cold $T_2$ module side temperatures*

## Results of computer design of a thermoelectric generator

Computer model comprises 5 sections, each of which has landing pads for 8 thermoelectric modules (Fig. 3). Each section has $N_i$ channels of diameter $d_i$ for passing of heat carrier. In so doing, the total cross-sectional area of channels in each section was the same, and increasing the number of channels with a simultaneous reduction of their diameter was achieved by increasing the area of heat exchanger of each successive section.

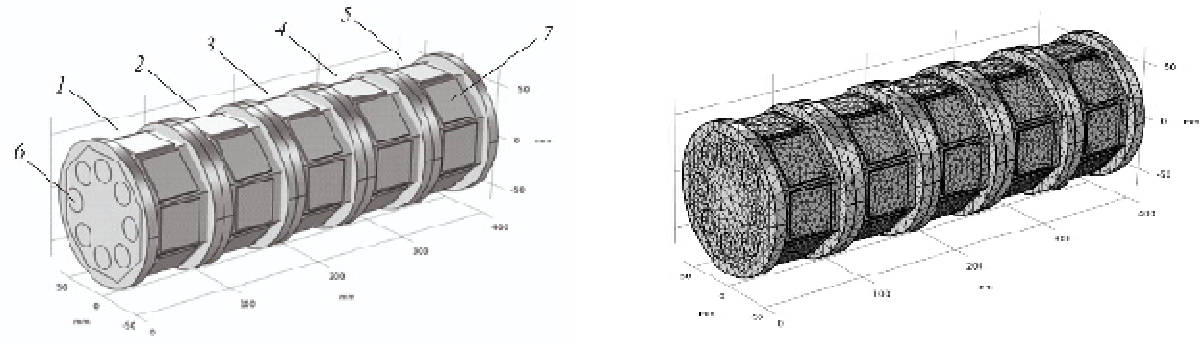


*Fig. 3. Computer model of the hot heat exchanger of thermoelectric generator in the Comsol Multiphysics applied package: 1-5 – heat exchanger sections, 6 – channels for heat carrier passing; 7 – places of thermoelectric modules arrangement*

Optimal geometry of each section was determined from the condition of assuring optimal temperature mode on the hot side of all thermoelectric modules – about 280-300°C.

An example of temperature distribution in the hot heat exchanger of thermoelectric generator in the Comsol Multiphysics application package is given in Fig. 4.

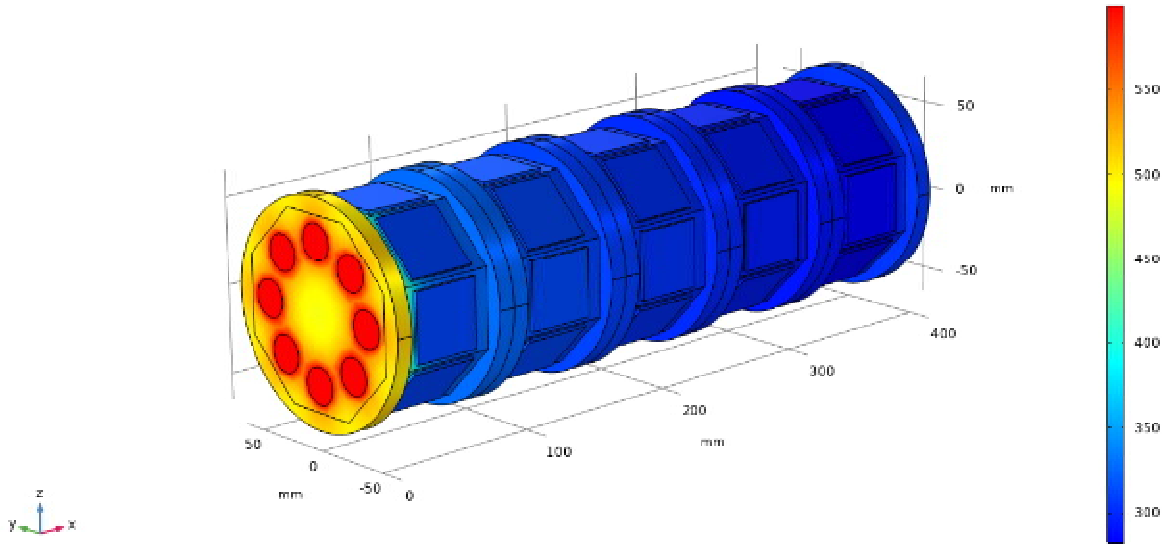


*Fig. 4. Example of temperature distribution in the hot heat exchanger of the generator*

Table 1 shows the computer simulation of the geometric parameters of the heat exchanger (number $N_i$ of channels of each section and their diameter $d_i$, area of the heat exchanger), which allow providing the required temperature mode.

Table 1.

*Results of optimization of the hot heat exchanger design*

| | Section 1 | Section 2 | Section 3 | Section 4 | Section 5 |
|---|---|---|---|---|---|
| Number of channels $N_i$ | 8 | 16 | 32 | 72 | 144 |
| Channel diameter $d_i$, mm | 21.2 | 15.0 | 10.6 | 7.1 | 5.0 |
| Heat exchanger area $S_{R(i)}$, m$^2$ | 0.037 | 0.053 | 0.075 | 0.112 | 0.158 |
| Average temperature of module landing pad $T_1(i)$, °C | 308.0 | 309.1 | 301.6 | 293.3 | 281.8 |

The temperature distribution of gas passing through the heat exchanger is shown in Fig. 5. Coordinate $x$ defines the position in the direction of the gas flow in relation to the heat exchanger.

In order to determine the temperature distribution in the cold heat exchangers of the heater (Fig. 6), the process of heat transfer from the thermoelectric module to the vehicle heating system by heat exchange between the cold side of the thermopile and the heat carrier flow, which circulates in the channels of the cold heat exchanger at speed $v$ and temperatures $T_{in.}$ and $T_{out.}$, respectively at the inlet and outlet of the heat exchanger was studied.

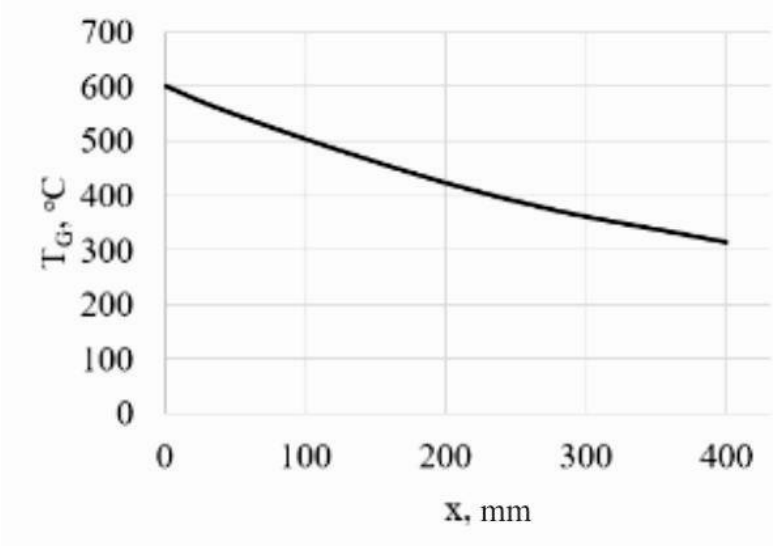


*Fig. 5. Temperature distribution of gas inside the hot heat exchanger of thermoelectric generator (for a heat exchanger design with the parameters given in Table 1)*

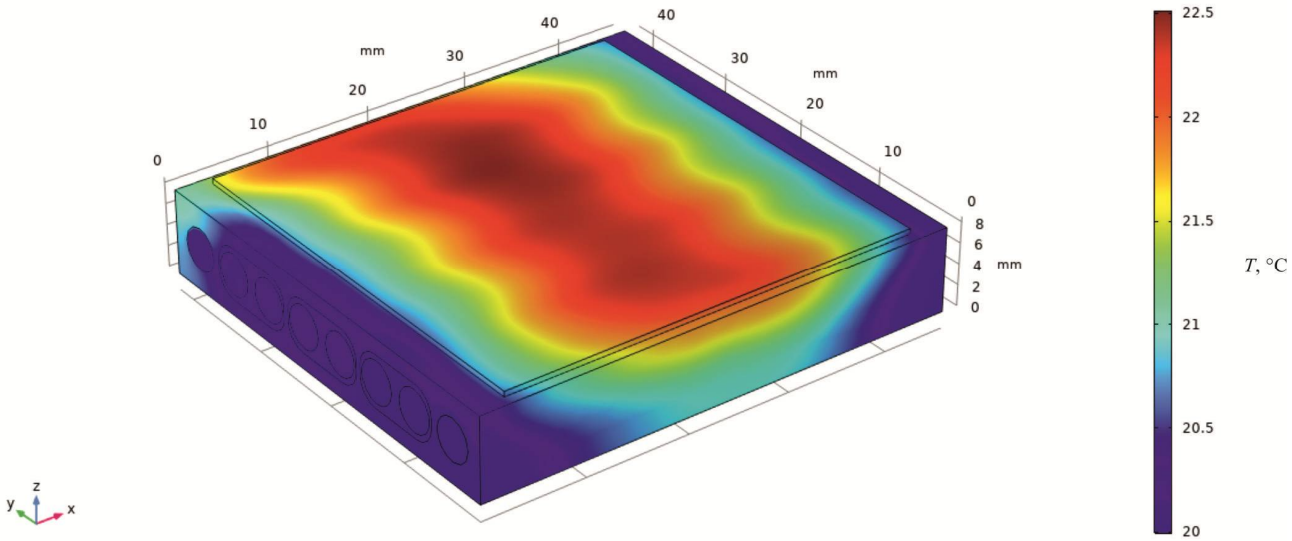


*Fig. 6. Example of temperature distribution in the hot heat exchanger of the generator*

Fig. 6 shows an example of a heat exchanger with channel diameter 4 mm with heat carrier consumption 0.05 $m^3$/h. Figs. 7, 8 also show the distributions of heat carrier velocity and temperature in the heat exchanger.

As a result of simulation, we obtained the dependences of temperature difference between the inlet and outlet from the cold heat exchangers on the geometry of channels and on the heat carrier consumption (Fig. 9).

*v*, m/s *T*, °C

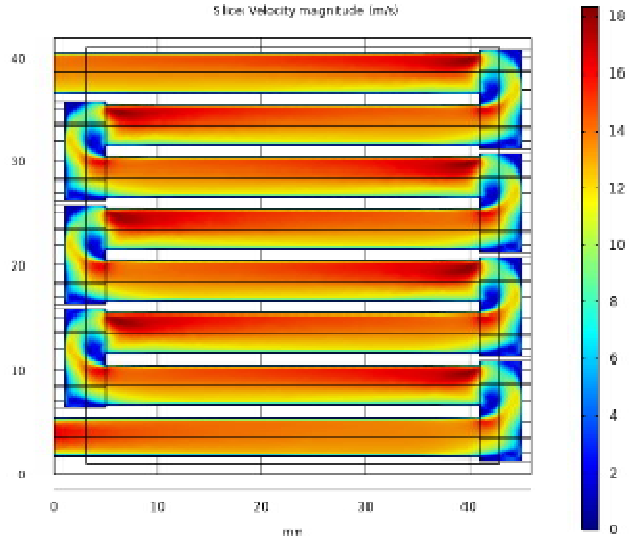


*Fig. 7. Example of distribution of heat carrier velocity in the cold heat exchanger of thermoelectric generator*

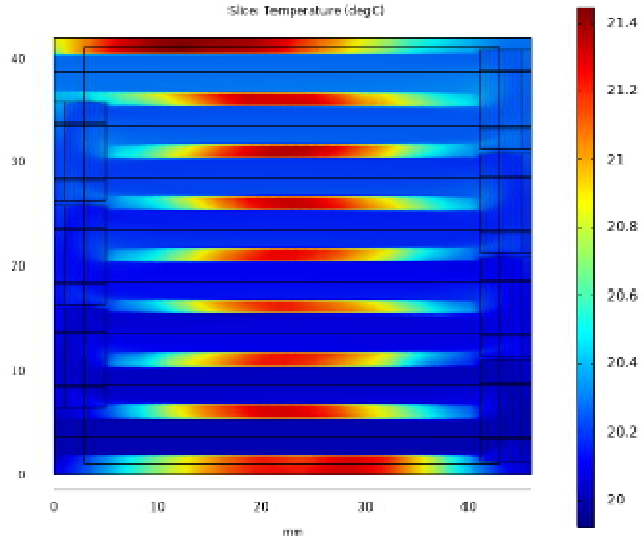


*Fig. 8. Example of distribution of heat carrier temperature in the cold heat exchanger of thermoelectric generator*

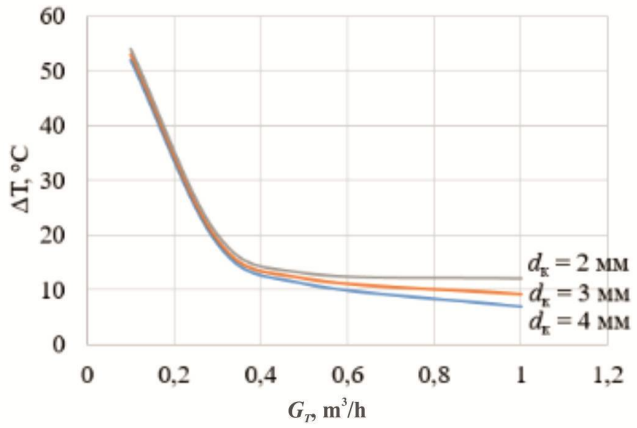


*Fig. 9. Dependence of temperature difference ΔT between the inlet and outlet of cold heat exchanger system on heat carrier consumption $G_m$ and channel diameter $d_к$*

For the case of heat exchanger system comprising 40 individual heat exchangers with channel diameter 4 mm, combined into one hydraulic loop by two series links, 20 pcs each, to ensure the necessary operating temperatures of the cold module side (30 - 50°C), the consumption of heat carrier pumped through the system should be 0.5 - 0.7 $m^3$/h.

The results served the basis for the design development of thermoelectric generator with electric power up to 350 W which will be sufficient for supply with electric energy of starting preheaters of the type PROHEAT M90 24V (with useful thermal power 26 kW and electric power consumption up to 230 W) or OJD30.8106010 (with useful thermal power 30 kW and electric power consumption up to 140 W). Such a system with account of thermal energy of thermoelectric generator (about 10 kW) will be equivalent in thermal power 36 - 40 kW (but autonomous) and will allow replacing the starting preheater of the type PJD - 44Ш (with useful thermal power 37 kW and electric power consumption up to 340 W), which is widely used in heavy-duty civil and military equipment.

## Conclusions

1. A physical, mathematical and computer models of a thermoelectric generator for the heat and electricity supply to heavy-duty vehicles were developed. Computer simulation has been used to determine the optimum design of heat exchanger systems for heat supply and removal, which allows to ensure the required operating mode of thermoelectric modules.
2. A design of thermoelectric generator of electric power up to 350 W and thermal power up to 10 kW was developed. Combined with a starting preheater of thermal power 25-30 kW, the generator creates an autonomous starting preheat system with thermal power up to 40 kW This system can replace a similarly powerful starting preheater and does not require the use of battery power.

## References

1. Tekhnycheskaia эkspluatatsyia avtomobylei: Uchebnyk dlia vuzov. 4-e yzd., pererab. y dopoln. / E.S. Kuznetsov, A.P. Boldyn, V.M. Vlasov y dr. - M.: Nauka, 2001, p. 535. [in Russion]
2. Reznyk L.H., Romalys H.M., Charkov S.T. Эffektyvnost yspolzovanyia avtomobylei v razlychnыkh uslovyiakh ekspluatatsyy. M.: Transport, 1989. – p. 128. [in Russion]
3. Pat. (UA) na vynakhid № 102303 MPK F01N 5/00 H01L 35/00. Termoelektrychne dzherelo zhyvlennia dlia avtomobilia / Anatychuk L.I., Mykhailovskyi V.Ia. – Opubl. 25.06.2013, biul. №12, Zaiavka u2011 13957 vid 28.11.2011. [in Ukrainian]
4. Pat. (UA) №72304. MPK: F01N 5/00; H01L35/00. Avtomobilnyi obihrivach z termoelektrychnym dzherelom zhyvlennia / Anatychuk L.I., Mykhailovskyi V.Ia. – Opubl. 10.08.2012, biul. №15, Zaiavka u2012 02055 vid 23.02.2012. [in Ukrainian]
5. Pat. (UA) №124999. MPK: F02N 19/10; H01L35/00. Avtomobilnyi obihrivach z termoelektrychnym dzherelom zhyvlennia / Maksymuk M.V. – Opubl. 25.04.2018, biul. №8, Zaiavka u2017 11819 vid 04.12.2017. [in Ukrainian]
6. Mikhailovsky V.Ya., Maksimuk MV Rational capacities of heat generators for preheating heaters of vehicles // Thermoelectricity. - №4.– 2015. - P.65-74.
7. Maksimuk M.V. Design of automobile pre-start heat source with thermoelectric generator. Diesel version // Thermoelectricity. - 2017. - P.32-43.
8. L.I. Anatychuk, V.V. Lysko. On the possibility of using thermoelectric generators for transport pre-heaters of high power // Thermoelectricity. - 2019, №3. - P. 80-92.

Submitted 10.05.2021

**Анатичук Л.І.** *акад. НАН України*
**Лисько В.В.** *канд. фіз.-мат. наук*

[1]Інститут термоелектрики НАН і МОН України,
вул. Науки, 1, Чернівці, 58029, Україна,
*e-mail: anatych@gmail.com*;
[2]Чернівецький національний університет
імені Юрія Федьковича, вул. Коцюбинського 2,
Чернівці, 58012, Україна

# КОМП'ЮТЕРНЕ ПРОЕКТУВАННЯ ТЕРМОЕЛЕКТРИЧНОГО ГЕНЕРАТОРА ДЛЯ ДЖЕРЕЛА ТЕПЛА ТА ЕЛЕКТРИКИ ДЛЯ ТРАНСПОРТНИХ ЗАСОБІВ ВЕЛИКОЇ ПОТУЖНОСТІ

*Розглянуто фізичну модель термоелектричного генератора для автономної системи передпускового розігріву транспортних засобів великої потужності. Шляхом комп'ютерного проектування визначено конструкції теплообмінників систем підведення та відведення тепла, які дозволяють забезпечити оптимальний режим роботи термоелектричних модулів. Розроблено конструкцію термоелектричного генератора електричною потужністю до 350 Вт, якої вистачатиме для живлення електричною енергією передпускових нагрівників тепловою потужністю 25-30 кВт. Така система, з врахуванням теплової енергії термоелектричного генератора, буде еквівалентною більш потужним передпусковим нагрівникам (36 – 40 кВт), але не потребуватиме при роботі використання електричної енергії акумулятора. Бібл. 8, рис. 9, табл. 1.*

**Ключові слова:** передпусковий нагрівник, термоелектричний генератор, фізична модель, комп'ютерне моделювання.

**Анатичук Л.И.** *акад. НАН Украины*
**Лисько В.В.** *канд. физ.-мат. наук*

[1]Институт термоэлектричества НАН и МОН Украины, ул. Науки, 1, Черновцы, 58029, Украина, e-mail: anatych@gmail.com ;
[2]Черновицкий национальный университет им. Юрия Федьковича, ул. Коцюбинского, 2, Черновцы, 58012, Украина

# КОМПЬЮТЕРНОЕ ПРОЕКТИРОВАНИЕ ТЕРМОЭЛЕКТРИЧЕСКОГО ГЕНЕРАТОРА ДЛЯ ИСТОЧНИКА ТЕПЛА И ЭЛЕКТРИКИ ДЛЯ ТРАНСПОРТНЫХ СРЕДСТВ БОЛЬШОЙ МОЩНОСТИ

*Рассмотрена физическая модель термоэлектрического генератора для автономной системы предпускового разогрева транспортных средств большой мощности. Путем компьютерного проектирования определены конструкции теплообменников систем подвода и отвода тепла, позволяющие обеспечить оптимальный режим работы термоэлектрических модулей. Разработана конструкция термоэлектрического генератора электрической мощностью до 350 Вт, которой будет хватать для питания электрической энергией предпусковых отопителей тепловой мощностью 25-30 кВт. Такая система, с учетом тепловой энергии термоэлектрического генератора, будет эквивалентна более мощным предпусковым отопителям (36 – 40 кВт), но не потребует при работе использования электрической энергии аккумулятора. Библ. 8, рис. 9. Табл. 1.*

**Key words:** preheater, thermoelectric generator, physical model, computer simulation.

## References

1. Tekhnycheskaia эkspluatatsyia avtomobylei: Uchebnyk dlia vuzov. 4-e yzd., pererab. y dopoln. / E.S. Kuznetsov, A.P. Boldyn, V.M. Vlasov y dr. - M.: Nauka, 2001, p. 535. [in Russion]

2. Reznyk L.H., Romalys H.M., Charkov S.T. Эffektyvnost yspolzovanyia avtomobylei v razlychnыkh uslovyiakh ekspluatatsyy. M.: Transport, 1989. – p. 128. [in Russion]
3. Pat. (UA) na vynakhid № 102303 MPK F01N 5/00 H01L 35/00. Termoelektrychne dzherelo zhyvlennia dlia avtomobilia / Anatychuk L.I., Mykhailovskyi V.Ia. – Opubl. 25.06.2013, biul. №12, Zaiavka u2011 13957 vid 28.11.2011. [in Ukrainian]
4. Pat. (UA) №72304. MPK: F01N 5/00; H01L35/00. Avtomobilnyi obihrivach z termoelektrychnym dzherelom zhyvlennia / Anatychuk L.I., Mykhailovskyi V.Ia. – Opubl. 10.08.2012, biul. №15, Zaiavka u2012 02055 vid 23.02.2012. [in Ukrainian]
5. Pat. (UA) №124999. MPK: F02N 19/10; H01L35/00. Avtomobilnyi obihrivach z termoelektrychnym dzherelom zhyvlennia / Maksymuk M.V. – Opubl. 25.04.2018, biul. №8, Zaiavka u2017 11819 vid 04.12.2017. [in Ukrainian]
6. Mikhailovsky V.Ya., Maksimuk MV Rational capacities of heat generators for preheating heaters of vehicles // Thermoelectricity. - №4.– 2015. - P.65-74.
7. Maksimuk M.V. Design of automobile pre-start heat source with thermoelectric generator. Diesel version // Thermoelectricity. - 2017. - P.32-43.
8. L.I. Anatychuk, V.V. Lysko. On the possibility of using thermoelectric generators for transport pre-heaters of high power // Thermoelectricity. - 2019, №3. - P. 80-92.

Submitted 10.05.2021

**Dmitrichenko M.F.,** *Doc. Tech. Sciences*
**Gutarevich Yu.F. ,** *Doc. Tech. Sciences*
**Trifonov D.M.,** *Cand. of Tech. Sciences*
**Sirota O.V.,** *C Cand. of Tech. Sciences*
**Shuba E.V.**, *Cand. of Tech. Sciences*

National Transport University
1, M.Omelianovycha-Pavlenka Str., Kyiv, 01010, Ukraine,
*e-mail: d.trifonov@ntu.edu.ua*

# ON THE PROSPECTS OF USING THERMOELECTRIC COOLERS TO MAINTAIN OPTIMAL AIR TEMPERATURE IN THE INTAKE MANIFOLD OF INTERNAL COMBUSTION ENGINE FOR IMPROVING ITS PERFORMANCE CHARACTERISTICS

*The paper deals with the problem associated with increasing the efficiency of the operation of road transport in conditions of high ambient temperatures, substantiates the need to take special measures to maintain the optimum air temperature at the engine inlet. According to the results of the analysis, it is established that the ambient temperature has a significant impact on the efficiency of the internal combustion engine. The use of a thermoelectric system is proposed, which makes it possible to maintain the optimum temperature in the intake manifold in order to improve the performance of the engine. Descriptions of the proposed thermoelectric system and the concept of its operation are presented. Bibl. 11, Fig. 4.*
**Key words:** internal combustion engine, natural and climatic factors, thermoelectric cooler, performance characteristics.

## Introduction

The transport industry is one of the basic sectors of the Ukrainian economy, has a developed network of roads, which creates the necessary prerequisites to meet the needs of transport users in the provision of transport services and the economic development of the national economy of the country. The current state of the transport industry does not fully meet the modern requirements for the effective implementation of energy-saving technologies and ensuring the priority of environmental safety requirements, which is due to the low level of implementation of modern technologies and the implementation of innovative policies in the transport industry. In this regard, the problem of increasing the efficiency of road transport operation is one of the most significant, which is confirmed by the National Transport Strategy of Ukraine for the period up to 2030 [1].

## Analysis of previous research

Modern designs of intake systems of internal combustion engines (ICE) through the use of various design solutions, first of all, provide a low concentration of harmful substances in the exhaust gas and high economic performance. At the same time, the performance indicators of internal combustion engines have faded into the background, which is caused by the strengthening of international standards for

environmental safety and fuel efficiency for road transport. As you know, the performance of internal combustion engines in different modes of operation, environmental and economic indicators depend not only on improving the design of the engine, but also on the efficiency of combustion of fuel-air mixture in engine cylinders, which in turn is determined by its qualitative and quantitative composition.

The effect of intake air temperature on the performance characteristics of internal combustion engines is widely covered in [2–6].

In works [7 - 9], based on the results of research work carried out to determine the optimal air temperature in the engine intake manifold, it is noted that the air temperature at which the optimal parameters of the engine operating cycle are provided is 40...60°C. In real conditions of vehicle operation, maintaining such a temperature regime of air at the inlet is practically impossible due to the influence of various changing factors, primarily climatic and road, as well as loading, speed and thermal modes of operation of the internal combustion engine. In addition, the turbocharger and other technology that boosts the engine also contribute to the increase in temperature under the hood of a modern engine. In this regard, the air temperature at the inlet of the internal combustion engine, depending on the operating conditions and the number of additional equipment, can vary widely, which significantly affects the work process (the filling of the cylinders with the air-fuel mixture and its quality deteriorate) and the heat balance of the engine.

It should be noted that the electronic engine control systems of modern cars equipped with various sensors to ensure the optimal composition of the air-fuel mixture, despite their technical excellence, do not fully take into account the influence of variable factors that manifest themselves during the operation of the car. For example, in hot climates, the temperature of the air in the intake manifold during engine operation at idle and partial loads rises to 80 ° C and above [10]. An analysis of changes in global temperature in relation to the average temperatures of 1951-1980 shows that the duration of periods of abnormally high temperatures has increased significantly on average over the past decades due to global climate trends (Fig. 1).

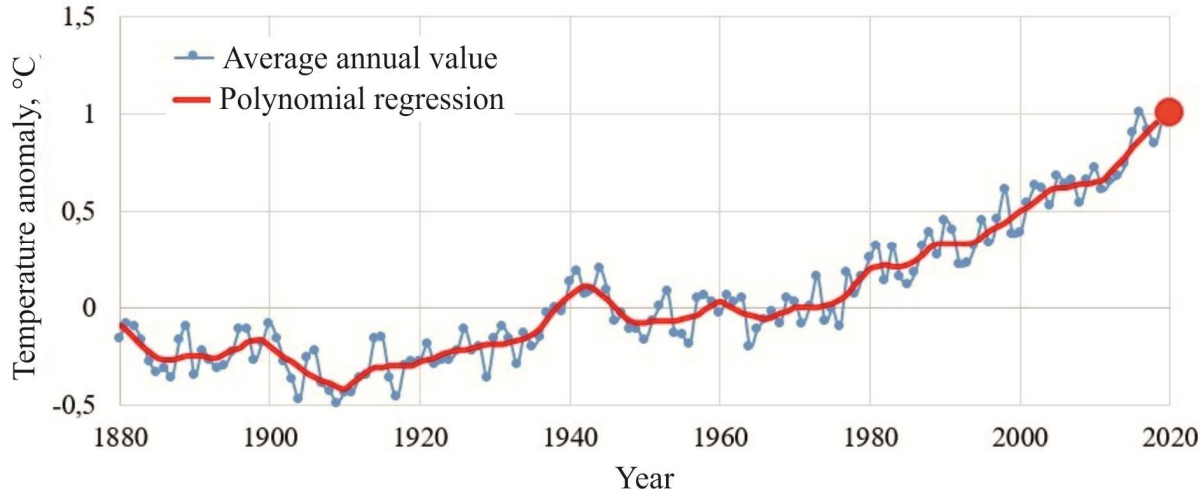


*Fig.1. Global land and ocean temperature index [11].*

Air cooling, in particular for turbocharged diesel engines, is widely used to improve engine volumetric efficiency by increasing air density and improving cylinder filling. This is usually done due to the air/air heat exchanger. Ambient air is used as a cooling medium (coolant), and therefore the degree of cooling of the air entering the engine is strictly related to the ambient temperature. Record-breaking high ambient temperatures in recent years lead to a significant decrease in the efficiency of the standard heat exchanger and, as a result, to a significant increase in intake temperature, which leads to a decrease in the

efficiency of road transport operation (including its energy performance).

Therefore, one of the promising ways to improve the performance of road transport in high ambient temperatures is to ensure optimal air temperature at the intake of the internal combustion engine.

In this regard, there is a need to develop methods and devices, taking into account modern technological solutions, to ensure the optimal temperature of the incoming air to the engine, in order to ensure the preparation of the optimal composition of the air-fuel mixture and its quantity, depending on its operating modes.

To solve this problem, the authors proposed an air-to-air thermoelectric system (Fig. 2), which automatically maintains the optimum air temperature in the engine intake manifold when the vehicle is operated at high ambient temperatures or high engine load.

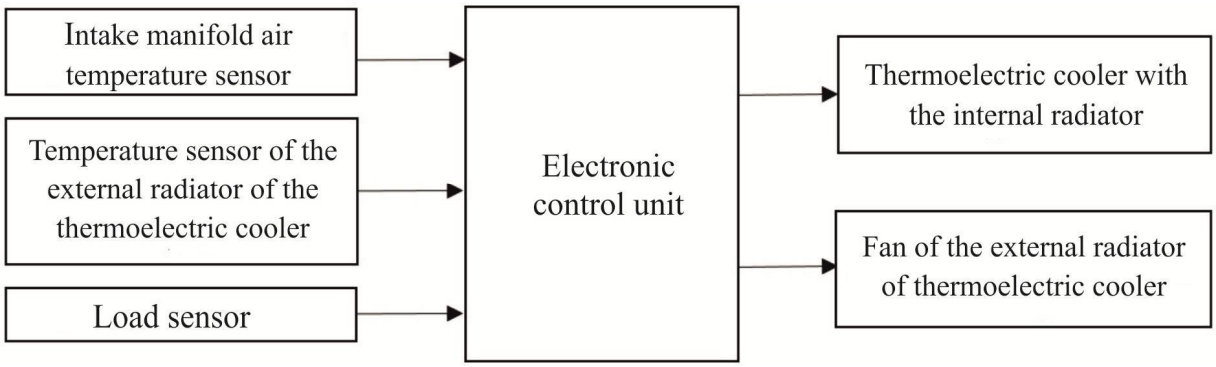


*Fig. 2. Block diagram of the proposed thermoelectric system*

The electronic control unit provides maintenance (stabilization) of the optimum air temperature in the intake manifold by controlling the thermoelectric cooler (TEC - Thermoelectric Cooler) and the fan of the external radiator of TEC with simultaneous monitoring and display of operating status and system parameters. Temperature stabilization is carried out by changing the electric power supplied to the TEC.

## Research results

The proposed thermoelectric system (Fig. 3) consists of an internal combustion engine, an intake manifold, an air cleaner, an electronic control unit, a thermoelectric converter with internal and external radiators, an external radiator temperature sensor, an external radiator fan, an air temperature sensor in the intake manifold, and a load sensor.

The main element of the proposed thermoelectric system is a thermoelectric module consisting of a thermoelectric converter, the principle of operation of which is based on the Peltier effect. The most important features of thermoelectric cooling modules are: the ability to cool the object below the ambient temperature, fairly accurate temperature control and small size. The use of thermoelectric modules often offers a simple solution to complex technical problems of thermal energy management and provides significant advantages over alternative technologies.

The principle of operation of the proposed thermoelectric system is as follows: during engine operation, the electronic control unit receives signals from air temperature sensors in the intake manifold and external radiator of the thermoelectric cooler and load sensor. Depending on the level of these signals, the electronic control unit smoothly changing the power on the thermoelectric converter provides the required temperature of the internal (cooling) radiator.

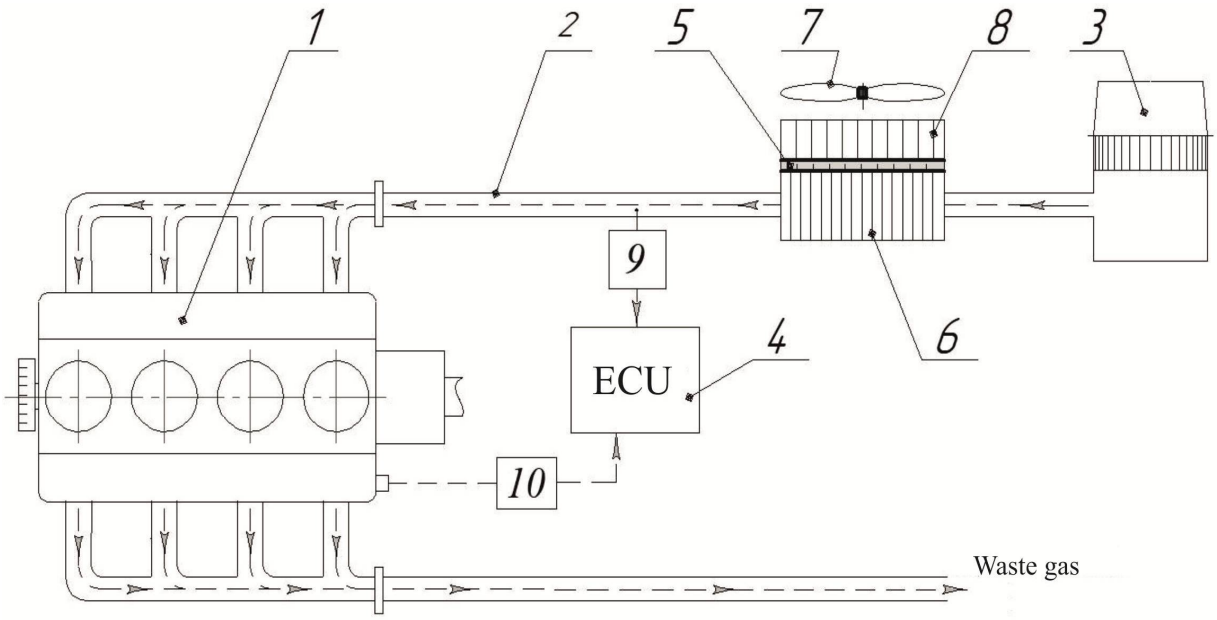


*Fig. 3.Block-diagram of the proposed thermoelectric system:*
*1-ICE, 2-intake collector, 3-air cleaner, 4-electronic control unit, 5-thermoelectric converter,*
*6-internal (cooling) radiator, 7-external radiator fan, 8-external radiator with temperature sensor,*
*9- air temperature sensor in the intake collector, 10- load sensor.*

In order to prevent a decrease in the efficiency of the thermoelectric system, the degradation of the thermoelectric module and its failure when exceeding the allowable heating temperature of the hot side of the thermoelectric converter, the electronic unit controls the fan of the external radiator (on and off), which facilitates the transfer of heat from the hot surface of the TEC in the underhood of the car.

The proposed thermoelectric system provides the following modes of operation:

– under conditions of optimal air temperature in the intake manifold, air from the air cleaner enters the engine cylinders through the disconnected thermoelectric converter and the intake manifold;

in conditions of exceeding the optimum air temperature in the intake manifold or in acceleration and full load modes, the electronic control unit connects the thermoelectric converter to the on-board network, which leads to a decrease in the temperature of the internal radiator, while the air temperature in the intake manifold decreases due to heat exchange of air from the air cleaner with the internal radiator of thermoelectric converter. Depending on the signal level of the air temperature sensor in the intake manifold, the electronic control unit, smoothly changing the power on the thermoelectric converter, provides the required temperature of the internal radiator, which leads to an improvement in the performance of the internal combustion engine.

At the Department of Engines and Heat Engineering of the National Transport University, an experimental sample of the proposed thermoelectric device (Fig. 4) was made and its functional tests were carried out to assess the possible effectiveness of the proposed approach to solving the above problem.

Functional studies to ensure the optimum air temperature at the engine inlet at high ambient temperatures were carried out in the engine test laboratory of the National Transport University. The experimental setup (Fig. 4) consists of a VW BBY engine installed on a brake test bench, a working sample of the proposed thermoelectric device, electronic thermometers with remote sensors, and a ceramic-metal heating element that heats the air at the inlet to about 60°C.

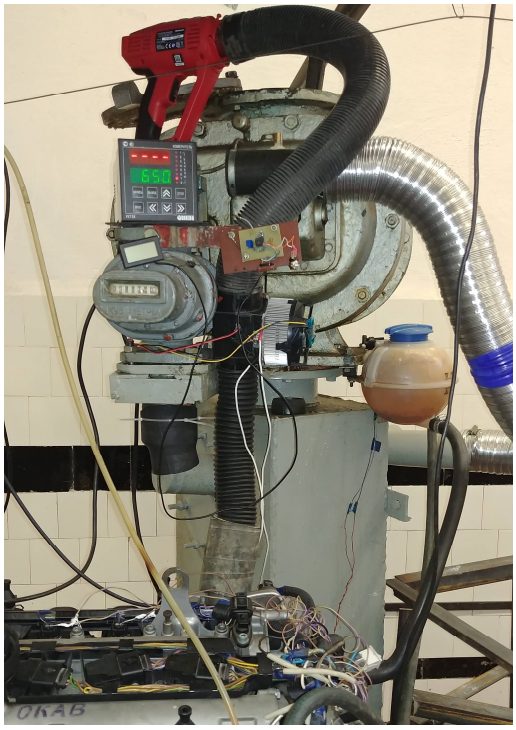

*Fig. 4. Experimental sample of the proposed device mounted on a VW BBY engine*

Based on the results of the first stage of experimental studies, the possibility of applying the approach proposed by the authors to the implementation of energy-efficient technologies in road transport was confirmed. The use of a thermoelectric system, the operation of which is based on the Peltier effect, makes it possible to reduce and maintain the set air temperature in the intake manifold.

In the future, it is planned to carry out computational studies in order to determine the number of thermoelectric modules and the required area of air heat-dissipating radiators of the thermoelectric module to ensure the required air temperature in the intake manifold and experimental studies in order to determine the expected efficiency of using the proposed device to improve the performance of internal combustion engines at high ambient temperatures and full loads.

## Conclusions

1. Based on the results of the research, a thermoelectric system is proposed that ensures the stabilization of the optimal air temperature in automatic mode in the engine intake manifold when the vehicle is operated at high ambient temperatures or high engine load.
2. Based on the requirements for temperature control systems, such as automatic maintenance of a given temperature in a given volume with a certain accuracy, regardless of its change in the environment, small weight and size, short time to enter the operating mode, low power consumption, the authors proposed the use of thermoelectric coolers, the operation of which is based on the Peltier effect.
3. The proposed device has a compact form factor compared to other technologies, is easy to implement and capable of providing the necessary design and operational characteristics, is environmentally friendly and does not require maintenance.
4. According to the results of functional tests of a working sample manufactured at the Department of Engines and Thermal Engineering of the National Transport University, the possibility of using the proposed thermoelectric system to reduce the air temperature in the intake manifold under conditions of

high ambient temperatures was confirmed.

## References

1. Pro shvalennia natsionalnoi transportnoi strategii Ukrainy na period do 2030 roku [Approval of the National Transport Strategy of Ukraine for the period up to 2030]. *Order of the Cabinet of Ministers of Ukraine No. 430-r issued on May 30, 2018* [in Ukrainian].
2. Shabalin D.V., Tereshchenko E.S. (2012).Vliianiie temperatury nadduvochnogo vozduha na rabochii process dizelnogo dvigatelia [Influence of charge air temperature on diesel engine operation]. *Vestnik SibADI*, 2 (24), 91-95 [in Russian].
3. Dmytrychenko M.F., Gutarevych Y.F., Trifonov D.M., Syrota O.V., Shuba E.V. (2018). On the prospects of using thermoelectric generators with the cold start system of an internal combustion engine with a thermal battery. *J.Thermoelectricity*, 4, 49-54.
4. Dmytrychenko M.F., Gutarevych Y.F., Trifonov D.M., Syrota O.V. (2020). The use of thermoelectric energy converters to reduce the influence of natural and climatic factors on the technical readiness of a vehicle. *J.Thermoelectricity*, 3, 56-68.
5. Dmytrychenko M., Gutarevych Y., Shuba Y., Syrota O., Trifonov D., Matijošius J. (2020) Improvement of fuel economy and starting properties of the diesel engine by heating the air at the inlet. *TRANSBALTICA XI: Transportation Science and Technology*, p. 494-503 [in Russian].
6. Birtok-Băneasă C, Raţiu S, Hepuț T (2017). Influence of intake air temperature on internal combustion engine operation, *IOP Conf. Ser.: Mater. Sci. Eng. Materials Science and Engineering* 163 012039.
7. Karnaukhov V.N. (2014). Optimizatsiia moshchnosti nagrevatelnogo elementa dlia podderzhaniia optimalnoi temperatury vozdukha vo vpusknom kollektore DVS [Optimization of the power of the heating element to maintain the optimum air temperature in the intake manifold of the internal combustion engine] *Electronic scientific journal: Modern Problems of Science and Education,* 3.
8. Karnaukhova I.V. (2014). Opredeleniie optimalnoi temperatury vozdukha vo vpusknom kollektore dvigatelia [Determining the optimum air temperature in the engine intake manifold]. *Vestnik SibADI*, 3(37), 7 – 12 [in Russian].
9. Karimkhodzhayev N., Dadaboyev R.M., Rakhmonov A.F. (2021). Vliianiie uslovii ekspluatatsii na iznosostoikost dvigatelia i ego detalei [Influence of operating conditions on the wear resistance of the engine and its parts]. *Universum: Technical Sciences: electronic scientific journal*, 4(85) [in Russian].
10. Akunov B.U., Kasymbekov K.J. (2019). Vliianiie temperatury vozdukha vo vpusknom kollektore dvigatelia na dlitelnost impulsa otkrytiia forsunki pri ekspluatatsii avtomobilia v razlichnykh usloviiakh [Influence of air temperature in the engine intake manifold on the duration of the injector opening pulse during vehicle operation in various conditions]. *Vestnik SibADI*, 1(65), 32-39.
11. Global climate change. https://climate.nasa.gov/vital-signs/global-temperature/.

Submitted 13.05.2021

**Дмитриченко М.Ф.** *докт. техн. наук*
**Гутаревич Ю.Ф.** *докт. техн. наук*
**Тріфонов Д.М.** *канд. техн. наук*
**Сирота О.В.** *канд. техн. наук*
**Шуба Е.В.** *канд. техн. наук*

Національний транспортний університет
вул. М. Омеляновича-Павленка, 1, м. Київ,
01010, Україна, *e-mail: d.trifonov@ntu.edu.ua*

# ПРО ПЕРСПЕКТИВИ ВИКОРИСТАННЯ ТЕРМОЕЛЕКТРИЧНИХ ОХОЛОДЖУВАЧІВ ДЛЯ ПІДТРИМАННЯ ОПТИМАЛЬНОЇ ТЕМПЕРАТУРИ ПОВІТРЯ У ВПУСКНОМУ КОЛЕКТОРІ ДВИГУНА ВНУТРІШНЬОГО ЗГОРАННЯ З МЕТОЮ ПІДВИЩЕННЯ ЙОГО ЕКСПЛУАТАЦІЙНИХ ХАРАКТЕРИСТИК

*У статті розглядається проблема, пов'язана з підвищенням ефективності експлуатації автомобільного транспорту в умовах високих температур оточуючого повітря, обґрунтовується необхідність прийняття спеціальних заходів для підтримання оптимальної температури повітря на впуску двигуна. За результатами аналізу встановлено, що значний вплив на ефективність роботи двигуна внутрішнього згорання здійснює температура оточуючого повітря. Запропоновано використання термоелектричної системи, яка дозволяє забезпечити підтримання оптимальної температури у впускному колекторі з метою підвищення експлуатаційних характеристик двигуна. Наведено опис запропонованої термоелектричної системи та принцип її функціонування. Бібл. 11, рис. 4.*
**Ключові слова:** двигун внутрішнього згорання, природно-кліматичні фактори, термоелектричний охолоджувач, експлуатаційні характеристики.

**Дмитриченко Н.Ф.,** *доктор техн. наук*
**Гутаревич Ю.Ф.,** *доктор техн. наук*
**Трифонов Д.Н.,** *канд. техн. наук*
**Сирота А.В.,** *канд. техн. наук*
**Шуба Э. В.,** *канд. техн. наук*

Национальный транспортный университет
ул. М. Емельяновича-Павленко, 1, г. Киев, 01010, Украина,
*e-mail: d.trifonov@ntu.edu.ua*

# О ПЕРСПЕКТИВАХ ИСПОЛЬЗОВАНИЯ ТЕРМОЭЛЕКТРИЧЕСКИХ ОХЛАДИТЕЛЕЙ ДЛЯ ПОДДЕРЖАНИЯ ОПТИМАЛЬНОЙ ТЕМПЕРАТУРЫ ВОЗДУХА ВО ВПУСКНОМ КОЛЛЕКТОРЕ ДВИГАТЕЛЯ ВНУТРЕННЕГО СГОРАНИЯ

*В статье рассматривается проблема, связанная с повышением эффективности эксплуатации автомобильного транспорта в условиях высоких температур окружающего воздуха, обосновывается необходимость принятия специальных мер по поддержанию оптимальной температуры воздуха на впуске двигателя. По результатам анализа установлено, что большое влияние на эффективность работы двигателя внутреннего сгорания оказывает температура*

*окружающего воздуха. Предложено использование термоэлектрической системы, позволяющей обеспечить поддержание оптимальной температуры во впускном коллекторе с целью повышения эксплуатационных характеристик двигателя. Представлено описание предлагаемой термоэлектрической системы и принцип ее функционирования. Библ.11, рис.4.*

**Ключевые слова:** двигатель внутреннего сгорания, природно-климатические факторы, термоэлектрический охладитель, эксплуатационные характеристики.

## References

1. Pro shvalennia natsionalnoi transportnoi strategii Ukrainy na period do 2030 roku [Approval of the National Transport Strategy of Ukraine for the period up to 2030]. *Order of the Cabinet of Ministers of Ukraine No. 430-r issued on May 30, 2018* [in Ukrainian].
2. Shabalin D.V., Tereshchenko E.S. (2012).Vliianiie temperatury nadduvochnogo vozduha na rabochii process dizelnogo dvigatelia [Influence of charge air temperature on diesel engine operation]. *Vestnik SibADI*, 2 (24), 91-95 [in Russian].
3. Dmytrychenko M.F., Gutarevych Y.F., Trifonov D.M., Syrota O.V., Shuba E.V. (2018). On the prospects of using thermoelectric generators with the cold start system of an internal combustion engine with a thermal battery. *J.Thermoelectricity*, 4, 49-54.
4. Dmytrychenko M.F., Gutarevych Y.F., Trifonov D.M., Syrota O.V. (2020). The use of thermoelectric energy converters to reduce the influence of natural and climatic factors on the technical readiness of a vehicle. *J.Thermoelectricity*, 3, 56-68.
5. Dmytrychenko M., Gutarevych Y., Shuba Y., Syrota O., Trifonov D., Matijošius J. (2020) Improvement of fuel economy and starting properties of the diesel engine by heating the air at the inlet. *TRANSBALTICA XI: Transportation Science and Technology*, p. 494-503 [in Russian].
6. Birtok-Băneasă C, Raţiu S, Hepuţ T (2017). Influence of intake air temperature on internal combustion engine operation, *IOP Conf. Ser.: Mater. Sci. Eng. Materials Science and Engineering* 163 012039.
7. Karnaukhov V.N. (2014). Optimizatsiia moshchnosti nagrevatelnogo elementa dlia podderzhaniia optimalnoi temperatury vozdukha vo vpusknom kollektore DVS [Optimization of the power of the heating element to maintain the optimum air temperature in the intake manifold of the internal combustion engine] *Electronic scientific journal: Modern Problems of Science and Education,* 3.
8. Karnaukhova I.V. (2014). Opredeleniie optimalnoi temperatury vozdukha vo vpusknom kollektore dvigatelia [Determining the optimum air temperature in the engine intake manifold]. *Vestnik SibADI*, 3(37), 7 – 12 [in Russian].
9. Karimkhodzhayev N., Dadaboyev R.M., Rakhmonov A.F. (2021). Vliianiie uslovii ekspluatatsii na iznosostoikost dvigatelia i ego detalei [Influence of operating conditions on the wear resistance of the engine and its parts]. *Universum: Technical Sciences: electronic scientific journal*, 4(85) [in Russian].
10. Akunov B.U., Kasymbekov K.J. (2019). Vliianiie temperatury vozdukha vo vpusknom kollektore dvigatelia na dlitelnost impulsa otkrytiia forsunki pri ekspluatatsii avtomobilia v razlichnykh usloviiakh [Influence of air temperature in the engine intake manifold on the duration of the injector opening pulse during vehicle operation in various conditions]. *Vestnik SibADI*, 1(65), 32-39.
11. Global climate change. https://climate.nasa.gov/vital-signs/global-temperature/.

Submitted 13.05.2021

## ARTICLE SUBMISSION GUIDELINES

For publication in a specialized journal, scientific works are accepted that have never been printed before. The article should be written on an actual topic, contain the results of an in-depth scientific study, the novelty and justification of scientific conclusions for the purpose of the article (the task in view).

The materials published in the journal are subject to internal and external review which is carried out by members of the editorial board and international editorial board of the journal or experts of the relevant field. Reviewing is done on the basis of confidentiality. In the event of a negative review or substantial remarks, the article may be rejected or returned to the author(s) for revision. In the case when the author(s) disagrees with the opinion of the reviewer, an additional independent review may be done by the editorial board. After the author makes changes in accordance with the comments of the reviewer, the article is signed to print.

The editorial board has the right to refuse to publish manuscripts containing previously published data, as well as materials that do not fit the profile of the journal or materials of research pursued in violation of ethical norms (for instance, conflicts between authors or between authors and organization, plagiarism, etc.). The editorial board of the journal reserves the right to edit and reduce the manuscripts without violating the author's content. Rejected manuscripts are not returned to the authors.

**Submission of manuscript to the journal**

The manuscript is submitted to the editorial office of the journal in paper form in duplicate and in electronic form on an electronic medium (disc, memory stick). The electronic version of the article shall fully correspond to the paper version. The manuscript must be signed by all co-authors or a responsible representative.

In some cases it is allowed to send an article by e-mail instead of an electronic medium (disc, memory stick).

English-speaking authors submit their manuscripts in English. Russian-speaking and Ukrainian-speaking authors submit their manuscripts in English and in Russian or Ukrainian, respectively. Page format is A4. The number of pages shall not exceed 15 (together with References and extended abstracts). By agreement with the editorial board, the number of pages can be increased.

To the manuscript is added:

1. Official recommendation letter, signed by the head of the institution where the work was carried out.

2. License agreement on the transfer of copyright (the form of the agreement can be obtained from the editorial office of the journal or downloaded from the journal website – Dohovir.pdf). The license agreement comes into force after the acceptance of the article for publication. Signing of the license agreement by the author(s) means that they are acquainted and agree with the terms of the agreement.

3. Information about each of the authors – full name, position, place of work, academic title, academic degree, contact information (phone number, e-mail address), ORCID code (if available). Information about the authors is submitted as follows:

authors from Ukraine - in three languages, namely Ukrainian, Russian and English;

authors from the CIS countries - in two languages, namely Russian and English;

authors from foreign countries – in English.

4. Medium with the text of the article, figures, tables, information about the authors in electronic

form.

5. Colored photo of the author(s). Black-and-white photos are not accepted by the editorial staff. With the number of authors more than two, their photos are not shown.

**Requirements for article design**

The article should be structured according to the following sections:

- *Introduction*. Contains the problem statement, relevance of the chosen topic, analysis of recent research and publications, purpose and objectives.
- *Presentation of the main research material* and the results obtained.
- *Conclusions* summing up the work and the prospects for further research in this direction.
- *References*.

The first page of the article contains information:

1) in the upper left corner – UDC identifier (for authors from Ukraine and the CIS countries);

2) surname(s) and initials, academic degree and scientific title of the author(s);

3) the name of the institution where the author(s) work, the postal address, telephone number, e-mail address of the author(s);

4) article title;

5) abstract to the article – not more than 1 800 characters. The abstract should reflect the consistent logic of describing the results and describe the main objectives of the study, summarize the most significant results;

6) key words – not more than 8 words.

***The text*** of the article is printed in Times New Roman, font size 11 pt, line spacing 1.2 on A4 size paper, justified alignment. There should be no hyphenation in the article.

**Page setup**: "mirror margins" – top margin – 2.5 cm, bottom margin – 2.0 cm, inside – 2.0 cm, outside – 3.0 cm, from the edge to page header and page footer – 1.27 cm.

**Graphic materials**, pictures shall be submitted in color or, as an exception, black and white, in .opj or .cdr formats, .jpg or .tif formats being also permissible. According to author's choice, the tables and partially the text can be also in color.

*Figures* are printed on separate pages. The text in the figures must be in the font size 10 pt. On the charts, the units of measure are separated by commas. Figures are numbered in the order of their arrangement in the text, parts of the figures are numbered with letters – a, b, .. On the back of the figure, the title of the article, the author (authors) and the figure number are written in pencil. Scanned images and graphs are not allowed to be inserted.

*Tables* are provided on separate pages and must be executed using the MSWord table editor. Using pseudo-graph characters to design tables is inadmissible.

*Formulae* shall be typed in Equation or MatType formula editors. Articles with formulae written by hand are not accepted for printing. It is necessary to give definitions of quantities that are first used in the text, and then use the appropriate term.

*Captions to figures and tables* are printed in the manuscript after the references.

*Reference list* shall appear at the end of the article. References are numbered consecutively in the order in which they are quoted in the text of the article. References to unpublished and unfinished works are inadmissible.

**Attention!** In connection with the inclusion of the journal in the international bibliographic abstract database, the reference list should consist of two blocks: CITED LITERATURE and REFERENCES (this requirement also applies to English articles):

CITED LITERATURE – sources in the original language, executed in accordance with the Ukrainian standard of bibliographic description DSTU 8302:2015. With the aid of VAK.in.ua

(http://vak.in.ua) you can automatically, quickly and easily execute your "Cited literature" list in conformity with the requirements of State Certification Commission of Ukraine and prepare references to scientific sources in Ukraine in understandable and unified manner. This portal facilitates the processing of scientific sources when writing your publications, dissertations and other scientific papers.

REFERENCES – the same cited literature list transliterated in Roman alphabet (recommendations according to international bibliographic standard APA-2010, guidelines for drawing up a transliterated reference list "References" are on the site http//www.dse.org.ua, section for authors).

**To speed up the publication of the article, please adhere to the following rules:**

- in the upper left corner of the first page of the article – the UDC identifier;
- family name and initials of the author(s);
- academic degree, scientific title;

begin a new line, Times New Roman font, size 12 pt, line spacing 1.2, center alignment;

- name of organization, address (street, city, zip code, country), e-mail of the author(s);

begin a new line 1 cm below the name and initials of the author(s), Times New Roman font, size 11 pt, line spacing 1.2, center alignment;

- the title of the article is arranged 1 cm below the name of organization, in capital letters, semi-bold, font Times New Roman, size 12 pt, line spacing 1.2, center alignment. The title of the article shall be concrete and possibly concise;
- the abstract is arranged 1 cm below the title of the article, font Times New Roman, size 10 pt, in italics, line spacing 1.2, justified alignment in Ukrainian or Russian (for Ukrainian-speaking and Russian-speaking authors, respectively);
- key words are arranged below the abstract, font Times New Roman, size 10 pt, line spacing 1.2, justified alignment. The language of the key words corresponds to that of the abstract. Heading "Key words" - font Times New Roman, size 10 pt, semi-bold;
- the main text of the article is arranged 1 cm below the abstract, indent 1 cm, font Times New Roman, size 11 pt, line space spacing 1.2, justified alignment;
- formulae are typed in formula editor, fonts Symbol, Times New Roman. Font size is "normal" – 12 pt, "large index" – 7 pt, "small index" – 5 pt, "large symbol" – 18 pt, "small symbol" – 12 pt. The formula is arranged in the text, center aligned and shall not occupy more than 5/6 of the line width, formulae are numbered in parentheses on the right;
- dimensions of all quantities used in the article are represented in the International System of Units (SI) with the explication of the symbols employed;
- figures are arranged in the text. The figures and pictures shall be clear and contrast; the plot axes – parallel to sheet edges, thus eliminating possible displacement of angles in scaling; figures are submitted in color, black-and-white figures are not accepted by the editorial staff of the journal;
- tables are arranged in the text. The width of the table shall be 1 cm less than the line width. Above the table its ordinary number is indicated, right alignment. Continuous table numbering throughout the text. The title of the table is arranged below its number, center alignment;
- references should appear at the end of the article. References within the text should be

enclosed in square brackets behind the text. References should be numbered in order of first appearance in the text. Examples of various reference types are given below.

**Examples of LITERATURE CITED**

*Journal articles*

Anatychuk L.I., Mykhailovsky V.Ya., Maksymuk M.V., Andrusiak I.S. Experimental research on thermoelectric automobile starting pre-heater operated with diesel fuel. *J.Thermoelectricity*. 2016. №4. P.84–94.

*Books*

Anatychuk L.I. *Thermoelements and thermoelectric devices. Handbook.* Kyiv, Naukova dumka, 1979. 768 p.

*Patents*

*Patent of Ukraine №* 85293. Anatychuk L.I., Luste O.J., Nitsovych O.V. Thermoelement.

*Conference proceedings*

Lysko V.V. *State of the art and expected progress in metrology of thermoelectric materials.* Proceedings of the XVII International Forum on Thermoelectricity (May 14-18, 2017, Belfast). Chernivtsi, 2017. 64 p.

*Authors' abstracts*

Kobylianskyi R.R. *Thermoelectric devices for treatment of skin diseases*: extended abstract of candidate's thesis. Chernivtsi, 2011. 20 p.

**Examples of REFERENCES**

*Journal articles*

Gorskiy P.V. (2015). Ob usloviakh vysokoi dobrotnosti i metodikakh poiska perspektivnykh sverhreshetochnykh termoelektricheskikh materialov [On the conditions of high figure of merit and methods of search for promising superlattice thermoelectric materials]. *Termoelektrichestvo - J.Thermoelectricity,* 3, 5 – 14 [in Russian].

*Books*

Anatychuk L.I. (2003). *Thermoelectricity. Vol.2. Thermoelectric power converters*. Kyiv, Chernivtsi: Institute of Thermoelectricity.

*Patents*

*Patent of Ukraine №* 85293. Anatychuk L. I., Luste O.Ya., Nitsovych O.V. Thermoelements [In Ukrainian].

*Conference proceedings*

Rifert V.G. Intensification of heat exchange at condensation and evaporation of liquid in 5 flowing-down films. In: *Proc. of the 9th International Conference Heat Transfer.* May 20-25, 1990, Israel.

*Authors'abstracts*

Mashukov A.O. *Efficiency hospital state of rehabilitation of patients with color carcer.* PhD (Med.) Odesa, 2011 [In Ukrainian].